EXON SKIPPING PEPTIDE-PMOS FOR CORRECTION OF DYSTROPHIN IN MOUSE MODELS OF DUCHENNE MUSCULAR DYSTROPHY

CORINNE ANNE BETTS

THESIS SUBMITTED FOR THE DEGREE OF DOCTOR IN PHILOSOPHY

FACULTY OF MEDICAL SCIENCES
DEPARTMENT OF PHYSIOLOGY, ANATOMY AND GENETICS
ST EDMUND HALL

Acknowledgements

I would first like to thank the Muscular Dystrophy Campaign for their generous support and funding for this DPhil. It has been a true pleasure to be a DPhil ambassador for this charity. Meeting the warm and friendly people whom tirelessly raise money for this charity has been awe inspiring.

I would like to thank the Wood laboratory and in particular Prof. Matthew Wood for his invaluable support and advice throughout this DPhil. He has provided an open environment for me to thrive and his encouragement and advice have moulded me into the scientist I am today, for which I am truly grateful. I would like to thank Dr. Suzan Hammond. Not only was she my co-supervisor but a close friend and has always ensured the best for me throughout my DPhil. Her advice and guidance have been invaluable and I knew I could approach her with any issue no matter how big or small. Thank you also to Prof. Haifang Yin, for without her initial help at the start of my University career, I would not be here.

I would like to thank the Duchenne muscular dystrophy group members, particularly Dr. Graham McClorey, whom I knew I could approach with any question. He too is a close friend whom has made the laboratory such a pleasure to work in. Thank you to Caroline Godfrey, Tom Merritt, Andrew Douglas, Yoshi Aoki, Taeyoung Koo, Raquel Mazano and all other past Duchenne group members. A huge thank you also to Dr. Carolyn Carr whom taught me how to MRI and analyse the data. This is an exceptionally complex procedure and therefore her patience whilst teaching me was unparalleled. Her approachable nature, help and advice have been invaluable.

To the rest of the Wood laboratory, past and present, we are more like a family then work colleagues. I have had the great pleasure to work with such talented and inspiring scientists. These are the people that make this laboratory so difficult to leave. We are a group of people thrown together from many walks of life and very different interests, yet we are bound together by a common thread. Thank you to past colleagues whom I deeply miss. You know who you are (SS). A huge thank you also to my present laboratory family that make this laboratory such a wonderful place to work.

To my husband, Jonathan Betts, my rock. I thank him for his unfailing love and support throughout the years. He has supported me in every choice I have made, even to his own detriment. Thank you also to my family for their love and support and for providing me with a wonderful place to escape, outside of studying. Finally to the big guy upstairs, for the strength to keep me going, when I didn't think I had anything left!

Abstract

EXON SKIPPING PEPTIDE-PMOS FOR CORRECTION OF DYSTROPHIN IN MOUSE MODELS OF DUCHENNE MUSCULAR DYSTROPHY

CORINNE ANNE BETTS — **DOCTOR IN PHILOSOPHY**
ST EDMUND HALL — **TRINITY TERM 2014**

Duchenne muscular dystrophy (DMD) is a fatal, muscle-wasting disorder due to mutations/deletions in the dystrophin gene. Whilst improvements in palliative care have increased the life expectancy of patients, cardiomyopathy and respiratory complications are still the leading causes of death. A potential therapy for the treatment of DMD is antisense oligonucleotides (AOs), which modulate dystrophin pre-mRNA splicing to restore the dystrophin reading frame and generate a truncated functional protein. Conjugation of AOs to cell penetrating peptides (CPP), such as Pip5e-, significantly improves delivery to skeletal muscles and to the heart, which is imperative given the impact of cardiomyopathy to mortality. However, it should be noted that the contribution of skeletal muscles, such as the core respiratory muscle, the diaphragm, in dystrophic cardiopulmonary function is poorly understood.

The specific aims of the work in this thesis were to (i) understand the effect of the diaphragm on cardiac function using magnetic resonance imaging (MRI), (ii) screen a number of derivatives of Pip5e (Pip6) in an effort to discover further promising peptides and define the properties integral to heart penetrating capacity, and (iii) assess whether Pip6-PMOs restore cardiac function (MRI) following a repeat, low dose regimen. In short, the specific restoration of dystrophin in the diaphragm of the dystrophic mouse model, the *mdx* mouse, did not improve cardiac function, highlighting the importance of a body-wide therapy. The screening of multiple Pip5e-PMO derivatives revealed 3 promising peptides with improved cardiac splicing capacity; however, serial deletions of amino acids from the central core resulted in the diminution of dystrophin restoration, possibly due to a reduction in hydrophobicity. Finally, the Pip6-PMO treatment regimen substantially restored dystrophin protein (28% in heart) and stabilised cardiac function, even with an increased work load. In conclusion, this study illustrates the importance of a body-wide treatment, such as the CPP strategy (Pip-PMO). These Pip-PMO conjugates demonstrate high dystrophin restoration in a number of muscles, including cardiac muscle, and have a beneficial effect on cardiac function.

List of Abbreviations

%RS- percentage recovery score

2'OMePS- 2'O methyl phosphorothioate

3D- three dimensional

5aa- 5 amino acid

AAV- adeno-associated virus

ACE- angiotensin-converting enzyme

A-Hex- amino hexyl

ALT- alanine aminotransferase

AO-antisense oligonucleotide

AST- aspartate aminotransferase

ß-blockers- beta-blockers

B-Ala- beta alanine

BMD- Becker muscular dystrophy

BPM- beats per minute

B-PMO- $(RXRRBR)_2$-PMO

BUN- blood urea nitrogen

BW- body weight

CK- creatine kinase

CO- cardiac output

CO_2- carbon dioxide

C-terminal- carboxy terminal

CPP- cell penetrating peptide

DAG- dystrophin-associated glycoprotein

DCM- dilated cardiomyopathy

dKO- double (utrophin/dystrophin) knock-out

EBD- Evan’s blue dye

ECG- electrocardiogram

EDV- end diastolic volume

EF- ejection fraction

ESE- exonic splicing enhancer

ESV- end systolic volume

eNOS- endothelial nitric oxide synthase

hDMD- human Duchenne muscular dystrophy

HR- heart rate

iNOS- inducible nitric oxide synthase

IP- intraperitoneal

IV- intravenous

LDH- lactate dehydrogenase

LGE- late gadolinium enhancement

LV- left ventricle

MOE- 2'-O-methoxyethyl phosphorothioate

MRI- magnetic resonance imaging

mRNA- messenger ribonucleic acid

NMJ- neuromuscular junction

NO- nitric oxide

nNOS- neuronal nitric oxide synthase

NOX- NADPH oxidase

Nppa- atrial natriuretic peptide

N-terminal- amino terminal

O_2- oxygen

PDE5- phosphodiesterase 5

Pip- PNA/PMO internalisation peptide

PMO- phosphorodiamidate morpholino oligomer

PNA- peptide nucleic acid

PTC- premature termination codon

qRT-PCR- quantitative real time polymerase chain reaction

R6-Pen- Penetratin derivative with 6 arginine residues

Radiofrequency- RF

READ- read through evaluation and assessment by dual receptor (mouse model)

ROS- reactive oxygen species

rRNA- ribosomal RNA

RT-PCR- reverse transcription polymerase chain reaction

RV- right ventricle

$(RXR)_4$- arginine-aminohexyl-arginine chain

SACS- stretch activated calcium channels

SERCA- sarcoplasmic reticulum calcium ATPase

snRNPs- small nuclear ribonucleoproteins

SR- sarcoplasmic reticulum

SV- stroke volume

TP10- transportan 10

tRNA- transfer RNA

TTE- transthoracic echocardiography

XLDCM- X-linked dilated cardiomyopathy

Table of Contents

Chapter 1. Introduction

Cardiac Morphology and Function

The heart is an integral component of the cardiorespiratory system, delivering deoxygenated blood to the lungs, and pumping oxygenated blood to the rest of the body. Cardiac myocytes are mono-nucleated, striated muscle cells, which form a branching network referred to as the functional syncytium (Textbook: [1]). These myocytes connect via specialised cell membranes called intercalated disks. Gap junctions within these intercellular regions permit cell-to-cell conduction following electrical stimuli, thereby allowing the heart to contract as a unit.

The heart is composed of 3 layers namely the outer epicardium, the middle myocardium and inner endocardium. It is enclosed within a double walled sac called the pericardium, which protects and anchors the heart to its surroundings. The gross anatomy of the heart comprises 4 chambers; the right atrium and ventricle, and the left atrium and ventricle. Deoxygenated blood from the body enters the right atrium via the superior and inferior vena cava. The right atrium depolarises, expelling the blood into the right ventricle via the tricuspid valve. The right ventricle, in turn, undergoes depolarisation thereby sending the deoxygenated blood along the pulmonary artery to the lungs. The blood undergoes carbon dioxide (CO_2) and oxygen (O_2) exchange in the lungs, and is returned to the left atrium via the pulmonary vein. The atrium depolarises, pushing the blood through the mitral valve, into the left ventricle. The oxygenated blood is

finally expelled from the left ventricle, and delivered to the rest of the body via the aorta.

The fine balance of the cardiac cycle may be disrupted by pathological conditions (ischemia, hypotension) or intrinsic cardiomyopathic mediators (conduction issues, damage) which may have a detrimental effect on cardiac function. This, in turn, has wide reaching implications for the rest of the body. Indeed, cardiomyopathy is prominent in Duchenne Muscular Dystrophy (DMD) patients, which leads to heart failure, and will be discussed in detail (**Disease Progression in Patients- Cardiomyopathic Progression**).

Magnetic Resonance Imaging- Brief Overview

Magnetic resonance imaging (MRI) is a powerful imaging tool used to investigate human anatomy in the context of health and disease. This technology has many applications, ranging from neuroimaging [2], musculoskeletal [3], liver and gastrointestinal tract [4, 5], cardiovascular and oncology imaging [6]. Indeed, clinicians overseeing DMD patient care often utilise MRI to determine the extent of musculoskeletal wasting [7], and more recently to assess the progression of cardiomyopathy [8].

The major components of an MRI system include the primary magnet, gradient coils and radiofrequency (RF) coils. The MRI system measures the spin of hydrogen atoms in a magnetic field in order to produce an image [9]. The abundance of hydrogen atoms in our body (70% water) and the presence of a single proton and circulating electron make it the ideal atom for use in MRI. Introduction to a strong magnetic field and RF pulses, excites the hydrogen atoms which generates a signal which may be recorded. The gradient coil is a secondary magnetic field, which allows slice selection and localisation.

MRI provides high spatial resolution which allows tissue characterisation, volume and functional assessment [10]. The enormous advantages of this technique are its non-invasiveness and high reproducibility which allows constant assessment at various stages. Cardiac MRI may be enhanced using contrasting agents, such as gadolinium, which accumulates in the

interstitial space following myocardial injury [11]. MRI was utilised in this thesis, as it was considered the ideal method to assess cardiac function in *mdx* mice.

Neuromuscular Disorders and Muscular Dystrophy

Neuromuscular disorders are a group of inherited or acquired diseases which develop following compromisation of the neuromuscular system. This involves disruption of integral neuromuscular unit components, such as the motor neurons, peripheral nerves, neuromuscular synapses or skeletal muscle itself (review: [12]).

A subset of neuromuscular disorders, muscular dystrophies, are the result of genetic mutations in structural proteins, signalling molecules and enzymes [13]. Disruption of the muscle sarcolemma leads to a cascade of pathological events including inflammation, cell necrosis and cell death. Extensive fibrotic deposition occurs which replaces muscle mass, thereby resulting in progressive muscle weakness and skeletal muscle wasting. More than 30 muscular dystrophies exist which vary in distribution and severity. The most severe form of muscular dystrophy is DMD.

Duchenne Muscular Dystrophy

The Duchenne Muscular Dystrophy Phenotype

DMD is a severe, X-linked, neuromuscular disorder caused by the absence of dystrophin protein [14]. This disease is the most common paediatric muscular disorder with a prevalence of 1 in 3500 to 5000 boys [14, 15]. Patients remain undiagnosed until about 2 years of age, at which stage they exhibit delays in motor development and skeletal muscle weakness [16]. Early diagnosis is often made following observation of Gower's movement, whereby patients experience difficulty getting up from the floor due to pelvic girdle and lower extremity weakness [17]. Between the ages of 6-10, patients develop muscle contractures, scoliosis and overt signs of musculoskeletal wasting and, by 10-12 years of age, patients are generally non-ambulant.

Early indicators of cardiomyopathy, such as tachycardia, manifest at 5-6 years of age. Cardiomyopathy then progresses to left ventricle (LV) dilation and wall thickening, a decrease in fractional shortening, and electrocardiogram (ECG) abnormalities [18, 19]. By 10-12 years of age, most patients exhibit signs of cardiomyopathy which are further compounded by respiratory involvement. Indeed cardiomyopathy contributes significantly to death amongst DMD patients [20] even with the advent of interventative respiratory support and cardiac drugs. Thus it is critically important that an effective treatment be developed for DMD, which also targets the heart. Antisense oligonucleotides (AOs) are a

promising therapeutic modality that may be manipulated to reach the heart and will be discussed in greater detail.

The Dystrophin Gene

Dystrophin is located on the human Xp21 gene locus [21] and is the largest human gene (2.4Mb) comprising 79 exons. The absence of dystrophin in DMD is due to deletions (60-65%), small mutations (including intronic deletions or exonic insertions; 20-35%) or duplications (5-15%) [22] which are transmitted either by carrier (maternal) or are spontaneous *de novo* mutations, owing to the enormous size of the gene [23]. Familial transmission in isolated cases accounts for approximately 27% of deletion mutations and between 55-63% of small mutations and duplications [24, 25]. These mutations or deletions disrupt the reading frame of dystrophin messenger (m)RNA, thereby preventing the translation of functional protein [26-28]. Becker muscular dystrophy (BMD) is the milder allelic form of the disease resulting from in frame deletions, which result in a truncated, but functional, protein [29].

Dystrophin Isoforms

A number of dystrophin isoforms exist, including full length (427kDa), 260kDa (Dp260), 140kDa (Dp140), 116kDa (Dp116) and 71kDa (Dp71) proteins [22] (**Fig. 1.1**). There are three full length isoforms which are derived from independent promoters designated ‘brain’, ‘muscle’ and

‘Purkinje’. These names denote the predominant tissue in which they are expressed (see **Fig. 1.1**). The muscle isoform is expressed in cardiac and skeletal muscle with low level expression in glial cells of the brain. It consists of 4 structural domains: the amino (N)-terminal which binds to actin, a central domain containing 24 spectrin repeats, a third cysteine rich domain, and a carboxy (C)-terminal domain. The C-terminal binds with several other proteins to form the dystrophin-associated glycoprotein complex (DAG; see **Fig. 1.2**) which includes the α- and ß-dystroglycans, α- ß- δ- γ- and ε-sarcoglycans, sarcospan, α- and ß-syntrophins, α-dystrobrevin and neuronal nitric oxide synthase (nNOS) [30].

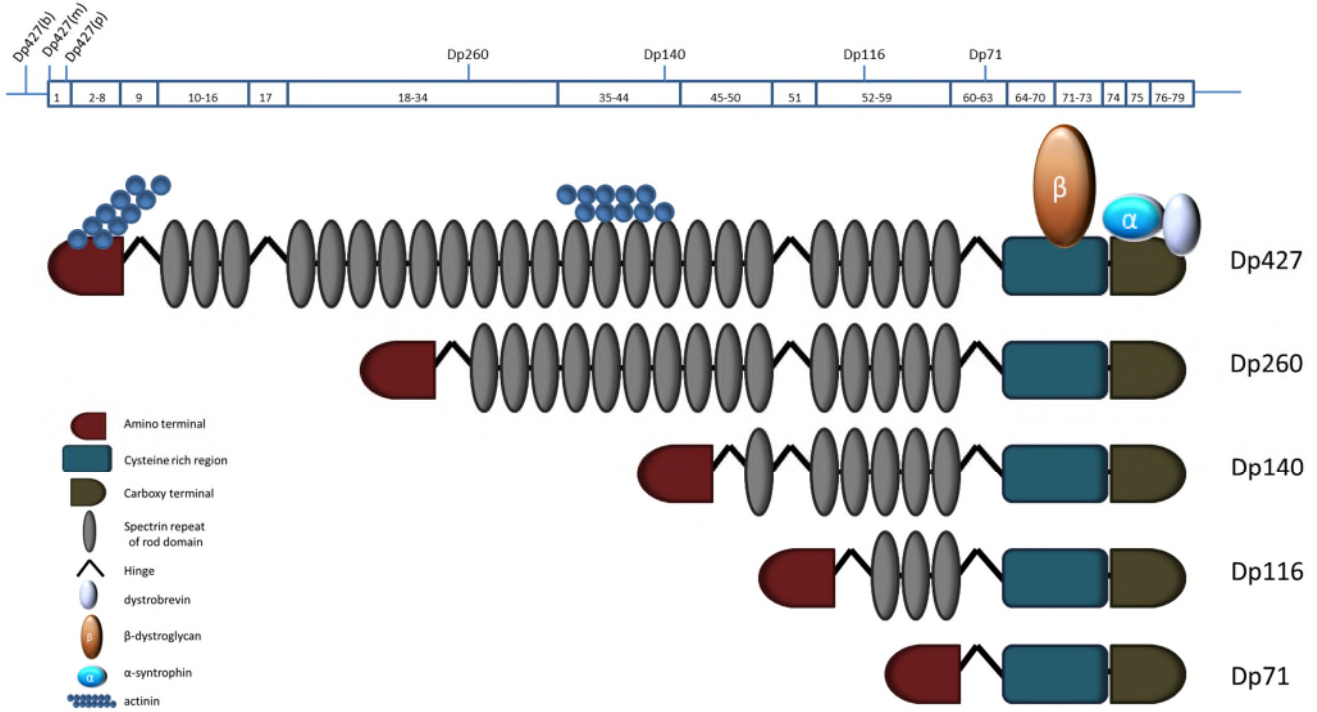

Figure 1.1. Dystrophin isoforms Dp427, Dp260, Dp140, Dp116, and Dp71 showing various domains and dystroglycan associated protein binding sites. The figure legend on the left lists the major components of the dystrophin protein namely the amino terminal (red), spectrin repeats (dark grey), cysteine rich region (blue) and carboxy terminal (green). It also illustrates hinge regions and the relevant dystrophin associated glycoprotein components that bind to Dp427; β-dystroglycan (brown), α-syntrophin (light blue) and dystrobrevin (light grey) at the carboxy end and actin at the amino end and rod domain. Dp260, Dp140, Dp116 and Dp71 do not have an actin binding domain, but retain the other dystroglycan binding sites. The bar above illustrates the dystrophin gene with 79 exons and the promoter sites for each isoform. Adapted from figure by Dr Graham McCLorey

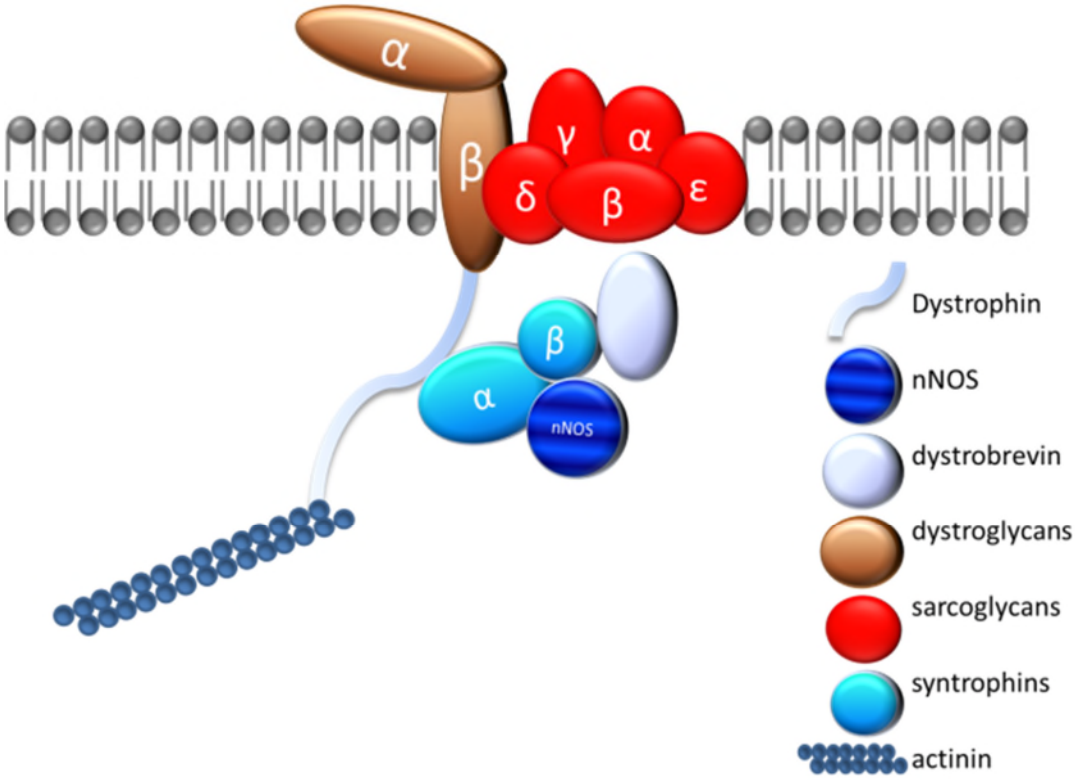

Figure 1.2. The dystrophin-associated glycoprotein complex. Illustration showing the orientation of dystrophin (grey ribbon) with the dystrophin-associated glycoprotein (DAG) complex and actin at the sarcolemma (dark grey hydrophobic molecules). Dystrophin is attached to the DAG at the carboxy terminus. The DAG consists of α-and β-dystroglycans (brown), 5-sarcoglycan subunits (red), α- and ß-syntrophins (light blue), dystrobrevin (grey) and neuronal nitrous oxide synthase (dark blue). Dystrophin is attached to actin at the amino terminus.

The function of dystrophin in the DAG complex is to link F-actin to the extracellular matrix, thus stabilising the sarcolemma against stress induced damage [31]. It also allows the dissipation of mechanical force to the extracellular matrix, thereby protecting myocytes from physical damage. In addition, dystrophin is involved in cellular communication either by directly regulating membrane-associated proteins or via calcium and nitric oxide (NO) second messenger cascades [32]. This will be discussed in greater detail (**Dystrophin in the cell**).

The shorter dystrophin isoforms lack the actin-binding domain, but retain the cysteine rich region and C-terminus which bind to dystroglycan, dystrobrevin and syntrophin (see **Fig. 1.1**) [22]. The Dp260 isoform is exclusively expressed in the retina along with full-length isoforms. Absence of these dystrophin isoforms in the retina have been associated with disturbances in retinal electrophysiology (particularly reduced b-waves) [33]. Dp140 is expressed in the brain and deletions of this isoform results in severe cognitive and intellectual disability [34]. This isoform is also expressed in retina and kidney tissues, whereas Dp116 is exclusively expressed in adult peripheral nerves. In contrast, Dp71 is expressed in all tissues with the exception of skeletal muscle and is believed to play a role in multiple cellular processes including cell adhesion, water homeostasis, cell division, and nuclear architecture [35].

Dystrophin Isoforms in Heart

Full length dystrophin, Dp427, and the shorter Dp71 isoform are the prevalent isoforms expressed in the heart [36]. The full length isoform is located at the cardiac sarcolemma and T-tubules whereas Dp71 is only present in the T-tubules. Direct comparison of *mdx* mice (Dp427 absent) and DMD null mice (Dp427 and Dp71 both absent) revealed similar myocardial fibrosis progression which demonstrated that Dp427 is the essential isoform required to prevent the onset of cardiomyopathy [36].

BMD and X-linked dilated cardiomyopathy (XLDCM) both present with dystrophin mutation/deletions and cardiac involvement. Although BMD generally presents with gradual skeletal muscle deterioration, 70% of patients develop cardiomyopathy and heart failure is the predominant cause of death [37] (note: BMD patients develop cardiomyopathy much later then DMD patients, and is fatal usually at 50-60 years of age). It was this observation that led to the idea that the location of the mutation/deletion within the dystrophin gene correlated with the severity of cardiomyopathy. Indeed this was confirmed and it was revealed that deletions which affected the amino-terminal domain (muscle promoter, exon 1 or intronic regions) were associated with early-onset DCM (mid-20's), whereas deletions in the rod domain and hinge 3 region resulted in later onset DCM (mid-40's) [23].

Duchenne Muscular Dystrophy- Disease Progression in Patients

Skeletal Muscle Progression

DMD first manifests with general muscle weakness, abnormality in gait, and typical Gower's movement, which is characterised by difficulty getting up from the floor and climbing the stairs [16, 17]. Weakness starts in the proximal muscles and descends symmetrically down both lower extremities [38]. This progressive weakness causes further changes in posture and gait. During the early ambulatory stage, patients exhibit plantar flexation and a compensatory increase in hip flexation in an attempt to clear the foot from the floor when taking a step. Muscles continue to weaken resulting in changes to body alignment and this is termed the transitional ambulatory stage. Patients widen their base for support and increase arm swinging and trunk leaning to compensate for weakness in the gluteus medius. During this stage, patients exhibit poor hip extensor strength and they tend to lean back to shift their body weight posterior to the hip joints. Quadriceps strength declines also. At late stages of ambulation, further changes in body alignment are observed and patients are prone to falling more regularly due to muscle weakness. Secondary to muscle weakness, joint contractions in the hip extensor [39] and plantar extensor of the ankle [40] manifest thereby limiting the movement within these joints. Scoliosis generally occurs as patients become wheel chair bound. The curvature of the spine restricts lung capacity and thus has a profound negative impact of respiratory function [41].

The continual replacement of collagen and fat tissue for muscle, leads to progressive muscle wasting and weakness. Dystrophic muscles are particularly susceptible to contraction-induced damage, which initially provoke cycles of regeneration [42, 43]. However, after a number of cycles of regeneration, muscle fibres are eventually replaced with fibrous connective tissue and fat, which render the muscle ineffective. In addition, the damaged muscle is unable to regulate local blood flow, which leads to ischemia [44]. Muscle ischemia further exacerbates the skeletal muscle pathology.

Other issues that occur in DMD patients that are overshadowed by the more severe skeletal muscle phenotype include neurological disorders, osteoporosis, and gastrointestinal dysfunction. DMD patients exhibit cognitive difficulties, such as a significant learning disability, poor reading and memory function, and low verbal IQ [45]. It has been suggested that these cognitive issues are due to the absence of dystrophin in the cerebellum [46]. The decline in cognitive function appears to also correlate with an increase in amyloid beta peptide, which is suggested to cause brain damage in patients [47]. Patients also suffer from osteoporosis due to low bone density [48], which is compounded by the prolonged use of corticosteroids [49]. One study revealed that 21% of patients had experienced a fracture in their lifetime and that these fractures had a substantial impact on mobility [50]. Dysfunction of the oropharyngeal,

oesophageal and gastric tracts are also prevalent amongst these patients [51]. These events underscore the vast extent of this debilitating disease on the human body.

Respiratory Involvement

DMD patients exhibit symptoms of respiratory muscle weakness from about 10-14 years of age. Respiratory complications are the major contributor to death amongst DMD patients and stem primarily from progressive restrictive ventilation defects, chronic hypoventilation and pulmonary infections (inability to cough and clear airways) [52]. The deterioration in respiratory muscles results in respiratory insufficiency. DMD patients exhibit reduced vital capacity and forced respiratory volume with reduced maximal inspiratory pressure as the disease progresses [53]. Impaired respiration accentuates pulmonary hypertension thus contributing to RV failure [54]. Moreover respiratory muscle weakness in patients leads to hypoventilation, hypercapnia and hypoxemia [55]. Ventilatory support is thus implemented to ensure adequate ventilation and coughing reflex when respiratory involvement is apparent.

Cardiomyopathic Progression

The deterioration of heart, cardiomyopathy, is a prominent event in DMD patients. Patients first exhibit left ventricle (LV) dilation and wall thickening (hypertrophy) accompanied by decreased fractional shortening and

electrocardiogram (ECG) abnormalities [18, 19, 37, 56]. As the cardiomyopathy progresses, the heart weakens, dilates and struggles to pump blood adequately around the body. This event is known as dilated cardiomyopathy (DCM). It is estimated that 25% of patients under the age of 6 years present with DCM, which escalates to 59% by 10 years of age and is prevalent in all patients by adulthood [19]. The degree of cardiac involvement varies between patients, but by 20 years of age most patients exhibit a low LV ejection fraction (EF) due to systolic dysfunction [8]. Whilst respiratory complications are still the major cause of death amongst patients [52], cardiomyopathy also contributes significantly to mortality [20].

ECG abnormalities are amongst the first observable cardiac events that occur in DMD patients. Monitoring heart ECG is a valuable diagnostic tool which records the repolarisation and depolarisation of the atria and ventricles during the cardiac cycle. The initial small P wave denotes atrial depolarisation, which is followed by the QRS complex (ventricular depolarisation) and T wave (ventricular repolarisation). ECG abnormalities in DMD patients present with altered R wave and deep Q wave, and an R/S ratio greater than 1 [57]. Approximately 50% of patients also display a shortened PR phase, whilst a smaller population also exhibit QT prolongation [58]. ECG and Holter ECG studies (ECG assessment required for greater than 24h) revealed tachycardia in approximately 26% of patients, and an increase in pathological heart rate variability (51%)

[18]. These ECG abnormalities have been associated with conduction defects [59], morphological changes to cardiac muscle (thin and thick myofibres) and myocardial fibrosis [58]. Indeed, the deep Q wave has been attributed specifically to lateral wall scarring [60].

LV dysfunction occurs when hypertrophy manifests. Hypertrophy is the thickening of the heart wall in order to sustain an increase in wall stress imposed by pressure/volume overload. This further undergoes maladaptive remodelling whereby the heart dilates, developing into DCM [8]. Generally cardiomyopathy is asymptomatic due to limitations in physical activity or is overlooked due to difficulties during cardiac assessment as a result of scoliosis. Traditionally transthoracic echocardiography (TTE) is utilised for assessment, but severe scoliosis hampers the ability to accurately measure cardiac function and therefore function is often estimated. Consequently pathological changes are detected at an advanced stage of the disease and treatment may be employed too late. New MRI techniques can successfully calculate circumferential strain in DMD patients and observe the gradual decline in follow up assessments when parameters such as EF generally fluctuate [8, 61, 62]. This innovative technique therefore provides a sensitive indicator of early systolic dysfunction.

Myocardial fibrosis correlates with a decline in function and therefore monitoring fibrotic progression is imperative. Fibrotic involvement is prevalent in 17% of patients under 10 years, 34% between 10-15 years and 59% older than 15 years of age [63]. Focal necrosis initially manifests at the posterobasal region of the LV free wall and gradually migrates towards the apex and the septum [64]. It further progresses to the outer half of the ventricular wall whilst the right ventricle (RV) free wall and atria generally remains unscarred.

Dystrophic Phenotype in the *mdx* Mouse Model

A mouse model of DMD, the *mdx* mouse, is widely utilised. The *mdx* mouse is the result of a spontaneous mutation in an inbred colony of C57BL/10 wild type mice, discovered in the mid-80's [65]. This single point mutation in exon 23 encodes a premature termination site thus preventing the production of dystrophin protein [65, 66]. Early studies revealed elevated plasma levels of creatine kinase (CK) and pyruvate kinase and irregular histological features, including variations in fibre size, degeneration of fibres and centralised nuclei [65]. At 3-4 weeks of age, skeletal muscle undergoes a massive round of fibre degeneration, followed by continuous degeneration-regeneration bouts. This event slow down at approximately 10 weeks of age [67]. The specific force and power in skeletal muscle declines with age [68]. *Mdx* mice undergo severe muscle necrosis, which is compensated for by regeneration, however the regenerative capacity decreases with age whilst necrosis continues and

thus fatty tissue deposition occurs [69]. Older *mdx* mice better resemble the pathological progression observed in patients.

Respiratory dysfunction is also observed in *mdx* mice and correlates with degeneration of the diaphragm as the disease progresses with age. Whole body plethysmography revealed reduced tidal volume, respiratory rate and minute ventilation under normoxia [70], and blunted hypoxic ventilatory reflex when exposed to mild hypoxia [71]. Arterial blood samples from *mdx* mice also revealed low blood O_2 levels and pH, and elevated CO_2. In addition, dystrophin is absent in the carotid body of *mdx* mice which may explain the impaired chemosensory drive.

Mdx mice also display a cardiac phenotype. The mice exhibit a very similar progression to DMD patients including early ECG abnormalities [58, 72], and progressive LV dysfunction leading to DCM [73, 74], the progression of which is described in **Fig. 1.3**. The major disparity between *mdx* mice and DMD patients is that RV involvement does not occur in all DMD patients; *mdx* mice exhibit RV dysfunction prior to LV changes. Interestingly BMD patients also exhibit RV changes prior to LV, analogous to *mdx* cardiac progression. DMD patients generally receive early ventilatory intervention due to the rapid deterioration in respiratory function. This intervention would be likely to improve pulmonary hypertension and thus may compensate for RV dysfunction. Perhaps this

is the reason for the marked disparity between patients and this model as ventilation is not implemented in mice and is possibly not required for BMD patients until a later stage.

Similarly to DMD patients, ECG recordings in conscious *mdx* mice have revealed tachycardia, decreased heart rate variability [75], deep Q waves, diminished S:R ratios and polyphasic R-waves [76] compared to controls. In addition, the QT and PR intervals are shorter in *mdx* mice and pharmacological autonomic blockade reveals an imbalance in autonomic function including decreased parasympathetic activity, increased sympathetic activity and dysregulation of heart rate.

A comprehensive cardiac MRI time course study (1, 3, 6, 9 and 12 months of age) accurately records the progression of the *mdx* cardiac phenotype [73]. RV dysfunction precedes LV and is evident from 3 months of age characterised by increases in RV systolic volume and subsequent reduction in the RV EF. An increase in myocardial fibrosis is apparent from 6 months of age. In addition, LV cardiac output (CO) deteriorates, followed by a reduction in stroke volume (SV) at 9 months and reduction in LV EF at 12 months. Overt signs of interstitial fibrosis occur at 7 months of age, which present as patches or transmural lesions by 10 months [77]. Although this model has been criticised for the late onset cardiac phenotype, it should be noted that, at 1 month of age, *mdx* mice exhibit

early intolerance to dobutamine stress [73]. These cardiac events illustrate the similarities between the human dystrophic cardiac phenotype and *mdx* mouse phenotype.

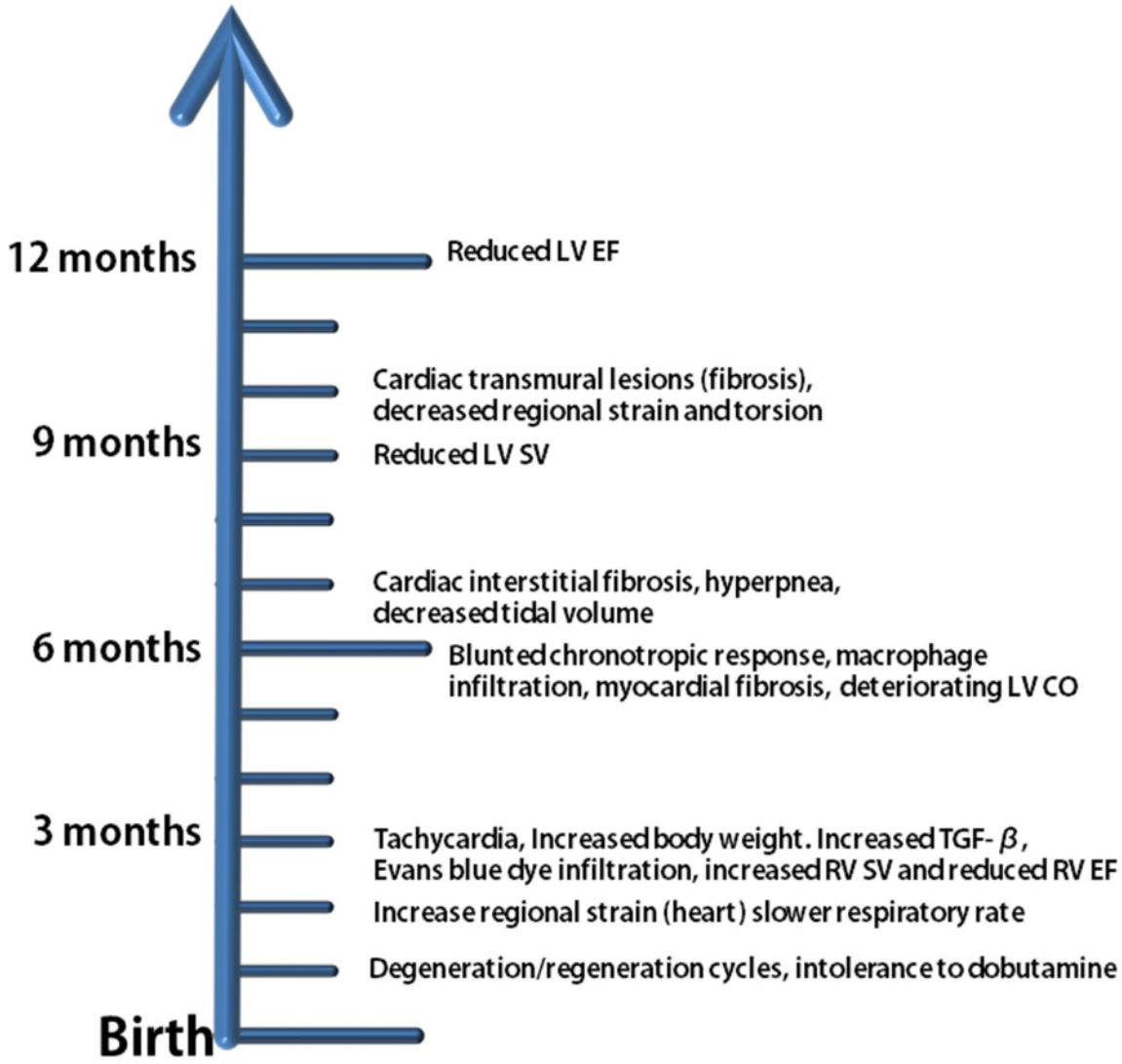

Figure 1.3. Timeline of events in *mdx* mice. The timeline lists the pathological cardiac and respiratory events that occur in the life of an *mdx* mouse. Initially signs of tachycardia and fibrosis occur, which progress into more obvious cardiac function changes and extensive fibrosis. Abbreviations: right ventricle-RV, left ventricle-LV, ejection fraction-EF, stroke volume-SV, cardiac output-CO.

Dystrophin at a Cellular Level

As mentioned, dystrophin stabilises the sarcolemma against stress induced damage by dissipating mechanical force and thereby protecting myocytes from physical damage [31]. The major events that occur in dystrophic tissue due specifically to the absence of dystrophin are (i) the influx of intracellular calcium and (ii) an imbalance of NO signalling (illustrated in **Fig. 1.4**) [32].

Calcium influx in skeletal muscle has predominantly been attributed to stretch activated channels (SACs) and reactive oxygen species (ROS) stimulation of Src. Dystrophin has been linked with the regulation of SACs which are markedly more active in *mdx* mice [78]. The mechano-sensitive channel Trpc1 was identified as the key SAC protein involved in calcium influx which is up-regulated in *mdx* mice. Trpc1 co-localises with Caveolin-3 which in turn binds to sarcolemmal protein ß-dystoglycan [79]. Reactive oxygen species production increases Src activity, which in turn activates the Trpc1 subunit thereby increasing calcium influx. ROS is an important mediator of other pathological events that occur in dystrophic tissue. Elevated ROS production has been attributed to a number of factors including mechanical stress, NOS production, mitochondrial respiration and NADPH oxidase (Nox) [78]. These events result in ROS and calcium mitochondrial overload with consequential mitochondrial membrane potential collapse [80]. Calcium influx may also be due to altered

expression of a sarcoplasmic reticulum (SR) channel, RyR1, which allows leakage from the SR [81].

The other major disruption leading to the pathological progression in DMD is the mislocalisation of nNOS which is usually anchored to the sarcolemma and is linked to dystrophin and α-syntrophin [82]. The primary role of nNOS is to allow the diffusion of NO into the nearby vasculature in order to counter α-adrenergic vasoconstriction [44, 83]. As this event is impaired, the protective vessel relaxation mechanism is compromised causing contraction-associated ischemic injury [84]. Ischemic injury contributes to the pathological progression of the dystrophic phenotype.

Calcium and nNOS Dysregulation in Heart

The role of dystrophin in the heart is similar to that of skeletal muscle; to protect the myocardium from mechanical stress and work induced damage [85]. Cardiomyocytes deficient in dystrophin display myocyte hypertrophy, atrophy and fibrosis [86]. Cardiac muscle undergoes similar calcium and NOS signalling pathways to skeletal muscle, however the following specific events have also been observed:

In addition to SACs, dystrophin has also been associated with dysregulation in L-type channels which also regulate calcium [87].

Dystrophin co-localises with this channel and modulates its function. The absence of dystrophin causes delayed inactivation of the channels which allows the prolonged influx of calcium, thereby increasing cytosolic and mitochondrial calcium levels, NADH production and ROS generation [88]. Altered L-type activation in heart has been associated with disturbed ECG recordings [89].

Several other channels/receptors and calcium handling proteins are dysregulated in *mdx* mouse hearts. The cardiac isoform of sarcoplasmic reticulum calcium ATPase (SERCA2), responsible for pumping cytosolic calcium back into the SR, is down-regulated in *mdx* hearts [90] and thus contributing to calcium mishandling. Another SR calcium release channel, which is associated with SERCA, the ryanodine receptor, is also dysregulated in *mdx* mouse hearts and may be further stimulated in a ROS environment, thereby increasing cytosolic calcium [91]. The imbalance of calcium handling proteins, such as calsequestrin, sarcalumenin and calpastatin, further contribute to the pathological progression [32]. The cardiac sodium channel, Na(v)1.5, is associated with dystrophin at the C-terminus and is down-regulated (protein levels) in *mdx* mice [92]. Na(v)1.5 is involved in cardiac excitability and conductance and thus a decrease of sodium current would result in ECG abnormalities.

A number of these receptors and channels have also been implicated in NOS regulation. NOS signalling in *mdx* hearts is severely disrupted; nNOS activity is significantly suppressed from 2 months of age and conversely inducible NOS (iNOS) activity increases. The significant increase in iNOS may be triggered by the influx of calcium, which induces the infiltration of macrophages and inflammatory mediators [72]. iNOS has been attributed to significant ECG abnormalities and arrhythmia in *mdx* mice. In addition to the sarcolemma, nNOS is also located at the SR with the ryanodine receptor and SERCA [82]. As discussed, SERCA2 and ryanodine receptor activation is disrupted in dystrophic hearts, which, combined with calcium fluctuations, result in disturbed nNOS and iNOS activity with consequential ECG abnormalities [90, 91]. It is clear that NOS signalling is integral to the homeostatic balance of the heart and indeed transgenic myocardial expression of nNOS in the *mdx* mouse improved NO signalling thus preventing fibrosis and myocarditis with improved/corrected ECG recordings [76]. It should also be noted that NOS disruption, which consequently disturbs NO signalling in the vasculature, significantly contributes to muscle ischemia [93].

It is thus clear that the absence of dystrophin in the cardiac cell leads to severe calcium dysregulation and NOS handling, which contribute significantly to cardiomyopathic progression. This is specifically due to the dysregulation of multiple channels, receptors and handling proteins which

increase calcium influx and ROS production. This results in further deterioration culminating in mitochondrial overload.

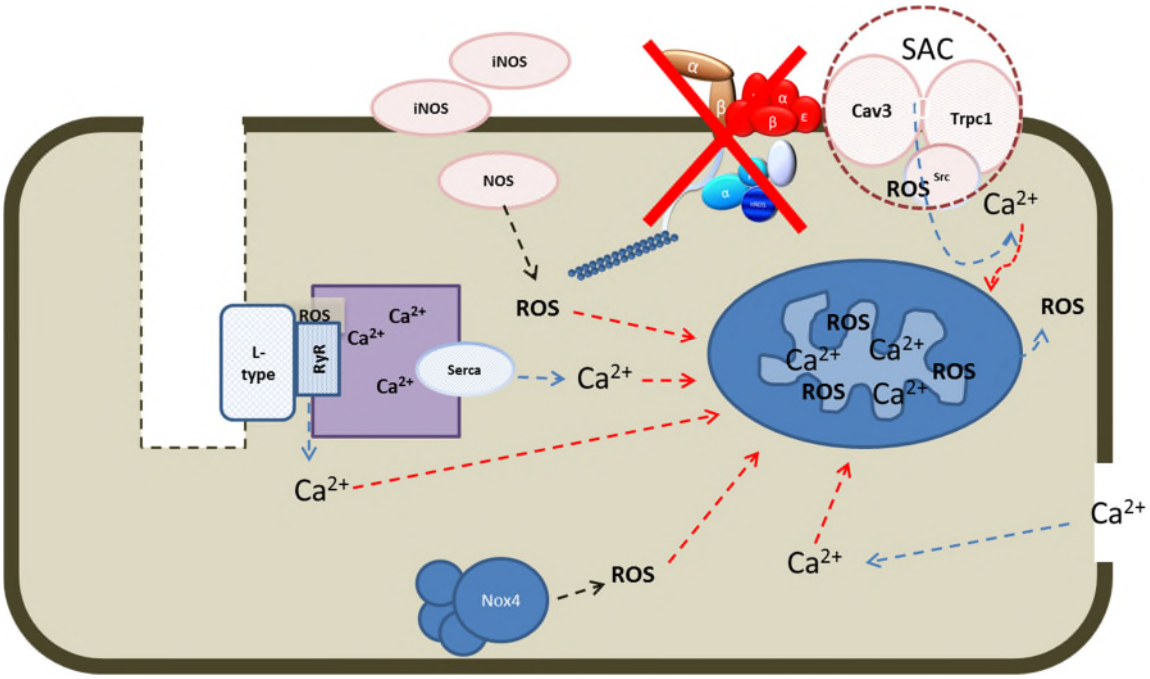

Figure 1.4. Disruption of calcium and NOS transients in the dystrophic cardiomyocyte. From right, sarcolemmal tears allow calcium influx. Top, Src activation by ROS activates Trpc1 and Cav3 allowing calcium influx. iNOS is up-regulated in dystrophin deficient cell due to calcium and macrophage recruitment which increases ROS. Left, L-type channels (located in T-tubule) remain open for longer allowing calcium influx. In addition RyR (activated by ROS) and SERCA are disrupted thereby releasing calcium from the sarcoplasmic reticulum. Nox4 further contributes to ROS production. Calcium and ROS overload in mitochondria causes membrane potential collapse.

Current Treatments for Duchenne Muscular Dystrophy

Current Clinical Applications

As there is currently no effective cure for DMD, therapy is limited to the management of symptoms. The three predominant approaches include corticosteroids for skeletal muscle, mechanical respiratory support and cardiac assessment and treatment. Corticosteroids markedly improve muscle strength and function [94] and have further been implicated in stabilising pulmonary function, prolonging ambulation and lowering the prevalence of scoliosis [95]. More recently, corticosteroids have also been associated with delaying the onset of cardiomyopathy by reducing the probability of developing cardiomyopathy by 4% for each year of corticosteroid treatment [96]. Unfortunately there are a number of side effects as a result of corticosteroid treatment, including Cushing's syndrome, short stature, hypertension, hyperglycemia, cataracts and osteoporosis [97]. Therefore, some patients decide to discontinue treatment whilst others modify the treatment regimen to minimise side effects. Patients are also encouraged to undergo physiotherapy in an effort to maintain functionality. It is recommended that they specifically stretch upper extremity muscles to limit contractures and attempt to maintain muscles required to control motorised wheel chairs [97].

Deterioration in respiratory muscles results in respiratory insufficiency and pulmonary hypertension. Mechanical support is thus implemented to maintain adequate ventilation and coughing reflex which is required as

soon as nocturnal hypoventilation is apparent [98]. The preferred respiratory support device is a non-invasive positive-pressure ventilation (NIPPV) machine with a mechanical insufflation-exsufflation device. This allows air to be expelled down the trachea which gradually increases pressure in the airway. This causes a rapid shift to a negative pressure causing deep expiration and allowing the coughing response. This interventative method has reduced mortality in DMD patients [99].

The approaches designed to specifically target cardiac involvement include angiotensin-converting enzyme (ACE) inhibitors, beta-blockers (ß-blockers) and diuretics [100].

ACE inhibitors are generally utilised following a decline in LV systolic function [101]. These inhibitors prevent the conversion of angiotensin-I to angiotensin-II, thus reducing circulating levels of the latter analogue. ACE inhibitors further inhibit kinase-II and increase bradykinin levels. These events reduce peripheral vascular resistance, improve endothelial function and prevent fibrosis and are thus recommended for patients with reduced LV systolic function. ACE administration in DMD patients (EF<55%) resulted in a significant improvement in cardiac function (relative to the pre-therapy results; $p<0.0001$) and delayed the progression of cardiomyopathy [102].

Beta-Blockers interfere with the binding of ß-receptors of the sympathetic nervous system control and act by reducing cardiac norepinephrine and O_2 consumption. They also retain anti-arrhythmic properties. This drug is used for patients with symptomatic, but stable, systolic dysfunction. The co-administration of ACE inhibitors, ß-blockers and diuretics is common practice and significantly improves cardiac function and survival in DMD patients [102, 103]. It should however be noted that metoprolol, a ß-blocker, resulted in deleterious effects on RV function when administered at early stages of cardiac progression [104], and thus demonstrates the importance of regular cardiac assessments.

Another less established technique that may be utilised for DMD patients who are unresponsive to other treatments is cardiac resynchronisation therapy. This method is considered if patients display a low LV EF accompanied by ventricular dyssynchrony (QRS>120ms) [105]. In these cases a bi-ventricular pacemaker, which allows the pacing of the septal and lateral walls of the LV, is surgically installed. A 5 year follow up in a DMD patient that underwent such a procedure exhibited marked improvement in cardiac function, specifically increased LV systolic function, improved LV EF (30% corrected to 45%) and a reduction in LV ED diameter. This study demonstrates the potential of this therapy for patients who do not respond to conventional interventative measures and that exhibit ventricular dyssynchrony.

Prospective Commercially Available Drugs: Pre-clinical studies

There are other commercially available drugs which may benefit patients and have therefore been investigated for their therapeutic potential in animal models of DMD. Poloxamer P188 is a synthetic copolymer which stabilises the sarcolemma and has been shown to improve the cardiac phenotype and even prevent isoproterenol/dobutamine induced cardiomyopathy/death [106, 107]. Sildenafil is a phosphodiesterase 5 (PDE5) inhibitor which enhances nitric oxide-cyclic guanosine monophosphate signalling (NO-cGMP). This signalling process is impaired in *mdx* mice and following administration of Sildenafil resulted in improved contractile performance, cardiac metabolism, sarcolemmal integrity [108] and reversed pathological cardiac dysfunction in *mdx* hearts [109]. It was also capable of improving muscle strength in the diaphragm thereby enhancing respiratory function [110]. Indeed the success of this inhibitor has prompted a human clinical trial in DMD patients (clinicaltrials.gov: NTC01168908). Other drugs, Losartan and Pirfenidone have been investigated for their anti-fibrotic properties as they inhibit TGF-ß expression, thereby reducing fibrosis and improving cardiac pathology and function [111, 112].

All these drugs have demonstrated encouraging results in animal models of DMD and indeed Sildenafil is already undergoing clinical trial for use in patients. These drugs may further present viable combinatory therapies

which may be administered with treatments specifically aimed at correcting/compensating for the dystrophin mutation.

Pre-clinical Therapeutic Approaches for DMD

An array of alternative therapies for the treatment of DMD are being investigated ranging from strategies directed at manipulation of dystrophin gene (aminoglycoside antibiotics), gene therapy (dystrophin splicing and mini dystrophin delivery by adeno-associated viruses-AAV), replacement of muscle fibres (stem cell therapies), and up-regulation of utrophin. Some of these therapies may be applicable to all DMD patients whereas some are mutation/deletion specific and will only be appropriate for a smaller subset of the DMD population. The relative success of each approach varies significantly, and the progress and obstacles encountered whilst developing these therapies will be discussed.

Ribosomal Read Through Therapy

Non-sense mutations in the DMD gene result in a premature stop codon (PTC) in the mRNA transcript, which prohibits the production of dystrophin protein. Ribosomal read-through therapies have been developed to combat these defects and could benefit 13-15% of DMD patients whose dystrophin gene contains PTCs [113]. Aminoglycoside antibiotics were the first compounds to be assessed for their read-through capacity and were shown to operate by binding to ribosomal (r)RNA, thereby causing a conformational change and allowing codon-anticodon pairing [114, 115]. They reduced the ability to distinguish between similar transfer (t)RNAs, allowing amino acids to bind to the stop codon thereby resuming translation. Systemic administration of gentamicin in *mdx* mice resulted in

the production of full length dystrophin and other physiological improvements [116]. Unfortunately, the clinical translation of this antibiotic did not demonstrate sufficient dystrophin production or clinical improvement in patients (2 DMD and 2 BMD patients received 7.5mg/kg gentamicin) [117]. Alternative gentamycin formulations and dosing regimens were also attempted with moderate improvements in dystrophin production or clinical importance [116, 118, 119].

The ribosomal read-through approach did however serve as a basis for further investigative studies in an attempt to identify non-aminoglycoside molecules to restore dystrophin in DMD PTC patients. High-throughput screening assays were employed, which identified PTC124 as a promising candidate [120]. The clinical applicability of PTC124 was initially questioned [121] but the recent publication of the Phase 2a clinical trial has renewed interest in this compound [122]. Patients were divided into 3 dosing cohorts and the drug was taken orally 3 times a day, over a 28 day period. Analysis revealed 61% of patients exhibited dystrophin expression and active plasma concentrations of compound.

Another high-throughput screen, utilising luciferase-independent assays in mice, identified 2 molecules, RTC-13 and RTC-14 with read-through potential [123]. Although *in vivo* application of RTC-14 exhibited poor

results, systemic administration of RTC-13 resulted in dystrophin expression in multiple muscles including the diaphragm and heart.

Another antibiotic, negamycin, was also investigated for its therapeutic potential and was directly compared to the unsuccessful gentamicin compound [124]. Negamycin was able to restore dystrophin in skeletal and cardiac muscle of *mdx* mice, and markedly reduced toxicity compared to gentamicin. More recently negamycin was compared to PTC124 in a transgenic mouse model called READ (read through evaluation and assessment by dual receptor) [125].The negamycin antibiotic was more potent than PTC124 and restored dystrophin and contractile function in *mdx* mice. These promising developments in read-through compounds demonstrate the potential of this technology to treat the subset of patients with PTCs.

Adeno-associated Viral Delivery of Micro/Mini-dystrophin

AAVs present another viable avenue of study with great potential for treating DMD. This approach relies on the delivery of the dystrophin gene which is loaded into an AAV vector. A number of serotypes with muscle tropism have been investigated and include AAV2 [126], AAV6 [127], AAV8 [128-130] and AAV9 [131-133]. Due to the large size of the dystrophin gene and its inability to be packaged into the AAV genome (4.7kb) [134] structure/function studies were performed to identify the

critical protein domains necessary for therapy. Functional, yet truncated mini- and micro-dystrophin constructs were developed that could be packaged into AAVs [135] and were shown to ameliorate the dystrophic phenotype [126, 128, 132]. AAV9 is the most promising vector identified, whereby a single AAV9-microdystrophin administration was capable of transducing the whole heart, in both neonate [132] and 2 month old *mdx* mice [133], with resultant improvement in ECG. It was also shown to improve resistance to dobutamine stress testing in 21 month old *mdx* mice [136]. AAV9 vectors have been explored for their ability to carry antisense oligonucleotide sequences (with U7 small nuclear RNA shuttle). Administration of AAV-U7snRNA revealed improvements in muscle force and dystrophic pathology and dystrophin restoration in the heart [131].

The major downfall regarding AAV administration is the concern regarding cellular and humoral immune response, which has been observed following administration of AAV2 and AAV6 in DMD dog models [126, 127]. One method of evading this issue is to use alternative delivery methods whereby micro-dystrophin/AAV8 vector is delivered via a catheter threaded through the femoral artery (study performed in macaque monkeys). This method resulted in 80% transduction in the targeted muscle (measured 3 months after administration) and exhibited no cellular response [129]. Immunosuppression is another method of safely administering AAV vectors [137].

These vectors are also being investigated for their potential to deliver other target genes that may attenuate the dystrophic phenotype, such as AAV8 to deliver a myostatin propeptide to enhance muscle growth [138], AAV6 for the delivery of micro-utrophin [139], and dominant negative forms of IKKα and IKKβ which reduced NF-kb signalling thereby promoting regeneration of muscle fibres and reducing fibrosis [140]. However there are still concerns regarding this therapy and whether it is clinically viable, as transduction using AAVs in dogs only lasts several months [128] and repeated administration is unfeasible due to the anticipated immunological response.

Cell Based Therapies

The general objective of cell based therapy is to promote muscle regeneration by taking cells from either patients (autologous) or from unaffected donors (allogeneic transfer) and introducing them into the individual to repopulate the muscle, thereby improving muscle function and pathology. Initial studies attempted to achieve this by myoblast transfer. Normal myoblasts were injected (intramuscularly) into *mdx* mice, which resulted in fusion with host muscle fibres and good dystrophin expression in *mdx* muscle [141]. However, when this was conveyed to patient trials, insufficient dystrophin was produced and no improvement in muscle function was observed [142]. Further studies have instilled some hope for this therapy, however poor dystrophin restoration combined with the inability of these cells to migrate long distances hampers the progress

of this method [143]. Since then, stem cells have been utilised due to their substantial self-renewal capacity and ability to differentiate. Muscle satellite cells are the ideal cellular candidate for DMD studies as they are tissue specific stem cells in skeletal muscle that may be triggered to proliferate for both self-renewal and differentiation into myogenic cells [144]. There are other stem cell lineages that have also been investigated due to their myogenic potential and ability to be systemically delivered. These include bone marrow-derived stem cells, mesenchymal cells and mesangioblasts [145, 146].

Studies investigating the utility of bone marrow derived cells revealed their migration to damaged areas, myogenic differentiation and regeneration of damaged fibres [147]. In addition, investigators found a sub-population of bone marrow cells, called side-population cells, which are also incorporated into *mdx* muscle [148]. Mesenchymal cells have been examined as another prospective regenerative population. *In vitro* correction and transplantation of these cells into *mdx* mice revealed high dystrophin positive fibres. These cells continued as satellite cells and therefore contributed to muscle regeneration [149]. CD133+ cells are another progenitor which can differentiate into muscle [150]. This is a promising avenue of research as CD133+ stem cells obtained from DMD patients and corrected *ex vivo* using a lentiviral vector, were successfully transplanted into scid/*mdx* mice [151]. Analysis revealed significant dystrophin expression and improved muscle morphology and function.

Further studies whereby autologous CD133+ stem cells were transplanted into DMD patients, demonstrated safety in phase 1 clinical trials [152].

Mesangioblasts are a blood vessel associated stem cell lineage. A study in cxmd dogs, whereby heterologous or autologous cells were virally transduced and administered, resulted in impressive dystrophin expression (5-70% fibres) and improved phenotype [153]. It should be noted that there was much controversy surrounding this study, particularly with reference to study design and interpretation of the results [154, 155] however it is still a viable and promising approach.

The pluripotency of embryonic stem cells and their ability to differentiate into the 3 germ layers underscores the immense therapeutic potential of this strategy. Indeed these stem cells have been shown to form mesenchymal cells which may be directed to form myotubes [156]. Recently a method of deriving induced pluripotent stem cells from any cell type (i.e. fibroblasts or blood) has been developed and has revolutionised the stem cell field. These stem cells are readily accessible from patients (skin biopsy or blood sampling), and exhibit pluripotency which allows them to differentiate into any cell type and may be easily propagated *in vitro* [157]. Myogenic progenitors may be derived from both embryonic and induced pluripotent stem cells and when transplanted into *mdx* mice provoked widespread dystrophin production [158]. This myogenic

potential, combined with the ability to easily obtain autologous cells, illustrates the capacity of this therapy.

Another cell mediated strategy is to use fibroblasts, which may be induced to form transplantable myoblasts. Fibrosis is prevalent in DMD patients and therefore fibroblasts are abundant. The over expression of MyoD in fibroblasts can cause the myogenic conversion of these cells [159]. These myoblasts may then fuse with existing muscle fibres. However a shortfall of this therapy is that it relies on intramuscular administration and therefore each muscle needs to be treated individually. One theory to counter this issue is systemic gene delivery to transduce fibroblasts *in vivo*. This would allow simultaneous and widespread treatment.

A number of these strategies rely on autologous transplantation/re-introduction and therefore do not negate the fact that dystrophic cells still retain an underlying defect in their genetic code. Therefore this approach will undoubtedly require a combination of gene and cell therapy for success.

Utrophin Up-regulation

Utrophin was first discovered whilst sequencing the dystrophin gene using a cDNA library [160]. A ‘dystrophin-like’ gene was identified which shared 83% homology with the dystrophin gene, of which the most critical component was the C-terminal, which links the DAG to the sarcolemma [160, 161]. Utrophin is expressed in all tissues [162], predominately in skeletal and smooth muscles [163, 164] but is also located at the neuromuscular junction (NMJ) and in glial and Schwann cells. Given the homology of utrophin with dystrophin, the up-regulation of this protein seems a very plausible approach for the treatment of DMD. Indeed higher utrophin levels have been observed in *mdx* mice which might account for the relatively mild phenotype observed in this mouse model [165]. The enormous advantage of utrophin up-regulation is that it is mutation independent and would therefore be applicable to all DMD patients. This approach has demonstrated some success in the *mdx* mouse model [166, 167].

One method of up-regulating utrophin is with the use of small molecules. Through extensive rounds of screening, the pharmaceutical company Summit Plc identified a small molecule, designated SMTC1100, which improved muscle physiology, increasing muscle strength and resistance to exercise induced fatigue [168]. Phase 1 clinical trials were temporarily halted due to low circulating levels of the drug; however in 2012 the drug was reinstated following improvements to the formulation. Summit Plc has

since reported that the treatment was well tolerated with high SMTC1100 plasma levels in patient cohorts (www.summitplc.com).

Another method of up-regulating utrophin is using an artificial zinc finger transcription factor, ‘Jazz’, which drives utrophin transcription [166]. ‘Jazz’ was transgenically induced in the *mdx* mouse model and resulted in improved sarcolemmal integrity and prevention of dystrophic progression [169]. More recently, investigators developed a viral approach whereby the ‘Jazz’ gene was systemically delivered in an AAV8 vector and was found to significantly improve the dystrophic phenotype in *mdx* mice [170].

Whilst utrophin up-regulation as a therapy holds great promise, it should be noted that up-regulation in heart, and therefore its ability to restore heart function, has not been addressed in any of these studies. In addition, utrophin up-regulation in skeletal muscle did not restore localisation of nNOS to the sarcolemma or protect fibres from exercise induced damage [171]. These critical issues highlight the shortfalls of this therapeutic approach.

Antisense Oligonucleotide-mediated exon skipping

Antisense Oligonucleotides

Antisense-oligonucleotides (AOs), one of the most promising approaches for the treatment of DMD [26-28], are short, single stranded DNA analogues, which are complementary in sequence to a specific pre-mRNA splice site. AOs initiate exon skipping through steric blockage of splice enhancers to remove the mutated exons, thereby restoring the reading frame and generating a truncated, but functional, dystrophin protein. In **Fig. 1.5b**, exon 50 is mutated and therefore exon 51 can be skipped by AO intervention to restore the reading frame (**Fig. 1.5c**).

The subsets of DMD patients that AOs can specifically treat include 79% of deletions, 91% of small mutations, and 73% of duplications which amounts to 83% of all DMD mutations [172]. However the downfall of this therapy is that it is mutation specific and only one exon may currently be targeted at a time. It is however noteworthy to add that multi-exon skipping is also being investigated. Current exon skipping efforts are therefore directed at the ‘hot-spots’ of deletions and mutations that would benefit the greatest number of patients; i.e. exons 44-53 and 2-20. Skipping of exon 51 would assist the greatest number of patients (13%) followed by skipping of exon 45 (8.1%), 53 (7.7%) and 44 (6.2%) (**Table 1.1**).

Table 1.1. Top 20 exon-skipping targets ranked according to the percentage of patients the therapy it is applicable to. Adapted from Aartsma-Rus [172]

Ranking	Exon	% All mutations
1	51	13%
2	45	8.1%
3	53	7.7%
4	44	6.2%
5	46	4.3%
6	52	4.1%
7	50	4.0%
8	43	3.8%
9	6&7	3.0%
10	8	2.3%
11	55	2.0%
12	2	1.9%
13	69&70	1.4%
14	19&20	1.1%
15	45&51	1.1%
16	58&59	1.1%
17	17	1.0%
18	7	1.0%
19	65&66	1.0%
20	43&44	0.9%

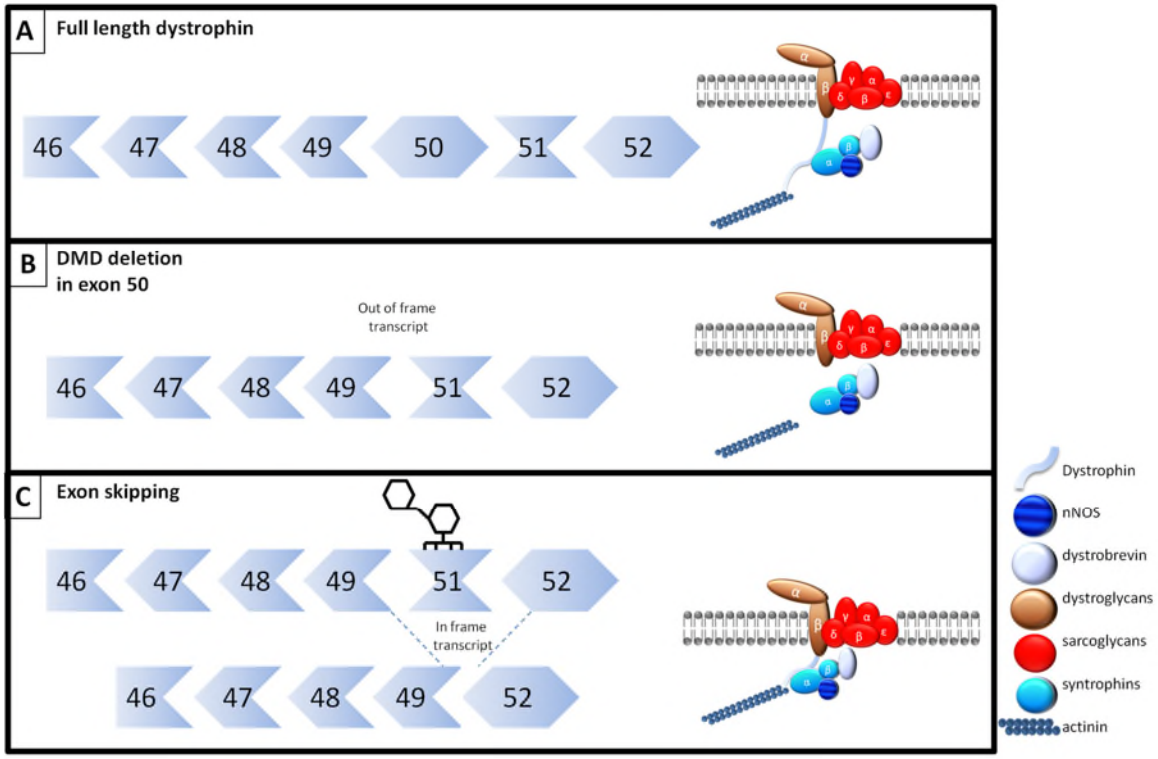

Figure 1.5. Illustration of the dystrophin reading frame in (A) unaffected individuals, (B) Duchenne patients, (C) and in the case of exon skipping. On the right is an illustration of dystrophin in relation to other dystrophin associated proteins in each of these cases. In the unaffected individuals (A), full length dystrophin is produced. However, in the case of a deletion, for example in exon 50 (B), the reading frame is disrupted resulting in an out of frame transcript and a non-functional protein. If an AO, such as a morpholino (PMO) is administered, it enables skipping of the exon (C) from the mature mRNA, resulting in a truncated but functional dystrophin protein[1].

[1] Image was first published in a review by Bentham Science Publishers, May 2013. Licence Number 3405981487254.

Antisense Oligonucelotide Chemistries for DMD

A number of AO chemistries for exon skipping in DMD patients have been investigated including 2'O methyl phosphorothioate (2'OMePS) [173], phosphorodiamidate morpholino oligomers (PMOs) [174], peptide nucleic acids (PNAs) [130], 2'-O-methoxyethyl phosphorothioate(MOE) [175] and locked nucleic acids (LNA) [176, 177]. The 2'OMePS and PMO chemistries have exhibited the greatest potential to date and have both progressed to clinical trial.

2'OMePS are antisense RNA analogues containing a methyl group at the 2'-position of the ribose ring (**Fig. 1.6** [178]). Although anionic, this AO does not assist with free uptake. In fact antisense efficacy is markedly better in neutral and cationic counterparts, such as PMOs and PNA respectively [179]. PMOs are neutrally charged compounds that contain a 6-sided morpholino residue and phosphorodiamidate linkages (**Fig. 1.6** [180]). These AOs exhibit enhanced stability, improved tissue concentration/kinetics and an excellent safety profile [181]. The neutral charge of the AO hinders its ability to enter tissue, however, it is believed that once the PMO has entered the tissue, it maintains a high tissue concentration [182-184].

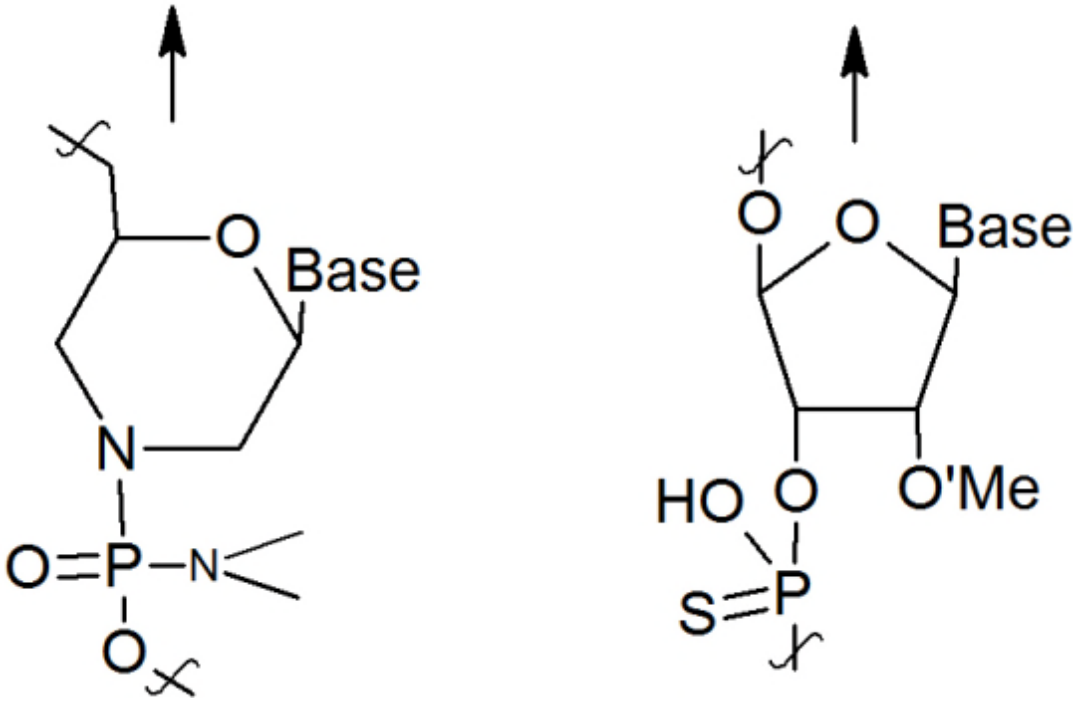

Figure 1.6. Chemical structure of phosphorodiamidate morpholino oligomer and 2'O methyl phosphorothioate oligonucleotides. The phosphorodiamidate morpholino oligomer (left) comprises a 6 sided morpholino residue with phosphorodiamidate linkage. 2'O methyl phosphorothioate (right) comprises a ribose ring with a methyl group at 2' position. These ribose rings are strung together by phosphorothioate linkages. This figure illustrates one residue and linker for each of the oligonucleotides. Usually they are comprised of multiple residues[2].

[2] Image was first published in a review by Bentham Science Publishers, May 2013. Licence Number 3405981487254.

Antisense Oligonucelotide Steric Blocking

AOs exert their effect by interfering with pre-mRNA splicing during the removal of introns for the generation of the mRNA transcript. Small nuclear ribonucleoproteins (snRNPs) and other splicing factors are involved in this process [185]. Generally the snRNPs bind to the target sequence and allow the binding of other snRNPs and splicing factors (**Fig. 1.7a**). Exonic splicing motifs (ESEs) are important exon recognition sites to which serine-arginine (S/R) rich domains bind. These S/R domains in turn interact with protein domains of splicing factors. AOs operate by sterically hindering the S/R-rich protein, thereby preventing the assembly of other splicing factors, and allowing the splicing of the desired exon (**Fig.1.7b**) [186].

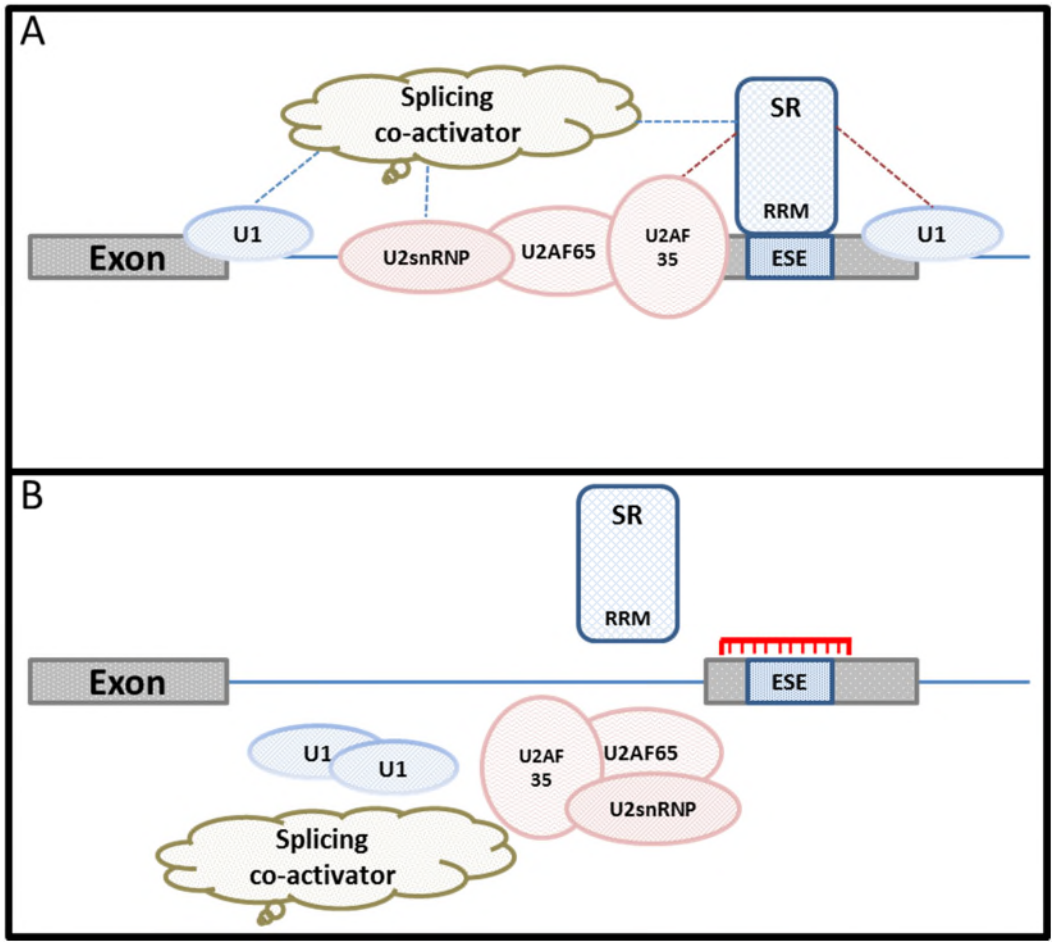

Figure 1.7. pre-mRNA splicing for removal of intronic sequences. (A) Normal pre-mRNA splicing showing binding of serine/arginine (S/R) protein (dark blue) to exonic splicing motifs (ESE) through its RNA-recognition motifs (RRM). This recruits U2 auxiliary factors (U2AF35 and U2AF65-pink) and other small nuclear ribonucleoproteins (snRNPs; U1-blue, U2-pink) and splicing factors (co-activator-green) to the target sequence. (B) Antisense-oligonucleotides (red) sterically blocks the serine/arginine rich region, thereby preventing the assembly of splicing factors (U2AF's, U2snRNP, U1 and splicing co-activators). Adapted from Cartegni [185].

Preclinical and Clinical Trials

Extensive pre-clinical studies in animal models have been pursued in order to assess the efficacy and safety of 2'OMe and PMO AOs prior to administration in human clinical trials. The first proof of principle studies utilising 2'OMePS were performed intramuscularly in *mdx* mice [187] and in the humanised DMD mouse model (hDMD; human *DMD* gene in chromosome 5) [188]. In both cases low levels of dystrophin restoration were observed. Even following regular high doses delivered systemically, this chemistry was only capable of inducing low levels of dystrophin protein; 3 injections of 100mg/kg resulted in 5% dystrophin in skeletal muscle [173]. Similarly, the PMO chemistry also required repeated high doses to produce dystrophin protein [174]. Seven weekly administrations of 100mg/kg PMO restored dystrophin expression in multiple skeletal muscles of the *mdx* mouse (10-50%) with improvements in muscle function and restoration of the DAPC [174]. However, it should be noted that no dystrophin was detected in hearts of treated mice. In fact, the only study whereby naked PMO has restored dystrophin in the heart (less than 2%), required very high doses (60mg/kg) of AO every 2 weeks, which was administered over an entire year [189].

Despite the modest restoration of dystrophin, there was some improvement in motor function [183] which was hoped would be sufficient to attenuate the dystrophic phenotype. Therefore both chemistries, PMO and 2'OMePS, have advanced to clinical trials targeting exon 51 (See

Table 1.2). The PMO chemistry owned by Sarepta (Eteplirsen) exhibits an exceptional toxicity profile whereby preclinical studies in *mdx* mice (highest dose at 960mg/kg) and cynomolgus monkeys (highest dose at 320mg/kg) demonstrated no drug-related effects on survival, body weight or a number of other clinical observations [190, 191]. The trials have progressed well demonstrating excellent safety [192, 193], and in mid-2013 Sarepta released an update of their most recent Phase IIb clinical trial. This study involved 12 boys who received 30 mg/kg, 50 mg/kg or placebo for 24 weeks (n=4) at which stage the placebo group were further divided and included in the treatment regimen [194]. Forty eight weeks post-administration, both doses resulted in significant dystrophin positive fibre expression, greater than 47%. A later assessment following 84 weeks of treatment revealed stable dystrophin expression and stabilisation in the 6 minute walk test (46 meters further then placebo test). Further results from the 120 week assessment confirm the stabilisation of the 6 minute walk test, but also revealed the remarkable stabilisation of pulmonary function (Sarepta press release, February 2014).

A short pharmacokinetic and safety study for the 2'OMe chemistry (Drisapersen) was performed in non-ambulatory boys who received a single-administration for a dose escalation study [195]. It was revealed that 6 mg/kg delivered subcutaneously was the maximal tolerated dose in these patients. Similar to the PMO trial, the 2'OMePS trial was progressing adequately [196], however in August 2013 GlaxoSmithKline revealed that

their randomised Phase III trial involving 186 boys did not meet the 6 minute walk test criteria; 6mg/kg per week over 48 weeks, subcutaneous administration. The boys receiving treatment walked on average an additional 10.33 m which was not significantly different to the placebo group.

Whilst the potential for PMO is still apparent the confounding issue regarding the chemistry is the low systemic restoration of dystrophin in skeletal muscle and the inability of these compounds to restore dystrophin in the heart [173, 174, 182, 183]. Recent literature has further emphasised the importance of restoring the cardiac phenotype in conjunction with correcting the skeletal muscle defect, as the absence of dystrophin in the heart combined with increased locomotor activity resulted in an advanced cardiac pathology [197]. It is therefore imperative that improvements in AO systemic delivery are pursued to ensure a clinically viable treatment for DMD, one that targets skeletal and cardiac muscle.

Table 1.2. Summary of all antisense oligonucleotide clinical trials pertaining to DMD. The table outlines the antisense oligonucleotide used, the clinical trial identifier, targeted exon, dosing regimen and phase of trial. Abbreviations: intramuscular- IM, subcutaneous- SC, intravenous- IV. Adapted from table from Taeyoung Koo

Compound	Clinical Trial Identifier	Targeted Exon Skipping	Dosing Regimen	Status of Trial
2'OMePS	-	Exon 51	0.8mg, single IM	Phase I [198]
2'OMePS	-	Exon 51	0.5, 2, 4 and 6mg/kg, 5 weekly SC; 6mg/kg, 12 weekly SC	Phase I/IIa [196]
2'OMePS	NCT01128855	Exon 51	3, 6, 9 and12mg/kg, 5 weekly SC	Phase I
2'OMePS	NCT01153932	Exon 51	6mg/kg, 48 weekly SC	Phase II
2'OMePS	NCT01462292	Exon 51	3 and 6mg/kg, 24 and 48 weekly SC	Phase II
2'OMePS	NCT01254019	Exon 51	6mg/kg, 48 weekly SC	Phase III
2'OMePS	NCT01480245	Exon 51	6mg/kg, 104 weekly SC	Phase III
2'OMePS	NCT01037309	Exon 44	0.5, 1.5, 5, 8, 10 and 12mg/kg, 5 weekly SC; 8mg/kg, 5 weekly IV	Phase I/IIa
PMO	NCT00159250	Exon 51	0.09 and 0.9mg, single IM	Phase I/II [192]
PMO	NCT00844597	Exon 51	0.5, 1, 2, 4, 10, 20mg/kg, 12 weekly IV	Phase Ib/II [193]
PMO	NCT01396239	Exon 51	30 and 50mg/kg, 24 weekly IV	Phase II
PMO	NCT01540409	Exon 51	30 and 50mg/kg, 80 weekly IV	Phase II
PS	-	Exon 19	0.5mg/kg, 4 weekly IV	Phase I/II [199]

Cell Penetrating Peptides

In an effort to improve delivery and tissue distribution of AOs, cell penetrating peptides (CPPs) as conjugates to these AOs are being assessed. CPPs are short peptide sequences which facilitate the delivery of AOs across the plasma membrane. They were first described in 1994 following the discovery of the homeodomain of Drosophila Antennapedia which was capable of traversing the membrane [200]. In order to determine the properties required for translocation, site-directed mutagenesis of the homeodomain was performed which led to the development of penetratin. Since the discovery of the Antennapedia homeodomain, peptide domains of 2 other proteins, HIV protein derived transactivating regulatory protein (Tat) [201] and Transportan [202], have been extensively investigated. Various derivatives of these peptides have been assessed and their properties exploited for their cargo delivery capacity. They have been shown to improve distribution to tissues, augment elimination half-life and increase tissue uptake and retention [203]. Factors contributing to the efficacy of the peptide include the length [204], charge [205], spacer length between cationic amino acids [204, 206], hydrophobicity [204] and affinity to heparin [204, 207].

Cell penetrating peptides investigated specifically for the treatment of DMD may be classified into two major groups, ‘non-covalent’ and ‘covalent’. The non-covalent class of peptides were derived for anionic AOs such as 2’OMePS, which due to its charge cannot be directly

conjugated to CPPs. Therefore, co-incubation of CPPs and 2'OMePS in certain molar ratios allowed the formation of stable nanoparticle complexes, which efficiently facilitate cellular delivery [208]. All studies focussed on non-covalent CPPs in the DMD field have been performed *in vitro* and therefore *in vivo* validation is still required to fully explore the therapeutic potential of these peptide-AOs. In short, a number of modifications of stearylated TP10 [209] has liberated CPPs capable of inducing high splice correction in an immortalised cell-line attained from *mdx* mouse myotubes, H2K *mdx* cells (PepFect6; [210] and PepFect14; [211]). The vast majority of literature pertains to covalent CPPs, specifically oligo-arginine derivatives, chimeric peptides, and Penetratin derivations. These CPPs are generally covalently linked to the charge neutral AO, PMO, via an amide linker [212, 213] at either the 3' [214] or 5' [215] end of the AO. A summary of CPP studies in DMD models is described in **Table 1.3**.

Table 1.2. Summary of all cell penetrating peptides developed and administered in mouse models of Duchenne muscular dystrophy[3]. TA- *tibialis anterior.*

Treatment	Route	Animal model	Dose	Regimen	Age of mice	Reference
Pip2b (PNA)	IM (TA)	*Mdx*	5ug	Single	6-8 weeks	Ivanova, 2008
TAT (PNA)	IM (TA)	*Mdx*	5ug	Single	2 months, 3 week and 6month	Yin, 2007
MSP (PNA)	IM (TA)	*Mdx*	5, 10 and 25ug	Single	2 months, 3 week and 6month	Yin, 2007
Pip5 series	IM (TA)	*Mdx*	5ug	Single	2 months	Yin, 2011
$(RXR)_4XB$	IP	*Mdx*	1, 2, 5, 10, 25mg/kg	1 dose	Neonates	Fletcher, 2007
$(RXR)_4XB$	IP	*Mdx*	5mg/kg	4 weekly	Neonates	Fletcher, 2007
$(RXR)_4XB$	IV	*Mdx*	25mg/kg	1 dose	6-8 weeks	Yin, 2008
$(RXR)_4XB$	IV	*Mdx*	6mg/kg	3 weekly	6-8 weeks	Yin, 2008
$(RXR)_4XB$	IP	dKO	25mg/kg	6 weekly	10 days	Goyenvalle, 2010
$(RXR)_4XB$	IP	dKO	5mg/kg	6 weekly	10 days	Goyenvalle, 2010
$(RXR)_4XB$	IP	dKO	25mg/kg	6 weeks, then monthly	10 days	Crisp, 2011
Screen of many CPP's; $(RXRRBR)_2XB$	IP	EGFP-654 mouse	12mg/kg	4 daily	7-8 weeks	Jearawiriyapaisarn, 2008
$(RXRRBR)_2XB$	IV	*Mdx*	6mg/kg	3 weekly	6-8 weeks	Yin, 2008
$(RXRRBR)_2XB$	IV retro-orbital	*Mdx*	30mg/kg	1 dose	4-5 weeks	Wu, 2008
$(RXRRBR)_2XB$	IV retro-orbital	*Mdx*	30mg/kg	6 biweekly	4-5 weeks	Wu, 2008
$(RXRRBR)_2XB$	IV retro-orbital	*Mdx*	30mg/kg	2 biweekly	4-5 weeks	Wu, 2008
$(RXRRBR)_2XB$	IV	*Mdx*	12mg/kg	2 cycles: 4 daily, 2 weeks rest	16 weeks	Jearawiriyapaisarn, 2010
$(RXRRBR)_2XB$	IV	*Mdx*	12mg/kg	2 cycles: 4 daily, 2 weeks rest	8 weeks	Jearawiriyapaisarn, 2010
$(RXRRBR)_2XB$	IV	*Mdx*	18.75mg/kg	Single	6 months old	Crisp, 2011
$(RXRRBR)_2XB$	IV	dKO	25mg/kg	23 weekly	10 days	Crisp, 2011
$(RXRRBR)_2XB$	IP	dKO	25mg/kg	23 weekly	10 days	Crisp, 2011
$(RXRRBR)_2XB$	IV	*Mdx*	12.5, 18.75 and 25mg/kg	Single	2 months	Yin, 2011
$(RXRRBR)_2XB$	IV	*Mdx*	18.75mg/kg	Single	6 months	Yin, 2011
MSP	IV	*Mdx*	25mg/kg	Single	6-8 weeks	Yin, 2009
MSP-B	IV	*Mdx*	3mg/kg	6 biweekly	6-8 weeks	Yin, 2009
B-MSP	IV	*Mdx*	3 mg/kg	6 biweekly	6-8 weeks	Yin, 2009
B-MSP	IV	*Mdx*	3 and 6mg/kg	Single, 6 biweekly	6-8 weeks	Yin, 2009
Pip5e	IV	*Mdx*	12.5, 18.75 and 25mg/kg	Single	2 months	Yin, 2011
Pip5e	IV	*Mdx*	18.75mg/kg	Single	6 months	Yin, 2011
Pip6's	IV	*Mdx*	12.5mg/kg	Single	4.5-5.5 months	Betts, 2012

[3] Table was first published in a review by Bentham Science Publishers, May 2013. Licence Number 3405981487254.

Covalently Attached CPPs

Oligo-Arginines

A number of studies have investigated polycationic amino acid chains for their CPP capacity. Serial modifications and optimisations have determined that oligo-arginines with 6-aminoheaxanoic acids (X) and/or β-alanines (B) spacers improved splicing-correction and rendered peptides serum stable [216] [205, 206, 217]. Splice correction was further improved as the number of X residues increased, but this contributed to cellular toxicity.

The $(RXR)_4$ peptide exhibited the best balance of attributes when considering splicing efficiency, serum stability and toxicity as a whole and was the first CPP conjugate to be administered in the *mdx* mouse model. This peptide was administered at a range of doses, at various time-intervals and via different delivery routes (**Table 1.3**). Generally, intraperitoneal (IP) administration resulted in high dystrophin restoration in the diaphragm [218, 219]. Multiple IP administrations produced ~100% dystrophin restoration in this tissue but low levels in skeletal muscles such as the *tibialis anterior*. Administration in the severe dKO (dystrophin-utrophin double knock out) mouse model additionally revealed improvements in mortality rate (usually between 6 and 20 weeks) and correction of deformities such as kyphosis (usually apparent in the dKO mouse model) [220] [221]. Single intravenous (IV) administrations induced

decent dystrophin exon skipping in skeletal muscle and diaphragm and approximately 50% exon skipping in heart [212].

Another comprehensive structure-activity study screening an array of 'RXR' derivatives in a high through-put, splicing reporter mouse model, EGFP-654, identified $(RXRRBR)_2$ peptide (B-peptide) as the lead candidate (**Table 1.3**) [214]. This peptide was deemed to be less effective than its predecessor, $(RXR)_4$, however was chosen based on its less toxic profile [206]. Higher administration of B-PMO delivered IV (retro-orbital route) again illustrated impressive exon skipping results notably in the heart and multiple administrations resulted in further restoration in heart (72%) [213]. Improvements in cardiac function such as resistance to dobutamine stress testing and improvements in end systolic volume (ESV) and EDV were also observed. Another study assessed cardiac function 6 months after the last administration, at which stage dystrophin would have been absent in the heart [214]. However these mice still displayed preserved diastolic function. Remarkably, another study undertaking various treatment and administration regimens resulted in no dystrophin restoration in heart, but still exhibited improvement in cardiac parameters (RV EF and CO restored to wild type levels) [222]. The authors postulated that the improvement in cardiac function in the absence of cardiac dystrophin may have been due to the restoration of dystrophin in the diaphragm which reduced pulmonary hypertension.

Chimeric Peptides

Chimeric peptides exploit the novel concept of conjugating traditional CPPs to ‘tissue specific motifs’ identified from phage display screens to develop an improved peptide [223]. The objective is to utilise the positive attributes of each component, specifically the delivery efficiency of the CPP and the tissue specificity of the phage motif. An example of this class of CPPs is B-MSP-PMO [223]. The phage motif, MSP peptide, revealed enhanced *in vivo* skeletal and cardiac muscle binding capacity [224] and was therefore investigated for its efficacy in DMD mouse models [223, 225].This peptide displayed strong dystrophin positive fibres in focal areas following intramuscular injection [130] and greater dystrophin correction over ‘naked’ PMO following systemic administration [225]. The B- and MSP- motifs were coupled in the configuration ‘B-MSP-PMO’ and revealed 2-5 fold improvement in skeletal muscle restoration compared to B-PMO (Note: no improvement in dystrophin restoration in cardiac muscle).

Another phage motif, T-9 (SKTFNTHPQSTP), was identified for its specificity in *mdx* quadriceps tissue, and exhibited improved specificity over the MSP peptide [226]. This motif requires further investigation but demonstrates an untapped resource whereby we could identify other motifs with heart or brain specificity which are certainly worth pursuing.

PNA/PMO Internalisation Peptide Series (Pips)

The PNA/PMO internalisation peptide (Pip) series was developed in collaboration with the Gait laboratory (Cambridge, MRC). The Pip parent peptide, Penetratin, was derived from the homeobox peptide of Drosophila Antennapedia (residues 43-58) [200, 227]. The addition of 6 arginine residues to the N-terminus of the Penetratin peptide, coined the new term R6-Penetratin (R6-Pen; see **Table 1.4**) [228]. Subsequent modifications were made to the R6-Pen peptide including the addition of a C-terminal cysteine residue and the utilisation of disulphide conjugation methods to develop the 'Pip' series [229]. These peptides conform to the traditional 'Pip' sequence containing a central hydrophobic core, flanked on either side by arginine rich sequences (**Fig 1.8**).

The original Pip peptides, Pip2a and Pip2b, were conjugated to a PNA AO which produced strong exon skipping and dystrophin positive fibres following a single intramuscular injection into the *tibialis anterior* muscle of the *mdx* mouse. Further alterations were made to this sequence and an extensive screen of a new series of peptides, Pip5 (Pip5e-o) now conjugated to PMO, was undertaken [230]. These derivatives retained the hydrophobic core sequence ILFQY, however differed in the composition and length of the flanking regions (see **Table 1.4**). The number of arginine residues ranged between 8 and 10, and the number and sequence of 'X' and 'B' spacer residues also varied in the flanking regions. All Pip5 derivatives were administered intramuscularly (*tibialis anterior* muscle) and

tissues were harvested. Pip5e-, Pip5j-, Pip5l-, and Pip5n-PMO resulted in the greatest number of dystrophin positive fibres. The first 3 Pips were administered IV and Pip5e-PMO was identified as the most efficient peptide-PMO conjugate inducing high levels of exon skipping and dystrophin restoration body wide including in the heart, following a single 25mg/kg IV administration. This peptide was directly compared to the B-PMO sequence and was shown to restore considerably greater dystrophin protein levels in the heart. The Pip5e- peptide forms the central focus of **Chapters 4 and 5** in which the hydrophobic core (ILFQY) is extensively investigated.

Figure 1.8. Schematic illustrating the traditional 'Pip' structure. The peptide comprises a central hydrophobic core, flanked on either side by arginine rich regions.

Table 1.3. Schematic illustrating the derivation of Pip series as it is known today including their sequences.

	Name	Peptide Sequence	Reference
Parent Peptide	Penetratin	RQIKIWFQNRRMKWK	Perez *et al.* and Derossi *et al.*,[200, 227]
First Generation CPP	R6-Pen	RRRRRRR QIKIWFQNRRMKWKKGG	Turner *et al.*, [228]
Second Generation CPP	Pip1	RXRRXRRXR-IKILFQN-RRMKWKK	Ivanonva *et al.*, [229]
	Pip2a	RXRRXRRXR-IdKILFQN-dRRMKWHKB	Ivanonva *et al.*
	Pip2b	RXRRXRRXR-IHILFQN-dRRMKWHKB	Ivanonva *et al.*
Third Generation CPP	Pip5e	RXRRBRRXR-ILFQY-RXRBRXRB	Yin *et al.*, 2011 [230]
	Pip5f	RXRRBRRXR-ILFQY-RXRXRXRB	Yin *et al.*, 2011
	Pip5h	RXRRXR-ILFQY-RXRRXR	Yin *et al.*, 2011
	Pip5j	RBRRXRRBR-ILFQY-RBRXRBRB	Yin *et al.*, 2011
	Pip5k	RBRRXRRBR-ILFQY-RXRBRXRB	Yin *et al.*, 2011
	Pip5l	RBRRXRRBR-ILFQY-RXRRXRB	Yin *et al.*, 2011
	Pip5m	RBRRXRRBR-ILFQY-RXRBRXB	Yin *et al.*, 2011
	Pip5n	RXRRBRRXR-ILFQY-RXRRXRB	Yin *et al.*, 2011
	Pip5o	RXRRBRRXR-ILFQY-RXRBRXB	Yin *et al.*, 2011

Aims of the work in this thesis

The specific aims of this thesis were to:

i. Determine the contribution of the diaphragm and accessory respiratory muscles to heart function in the *mdx* mouse, by restoring dystrophin in the diaphragm and assessing cardiac function using MRI.

ii. Screen a number of Pip5e-PMO derivatives, the 'Pip6' series, with potentially greater capacity to correct cardiac abnormalities over the current lead compound. Multiple techniques to measure dystrophin protein and exon skipping were utilised.

iii. Following the identification of a promising Pip6-PMO candidate, assess whether dystrophin restoration in the heart was capable of improving cardiac function using MRI.

Chapter 2. General Materials and Methods

The experiments were carried out in the Biomedical Sciences Unit, University of Oxford according to procedures authorised by the UK Home Office.

Synthesis of Peptides

Peptides were kindly synthesised by Dr Amer Saleh during his time at MRC LMB, Cambridge. The following excerpt was taken from the Pip6 manuscript (submitted to Molecular Therapy: Nucleic Acids): The PMO sequence (5'-GGCCAAACCTCGGCTTACCTGAAAT-3') was purchased from Gene Tools LLC. Peptides were conjugated to PMO through an amide linkage at the 3' end of the PMO, followed by purification by HPLC and analysed by MALDI-TOF . Peptide-PMO conjugates were dissolved in sterile water and filtered through a 0.22 µm cellulose acetate membrane before use.

Animals and Peptide Administration

C57BL/10 (C57BL/10ScSn, Harlan Laboratories) and *mdx* (C57BL/10ScSn-Dmd^{mdx}/J; Jackson Laboratories- stock number 001801) mice were used for all experiments. Before administrations, peptide-PMO conjugates were allowed to thaw and incubated for 30 minutes at 37^{0}C. Peptide-PMO was further water sonicated for 7 minutes before use and immediately prepared in 0.9% saline solution at the desired dose. The peptide solution was administered IV via the tail vein or IP in *mdx* mice.

Mice were sacrificed by CO_2 inhalation, and blood, muscles and other tissues harvested and snap-frozen in cooled isopentane before storage at -80^{0}C.

Immunohistochemistry and Quantification of Staining

Transverse sections of tissue samples were cut (8 µm thick) using an OTF500 Cryostat (Bright Instuments). Sections were blocked with 20% goat serum and 20% foetal calf serum in PBS for 2 hours. Sections were then co-stained with rabbit-anti-dystrophin (Abcam) and rat anti-laminin (Sigma), which was detected using secondary antibodies goat-anti-rabbit IgG Alexa 594 and goat-anti-rat IgG 488 respectively (Invitrogen). For quantification, 4 representative frames of the dystrophin and correlating laminin fields were taken for each section. Using ImagePro software, 10 regions of interest were randomly placed on the laminin image which was overlaid on the corresponding dystrophin image to attain the minimum and maximum fluorescence intensity for each section. Data were extrapolated and normalised relative to C57BL/10. Values were plotted on a scatter graph. The percentage recovery score was calculated using the following equation: (dystrophin recovery of treated *mdx* mice-dystrophin recovery of untreated *mdx* mice)/(dystrophin recovery of C57BL/10 mice-dystrophin recovery of untreated *mdx* mice); as described on the TREAT-NMD website (http://www.treat-nmd.eu/downloads/file/sops/dmd/*MDX*/DMD_M.1.1_001.pdf). Multi-level

statistics were performed using MlWIN statistics software package to compare multiple treatments at once.

Exon Skipping in mdx Mouse Tissues

Total RNA was extracted using TRIzol reagent (Invitrogen) following manufacturer's instructions. Briefly tissue was homogenised in 1 ml of TRIzol reagent and incubated for 10 minutes. Samples were centrifuged for a further 10 minutes at 12 000 g and supernatant was transferred to a new tube. Two hundred microliters of chloroform was added to each sample, mixed and incubated for 5-10 minutes. Samples were again centrifuged for 15 minutes at 12 000 g. Following centrifugation, the top, clear layer was collected and 500 µl of isopropanol was added, thoroughly mixed and incubated for 10 minutes. Samples were again centrifuged for 10 minutes at 12 000 g. The supernatant was discarded, and the pellet was washed with 1 ml of 70% ethanol. Samples underwent a final centrifuge spin; 5 minutes at 7 500 g. Again the supernatant was removed and the pellets were allowed to air-dry for 5 minutes. Samples were re-suspended in RNAse free water and underwent NanoDrop spectroscopy to measure RNA concentration.

RT-PCR: Four hundred nanograms of RNA template was used in a 50 µl reverse transcription reaction using One Step RT-PCR Kit (QIAGEN) and gene specific primers (see **Table 2.1**). Cycle conditions: 50˚C for 30

minutes, 30 cycles: 30 sec at 94ºC, 1 min at 58ºC, 2 min at 72ºC. Two microlitres of cDNA was amplified in a 50 µl nested PCR (QIAGEN PCR kit). Cycle conditions: 94 °C for 30 seconds, 58 °C for 1 minute, 72 °C for 1 minute for 24 cycles. PCR products were examined by electrophoresis on a 2% agarose gel. Samples were run on a 2% agarose gel and visualised using a Gel Dock System under UV light.

Quantitative real time PCR- Dystrophin: Two micrograms of RNA was reverse transcribed using a High Capacity cDNA Synthesis kit (Applied Biosystems). Exon skipping qPCR was performed using Syber green Kits (Applied Biosystems) and primer (IDT) in RNAse free water and run on the StepOne Plus Real-Time PCR system (Applied Biosystems). For primer sequences, see **Table 2.1.** Plasmids (total dystrophin and delta 23 skipped) were used for the standard curve.

Quantitative real time PCR- TaqMan: One microgram of RNA was reverse transcribed using a High Capacity cDNA Synthesis kit (Applied Biosystems). The cDNA was diluted 1:5 in RNAse free water and qPCR was performed using TaqMan Kits (Applied Biosystems) and primers (IDT) in RNAse free water and run on the StepOne Plus Real-Time PCR system (Applied Biosystems). The CT values from each run were extrapolated, underwent a power calculation (Pfafl conversion) and were further normalised relative to house-keeping genes Cyc1 (diaphragm) or Ywhaz (heart) For Integrated DNA Technologies (IDT) assay codes see **Table 2.2**.

Table 2.1 RT-PCR primers used for detection of dystrophin exon skipping

	Forward	**Reverse**
RT-PCR (Fo 20-26)	CAG AAT TCT GCC AAT TGC TGA G	TTC TTC AGC TTG TGT CAT CC
Nested PCR (Fi 20-26)	CCC AGT CTA CCA CCC TAT CAG AGC	CCT GCC TTT AAG GCT TCC TT
qRT-PCR ex19-20	GCCATAGCACGAGAAAAAGC	GCATTAACACCCTCATTTGC
qRT-PCR delta 23	GCG CTA TCA GGA GAC AAT GAG	GTT TTT ATG TGA TTC TGT AAT TTC CC

Table 2.2 qRT-PCR primers used for markers of disease progression. Gene name and Integrated DNA Technologies (IDT) Assay ID listed

Gene Name	Assay ID
Nppa	Mm.PT.58.8820983
Nox4	Mm.PT.58.12973594.g
Col1a	Mm.PT.58.5206680
Tgfb	Mm.PT.58.11254750
Ywhaz	Mm.PT.39a.22214831
Cyc1	Mm.PT.56a.10623647

Protein Extraction and Western Blot

Samples were homogenised in lysis buffer comprising 75 m*M* Tris-HCl (pH 6.5), 10% Sodium Dodecyl Sulphate and 5% 2-Mercaptoethanol. Lysed tissue was further heated at 100^0C for 3 minutes before centrifugation and removal of supernatant. Dilutions of samples (1/100) were prepared, of which 5 µl was loaded into a clear 96 well ELISA plate (performed in duplicate). An albumin standard curve, ranging between 0.125 and 1 mg/ml was also loaded in duplicate. Two hundred and fifty microliters of Bradford reagent (Sigma) was added to each well and allowed to incubate at room temperature for at least 10 minutes before undergoing caliometric spectroscopy. The concentration of each sample was extrapolated from the albumin standard curve. Between 10-15 µg protein of untreated and treated *mdx* sample, and between 5% and 50% C57BL/10 protein (positive control) was loaded onto a 3-8% NuPage Tris-Acetate gel (Invitrogen). Proteins were transferred onto PVDF membrane and further probed for dystrophin using DYS1 (Novocastra) and loading control, α-actinin (Sigma) or vinculin (Sigma) antibodies. Primary antibodies were detected using IRDye 800CW goat-anti mouse IgG (Licor). Western blots were imaged (LiCOR Biosciences) and quantified using the Odyssey imaging system.

Exercise Regimens

Two studies (**Chapter 3 and 5**) required exercise regimens that differed in frequency and duration. The Exer 3/6 treadmill (Columbus Instruments,

USA) was used to exercise these mice cohorts. Both protocols required adaption periods in order for the matched C57BL/10 and *mdx* mice to deal with the increase in work load. Thus they were initially allowed 2 minutes for familiarisation and the exercise regimen started at 5 m/min and was gradually increased in 1 m/min increments until the desired speed was attained. Generally mice exercised at 12 m/min for 45 minutes on each exercise session. Electric shock was not used for these studies as it was imperative that all mice ran for the same interim. If the electric shock system had been utilised, mice would have to have been removed from the exercise protocol after 2-3 shocks due to welfare issues (and as described in Animal Project Licence). Mice, particularly *mdx*, still required encouragement and therefore inflated gloves were placed in the electric shock area. Alternatively, a wooden paddle was used to gently encourage mice back onto the treadmill. Mice were monitored closely to ensure the welfare of the animals maintained.

Cardiac Cine-MRI

Mice were anaesthetised with isoflurane and placed in the supine position in a purpose-built cradle. Pins attached to the ECG electrodes were placed under the skin of the forepaws of the mouse and the respiration loop was taped across the abdomen (see **Fig 2.1**). Once the mouse was adequately secured, the cradle was lowered into a vertical-bore, 11.7T MR system (Magnex Scientific, Oxon, UK) with a 40 mm birdcage coil (Rapid Biomedical, Wurzburg, Germany; **Fig 2.1**). Images were acquired using a Bruker console running Paravision 2.1.1 (Bruker Medical, Ettlingen,

Germany; **Fig 2.1**). A 4 slice axial scan was run to locate the heart of the mouse within the magnet. A series of long-axis and short-axis scans were performed to ensure scans were taken in the correct orientation. Sort axis scans of the entire left and right ventricles were imaged by taking consecutive stacks of cine images in 1 mm thick increments. Additional parameters: Field of view: 25.6 X 25.6 mm, number of images per cardiac cycle: 20-30.

Figure 2.1. Figure illustrating the MRI procedure. Mice were anaesthetised and placed on their backs in a purpose built cradle (left). Electrocardiogram (ECG) leads were inserted under the skin of the paws (green leads) and the respiratory loop (yellow lead) was taped over the abdomen. The cradle was then inserted vertically into the 11.7T MR system (middle and right top). Mice were imaged using a Bruker console running Paravision 2.1.1 (right bottom).

MRI Analysis

Images were analysed using ImageJ software (NIH Image, Bethesda, MD) as previously described [73]. The epicardial and endocardial borders were drawn using the ImageJ free-hand tool at end-diastole and end systole (**Fig 2.2**) to calculate the LV mass, LV and RV end-diastolic (EDV) and end-systolic lumen volumes (ESV). These measurements assisted in calculating various other parameters such as SV, EF and CO. The SV is the volume of blood pumped out of a ventricle after each heartbeat (Equation 1), whereas the EF is the volumetric fraction of blood pumped out of each ventricle after each heartbeat (Equation 2). Cardiac output is the volume of blood pumped out of each ventricle per minute and therefore varies with heart rate (Equation 3):

Equation1: $SV = EDV - ESV$

Equation 2: $EF = \frac{SV}{EDV} \times 100\%$

Equation 3: $CO = SV \times HR$

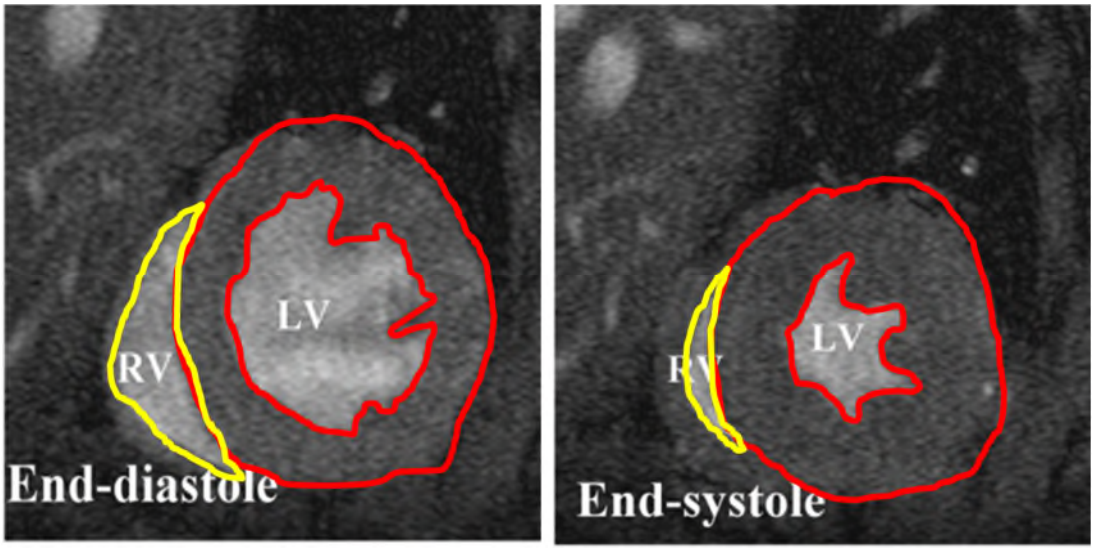

Figure 2.2. Cardiac parameters calculated using Image J software. The epicardial and endocardial borders of the left ventricle (LV, red) and right ventricle (RV, yellow) were drawn using the ImageJ free-hand tool at end-diastole and end systole. This allowed the calculation of LV mass and LV and RV end-diastolic (EDV) and end-systolic lumen volumes (ESV), which facilitates the calculation of stroke volume, ejection fraction and cardiac output (combined with heart rate).

Evans Blue Dye Infiltration

Mice were injected IP with 1% Evans blue dye (EBD; 10 µl/gram of mouse; Sigma) and *tibialis anterior*, diaphragm and heart tissues were harvested 20 hours later [231]. Tissues were cryosectioned (8 µm), soaked in acetone for 10 minutes, rinsed with PBS and mounted. The entire section was imaged using a Leitz DM RBE fluorescent microscope (Leica) and Axiovision Rel 4.7 Software (Zeiss). Images were manually reassembled and the surface area of EBD staining was calculated using the threshold function of ImageJ software.

Masson's Trichrome Staining

Heart tissues were cryosectioned (8 µm) and sent to the William Dunn School of Pathology lab, Oxford, for staining by Mr Richard Stillion. For the quantification of collagen in tissues, images of the entire section were taken and the percentage surface area of collagen deposition/trichrome staining was quantified using ImageJ threshold values.

Clinical Biochemistry

Plasma samples were extracted from the jugular vein of *mdx* mice immediately after sacrifice by CO_2 inhalation and centrifuged at 2 000 g for 5 minutes. The top, clear plasma layer was collected and stored at -80^{0}C until required. Analysis of liver and kidney toxicity and muscle damage was performed by the Mary Lyon Centre Clinical Pathology Lab, MRC,

Harwell, UK. These included alanine aminotransferase (ALT), aspartate aminotransferase (AST), blood urea nitrogen (BUN), albumin, bilirubin, CK and lactate dehydrogenase.

Statistical Analysis

All values, with the exception of immunohistochemical staining quantification, were reported as mean ± standard error of the mean (SEM). All statistically significant values were determined using a One-way ANOVA followed by a Tukey post-hoc test. For MRI analysis, Games-Howell Post-Hoc Test was also performed to correct for variance heterogeneity. Two-way ANOVAs were also performed on MRI data to determine interactions between exercise and mouse cohorts.

Chapter 3. Specific rescue of dystrophin in diaphragm does not restore cardiac function

Introduction

The importance of dystrophin in respiratory function

Respiratory muscle weakness is prominent in DMD patients from about 10-14 years of age. The majority of patients die from complications associated with the respiratory muscle weakness, including progressive restrictive ventilation defects, chronic hypoventilation and pulmonary infections [52]. Impaired respiration has a knock-on effect on cardiac function as it reduces pulmonary pressure, thus contributing to RV failure [54]. Improvements in palliative care, particularly the use of corticosteroids and ventilatory support, have reduced morbidity in DMD patients.

As the pathological development in DMD patients is due specifically to the absence of dystrophin, it is clear that the presence of this protein in diaphragm and accessory respiratory muscles (intercostal and sternomastoid muscles) is integral to prevent disease progression. Indeed gradual deterioration and fibrotic accretion in the diaphragm correlates closely with the decline in respiratory function [232]. The diaphragm, external intercostals and sternomastoid muscles are required for the process of inspiration, the internal intercostals and abdominal muscles are involved in expiration [233]. Generally when inspiratory weakness ensues, patients increase respiration frequency to maintain adequate ventilation.

However as respiratory weakness progresses, patients hypoventilate which increases blood CO_2 and decreases O_2. Weakness of expiratory muscles results in the inability to cough, which contributes to pulmonary infections. This demonstrates the importance of the diaphragm and accessory respiratory muscles (intercostal and sternomastoid muscles) on cardiorespiratory function.

AO restoration of dystrophin in the diaphragm

The restoration of dystrophin in all muscle groups would be ideal for the treatment of DMD; however this presents a major challenge. AOs and their exon skipping capacity to restore the dystrophin reading frame, and produce a truncated dystrophin protein, are actively being investigated for their therapeutic potential. However, AOs, such as PMO and 2'OMe, have limited restorative capacity due to moderate dystrophin restoration in skeletal muscles and no restoration of dystrophin protein in cardiac muscle [173, 174, 182, 183].

As discussed (**Chapter 1: Cell Penetrating Peptides**) peptide-conjugated AOs are considered a promising therapy for the treatment of DMD due to their capacity to improve delivery and tissue distribution of AOs. Multiple [222] or high doses [213] of a CPP, called B-PMO, the $(RXRRBR)_2$ peptide conjugated to PMO, is capable of restoring dystrophin in the heart.

Penetratin-derived Pip's, which have been developed by the Gait and Wood labs, also demonstrate cardiac dystrophin restoration [230, 234].

However, setting this encouraging progress aside for now, it is important to assess whether restoring dystrophin in the major respiratory muscle, the diaphragm, may improve cardiorespiratory function to an extent that would negate the requirement of dystrophin in heart. There is some encouraging evidence that the restoration of dystrophin in the diaphragm of mouse models of DMD has a profound beneficial effect on pulmonary [70] and cardiac function [222]. However, neither of these studies revealed the full story. The study on pulmonary function specifically restored dystrophin in the diaphragms of *mdx* mice, but did not assess cardiac function [70]. In contrast the study that assessed cardiac function employed a systemic delivery approach and therefore dystrophin was present in multiple skeletal muscles and not just the diaphragm [222]. It is therefore important to assess cardiac function in a model in which dystrophin is restored in the diaphragm alone.

Increased activity in *mdx* mice aggravates cardiomyopathy

Another important investigative avenue to consider is the consequence of increased locomotor activity on the dystrophic heart and cardiac function. Young untreated *mdx* mice allowed voluntary exercise exhibited significantly enlarged ventricles and thinner lateral ventricular walls of the

heart than sedentary *mdx* mice [235]. Twenty percent of these mice also had fibrotic lesions in the left ventricular myocardium, which usually only manifests in *mdx* mice older than 40 weeks of age. Although this study did not assess cardiac function, it is possible that these dramatic remodelling events in the heart would have had a profound effect on cardiac function.

Rationale for study

Respiratory function has a fundamental impact on cardiac function in the *mdx* mouse. It has been postulated that the major respiratory muscle, the diaphragm, may be sufficient to improve lung capacity thereby having a beneficial effect on cardiorespiratory function. It was therefore important to assess what impact restoration of dystrophin in the diaphragm has on cardiac function.

An increase in locomotor activity has a detrimental effect on cardiac histopathology in untreated *mdx* mice. As functional improvement of the diaphragm improves inspiratory lung function, this muscle alone may be sufficient to deal with the increased ventilatory response incurred in the event of exercise. This raises the question as to whether dystrophin restoration in the diaphragm is sufficient to stabilise or improve cardiac function in the absence of dystrophin in the heart.

In order to understand the impact of diaphragmatic dystrophin restoration on cardiac function and to assess the beneficial effects in the event of exercise, *mdx* mice were treated with B-PMO and underwent MRI to assess cardiac function. B-PMO readily restores dystrophin in skeletal muscle [222] and preliminary studies have shown that IP administration predominantly restores dystrophin in the diaphragm. Consequently, B-PMO was chosen for this study. In addition, a regular, but short-term, exercise regimen was developed to use within the treatment protocol.

Synopsis of findings

A number of right ventricle cardiac function parameters had deteriorated in the untreated *mdx* mice compared to C57BL/10 controls, changes that were amplified with exercised. Administration of B-PMO resulted in substantial dystrophin restoration in the diaphragm and negligible dystrophin restoration in peripheral muscles, such as *tibialis anterior* and accessory respiratory muscles. Restoration of dystrophin in the diaphragm did not improve cardiac function, which was significantly worse in the B-PMO treated mice than the C57BL/10 mice, with or without exercise. The pathology of the diaphragm, however, had improved as observed by Masson's trichrome and EBD uptake. These results indicate that restoration of dystrophin in the diaphragm alone was insufficient to correct cardiac function, whether or not mice were exercised.

Methodology

Six cohorts were studied, all utilising male mice; untreated unexercised *mdx* (*mdx*^{unex}; n=10), untreated exercised *mdx* (*mdx*^{ex}; n=10), C57BL0 unexercised (C57BL/10$^{unex;}$ n=10), C57BL/10 exercised (C57BL/10^{ex}; n=10), B-PMO treated unexercised *mdx* (B-PMO^{unex}; n=10) and B-PMO treated exercised *mdx* mice (B-PMO^{ex}; n=10). Mice underwent MRI at 24 weeks of age, and the exercise regimen took 3 weeks. Mice were exercised every second day (10 exercise bouts in total, **Fig. 3.1**. top). Treatment was administered prior to the exercise regimen and so the treated cohorts received a single, IP administration of 19 mg/kg B-PMO prepared in 0.9% saline solution at 21 weeks of age (**Fig. 3.1**, bottom). For the treated cohort, exercise commenced 1 day after IP administration. The exercise regimen was performed as follows: mice were allowed 2 minutes for familiarisation, then for the first 2 exercise days, mice were run at a speed of 5 m/min which was increased in 1 m/min increments to 12 m/min over a 45 minute period. The speed was maintained between 10 and 12 m/min for the following 2 exercise sessions, and the remaining sessions (6 bouts) sustained a speed of 12 m/min for the full 45 minute exercise period. All mice underwent cardiac cine-MRI at 24 weeks of age. Following MRI, mice were sacrificed by CO_2 inhalation, and tissues harvested and snap-frozen in dry-ice cooled isopentane before storage at -80^{0}C. Three to 4 mice from each cohort were injected IP with 1% EBD (10 µl/gram of mouse) and tissues harvested 20 hours later.

Tissues including the diaphragm, heart, *tibialis anterior*, intercostal and sternomastoid muscles were processed and analysed for the presence of dystrophin using standardised techniques; immunohistochemical staining, RT-PCR and western blot. The expression of cardiac injury and oxidative stress markers were assessed by qRT-PCR. Heart and diaphragm samples were cryosectioned and stained with Masson's trichrome to assess the deposition of collagen/fibrosis. Tissues from EBD-injected mice were cryosectioned, washed and mounted. Sequential images of the section were taken at 10x magnification and manually reconstructed using Adobe Photoshop CS5, so that a consolidated image of the entire section could be viewed. The surface area of EBD leakage was quantified relative to the total surface area of the section using ImageJ.

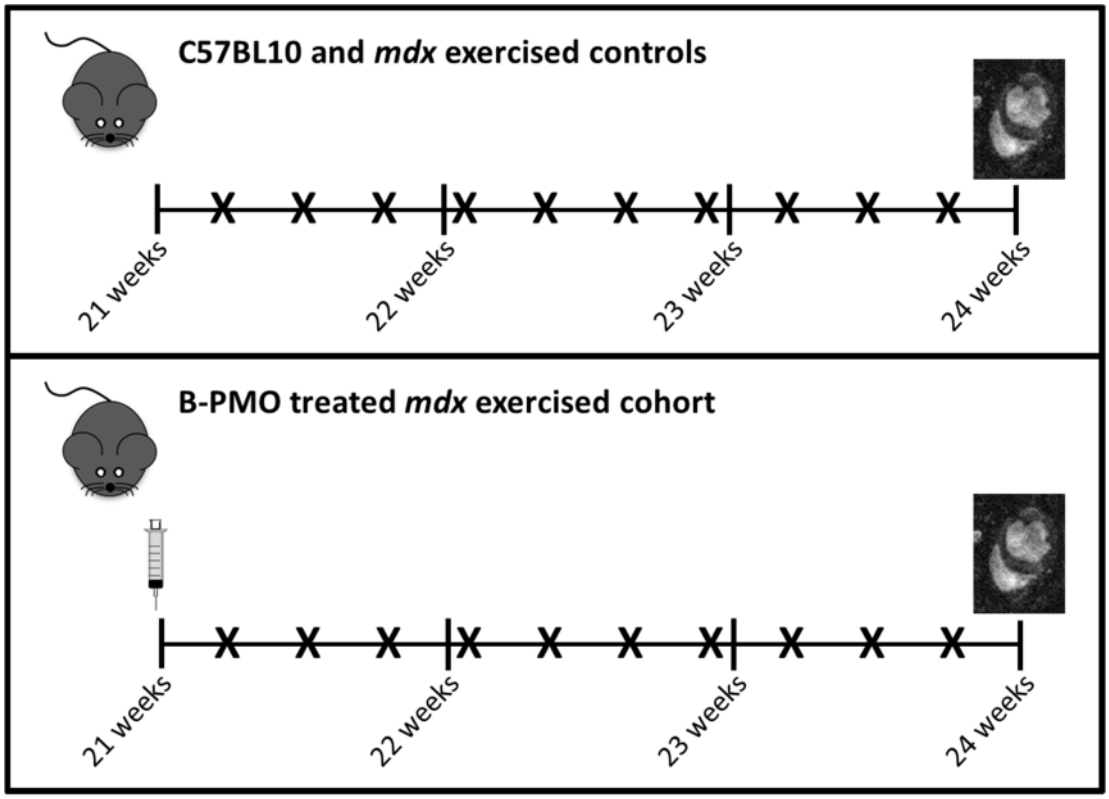

Figure 3.1. Schematic illustrating the B-PMO administration and exercise regimens used in this chapter. The exercise regime for the *mdx* and C57BL/10 cohorts (top) commenced at 21 weeks of age and continued for 3 weeks; 45 minutes exercise every 2 days. At 21 weeks of age the treated cohorts received a single intraperitoneal administration of 19 mg/kg B-PMO. All mice underwent cine-MRI at 24 weeks of age. X symbolises exercise bouts, image of syringe symbolises administration of B-PMO.

Results

Treatment with B-PMO restored high levels of dystrophin in the diaphragm of *mdx* mice

To assess whether dystrophin was restored in the diaphragm following the single IP administration of B-PMO, routine dystrophin splicing and protein restoration techniques, namely immunohistochemical staining, RT-PCR and western blotting were performed. Additional tissues assessed for the presence of dystrophin included the heart, *tibialis anterior* and accessory respiratory muscles, the intercostal muscles and sternomastoid muscles. Immunohistochemical staining for dystrophin protein in the B-PMO treated mice revealed widespread and high level expression in the diaphragm 3 weeks after administration (**Fig 3.2**). This was confirmed by quantification relative to a laminin counter stain (**Fig. 3.3**) and the percentage recovery scores (%RS) were calculated. The recovery score is a method of expressing the effect of a treatment by calculating the difference between the treated *mdx* and untreated *mdx* relative to the difference between the C57BL/10 and untreated *mdx* mice (see **Chapter 2: Immunohistochemistry and Quantification**). This gives an indication as to how much dystrophin was restored in the treated mice. The %RS for the diaphragm was approximately 100% (**Fig. 3.3**). Dystrophin expression in the *tibialis anterior* (%RS- 0-2%), intercostal (%RS- 12-14%) and sternomastoid muscles (0-6%) was very low and dystrophin protein recovery was completely absent in the heart (**Fig. 3.3**).

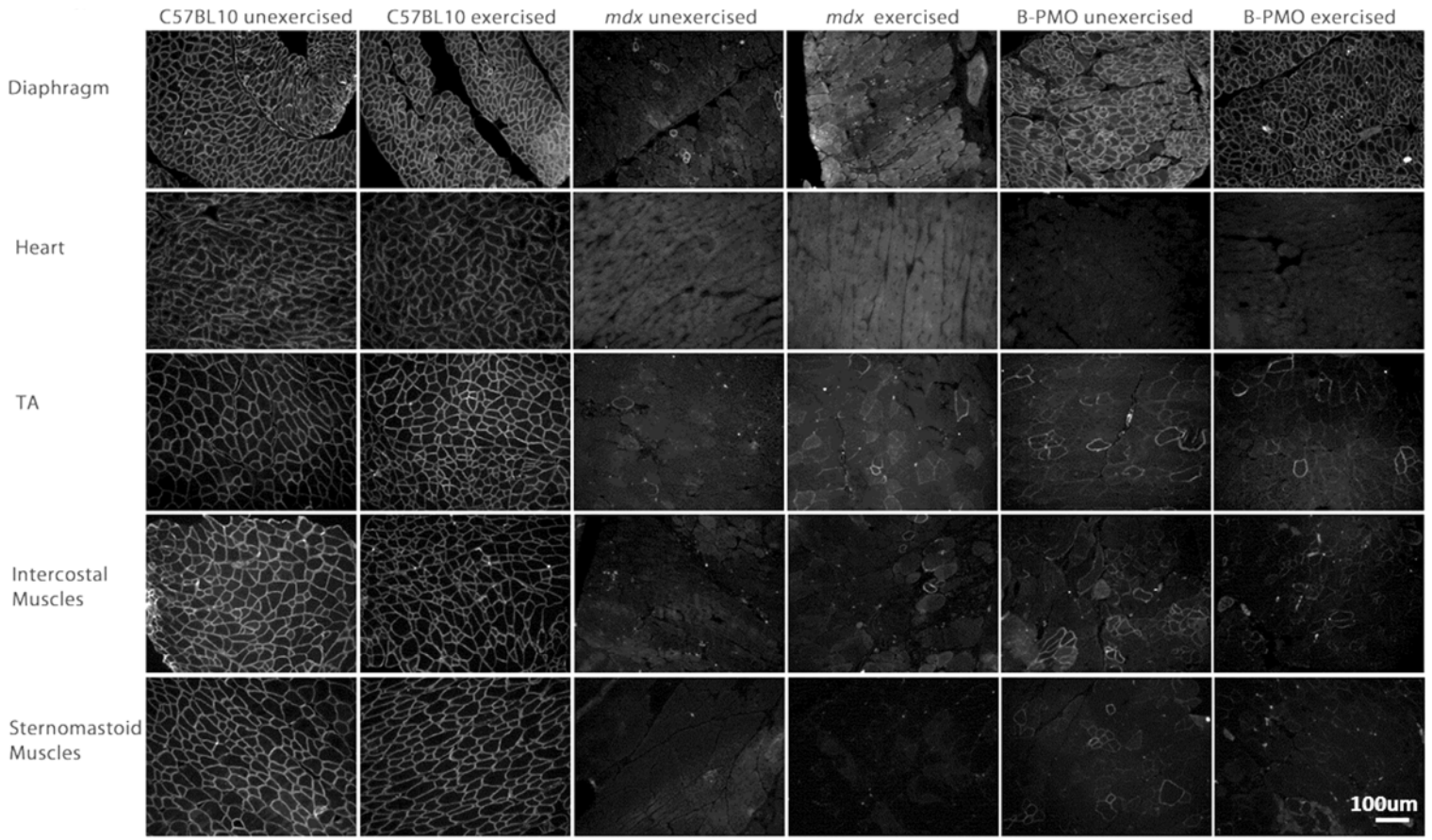

Figure 3.2. Immunohistochemical staining of dystrophin following B-PMO treatment. Dystrophin immunohistochemical staining of dystrophin protein in exercised and unexercised C57BL/10, *mdx* and B-PMO treated *mdx* mice showing the diaphragm, heart, *tibialis anterior*, intercostal and sternomastoid muscles. Tissues were harvested 3 weeks after B-PMO administration. Scale bar: 100 µm.

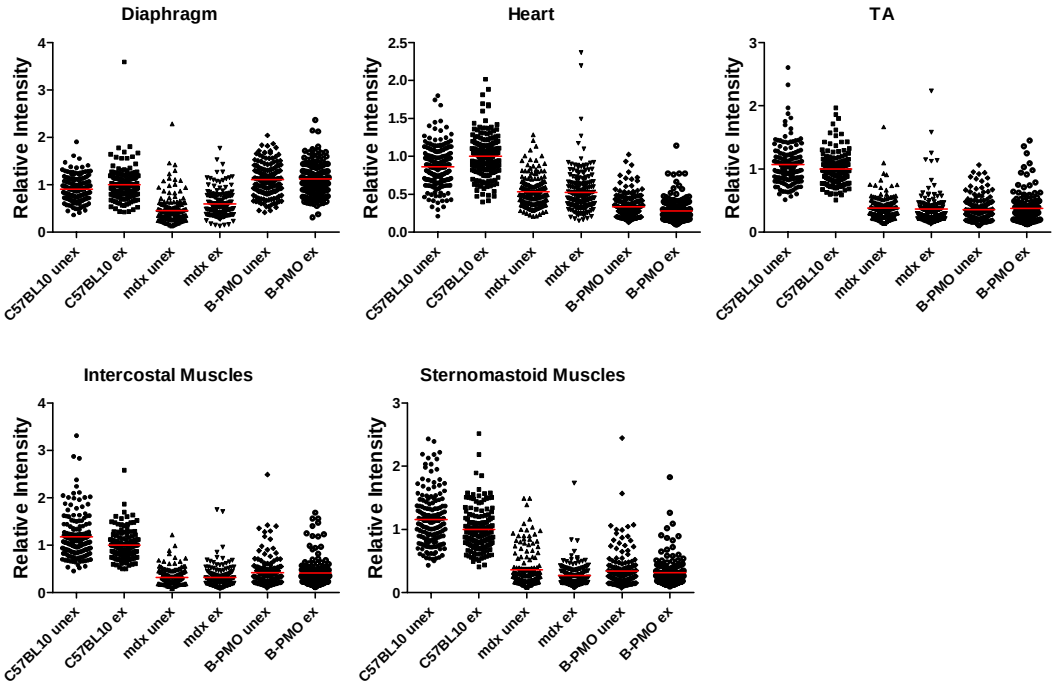

Figure 3.3. Immunohistochemical staining quantification of dystrophin following B-PMO treatment. Dystrophin immunohistochemical staining quantification of dystrophin protein in exercised and unexercised C57BL/10, *mdx* and B-PMO treated *mdx* mice in the diaphragm, heart, *tibialis anterior*, intercostal and sternomastoid muscles. Dystrophin expression was calculated relative to laminin co-stain for diaphragm, heart, *tibialis anterior*, intercostal and sternomastoid muscle. Quantification used 120 regions of interest; the intensity value of dystrophin relative to the corresponding intensity value of laminin, normalised to C57BL/10 unexercised. The box plots show the normalised relative intensity values for each region of interest. N=4 for each cohort.

These data were complemented by the RT-PCR and western blot results. The RT-PCR results displayed complete Δ23 splicing of the dystrophin transcript in diaphragm tissue of treated cohorts (**Fig. 3.4**), and the western blot data showed 41% and 17% dystrophin protein restoration in the B-PMO^{unex} and B-PMO^{ex} groups respectively (**Fig. 3.5**). The disparity in dystrophin protein restoration in the diaphragms of B-PMO^{unex} and B-PMO^{ex} ($p < 0.05$) may have been due to mechanical damage induced by the exercise regimen, which increased turnover of dystrophin in the B-PMO^{ex} group (therefore less dystrophin remaining). Δ23 splicing was relatively low in other tissues, and dystrophin protein restoration was approximately 1% in the *tibialis anterior* and sternomastoid, and 4% in intercostal muscles. Exon skipping and protein restoration was absent in the hearts of B-PMO treated cohorts.

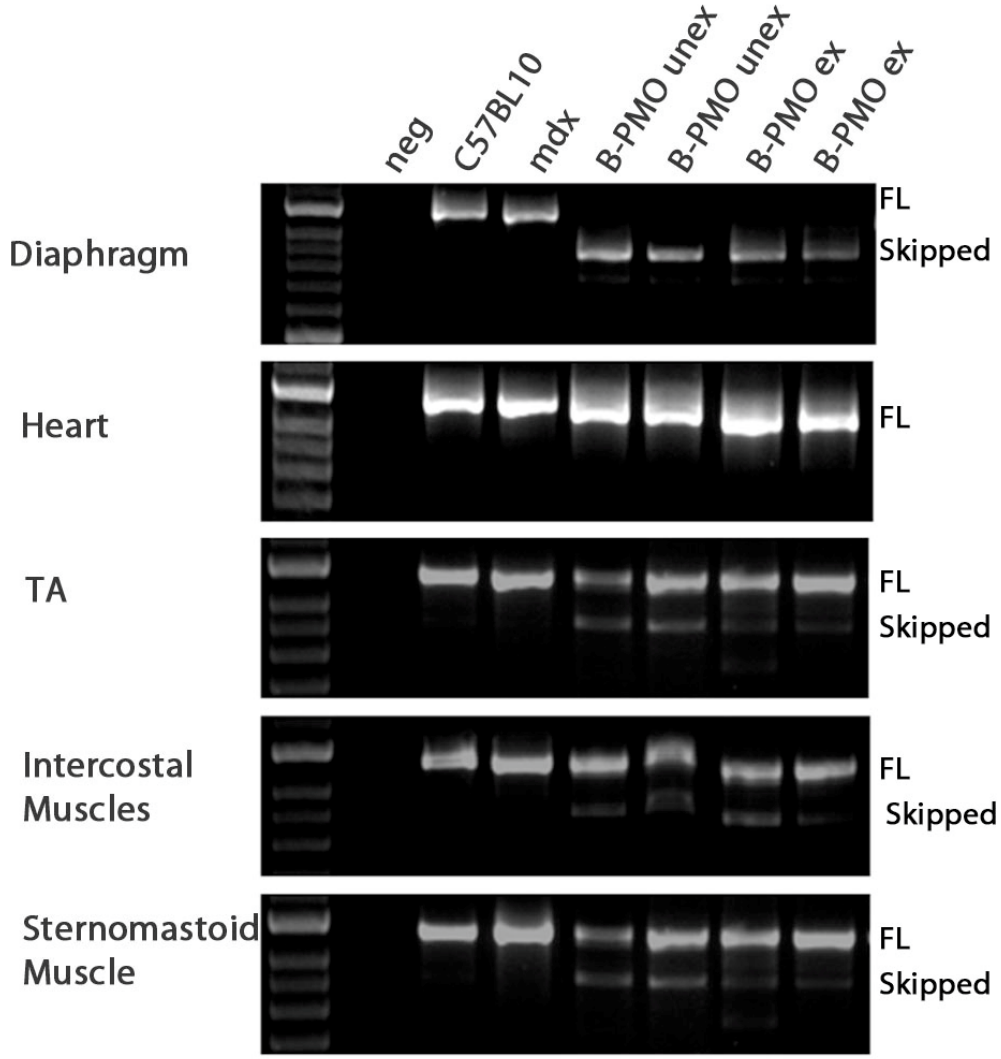

Figure 3.4. Dystrophin splicing in B-PMO treated mice compared to *mdx* untreated and C57BL/10 control groups. Representative images of reverse-transcriptase (RT) PCR illustrating Δ23 splicing in diaphragm, heart, *tibialis anterior*, intercostal and sternomastoid muscles of B-PMO treated cohort. The top band represents full length dystrophin (FL) and the lower band represents the skipped transcript (Skipped). Figure shows complete splicing of Δ23 transcript for diaphragm, and low levels of skipping for *tibialis anterior*, intercostal and sternomastoid muscles. No splicing present in heart samples. N=4 for each cohort.

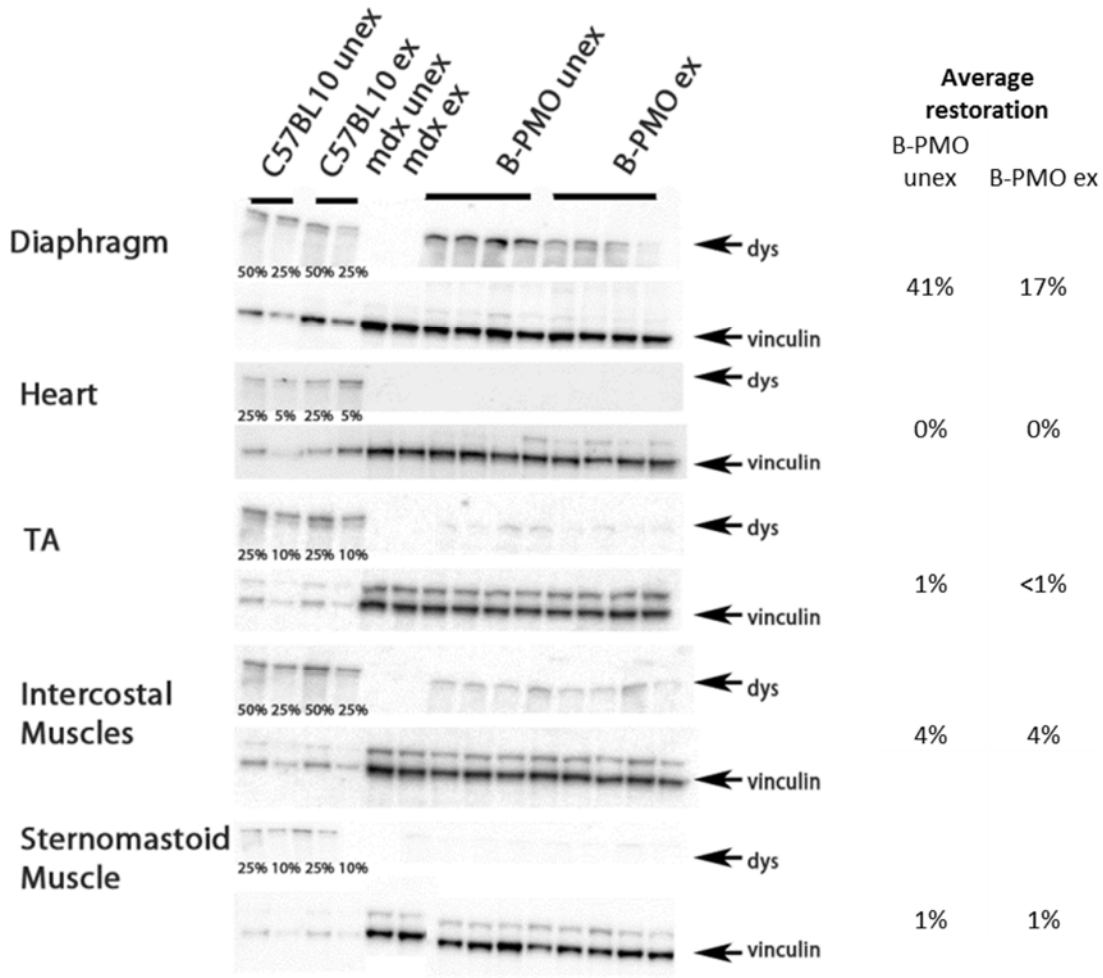

Figure 3.5. Dystrophin protein restoration in B-PMO treated mice compared to *mdx* untreated and C57BL/10 control groups. Representative images of western blots splicing in diaphragm, heart, *tibialis anterior*, intercostal and sternomastoid muscles of B-PMO treated mice. Ten-15 µg of protein was loaded and quantified relative to vinculin loading control. Average dystrophin restoration levels in treated mice shown relative to C57BL/10 exercised and unexercised cohorts shown on right. N=4 for each cohort.

Restoration of dystrophin in diaphragm did not restore cardiac function

Cardiac function of the unexercised *mdx* and B-PMO treated cohorts were compared with their C57BL/10 counterpart. All cardiac parameters were normalised to weight (with the exception of the EF which is presented as a percentage and is independent of weight). The *mdx*^{unex} cohort revealed lower LV CO function and a number of RV changes relative to C57BL/10^{unex} mice (**Fig. 3.6**). Regarding the right ventricle, SV was lowered, with subsequent reduction in EF and CO suggesting impaired contractility and efficiency. Similarly, the B-PMO^{unex} cohort revealed a lower left ventricle SV and CO relative to C57BL/10^{unex} mice (**Fig. 3.6**). Again, changes in multiple right ventricle parameters were observed in the B-PMO^{unex} group relative to C57BL/10^{unex} (**Fig. 3.6 and Table 3.1**). These findings indicate that significant restoration of dystrophin protein in the diaphragm (B-PMO^{unex} mice) did not improve cardiac function.

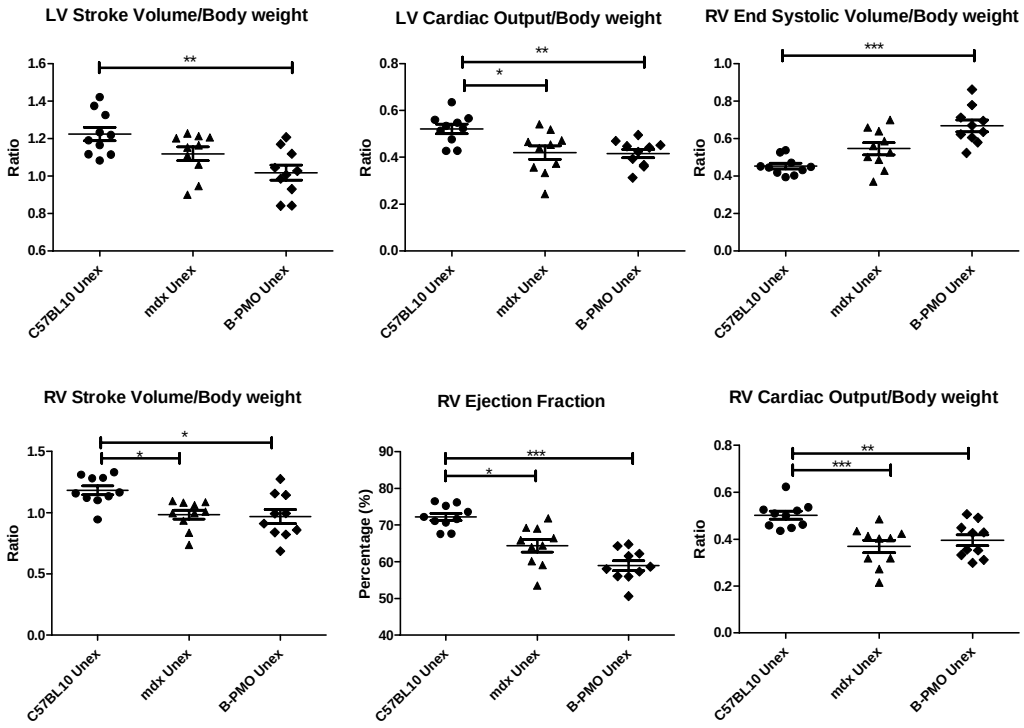

Figure 3.6.Cardiac function parameters measured by cine-MRI in unexercised *mdx* mouse cohorts. Scatter plot graphs illustrating individual mouse values, mean and standard error of the mean (SEM) for left ventricular (LV) and right ventricular (RV) functional parameters relative to body weight. Note: The exception to this was the ejection fraction which was represented as a percentage. B-PMO^{unex} and *mdx*^{unex} cohorts exhibited worse cardiac function then C57BL/10^{unex} mice. Statistical significance was determined using ANOVA followed by Tukey Post-Hoc Test or Games-Howell Post-Hoc Test to correct for variance heterogeneity. (*=p<0.001, **=p<0.01*=p<0.05). N=10 for each cohort.**

Table 3.1. Cardiac function parameters measured by cine-MRI for *mdx,* C57BL/10 and B-PMO treated cohorts. All parameters are presented relative to body weight (BW). Note: The exceptions to this were the ejection fraction which is represented as a percentage and heart rate calculated as beats per minute (BPM). Weights are in grams. Statistical significance was determined using ANOVA followed by Tukey Post-Hoc Test (^{TU}ANOVA). Games-Howell Post-Hoc Test was also performed to correct for variance heterogeneity (^{GH}ANOVA). Each cohort is compared to all other cohorts. * significantly different to C57^{unex}, + significantly different to *mdx*^{unex}, Δ significantly different to B-PMO^{unex}, □ significantly different to C57^{ex}, o significantly different to *mdx*^{ex} and x significantly different to B-PMO^{ex}. Number of symbols denotes significance i.e. ***=p<0.001, **=p<0.01*=p<0.05. N= 10 for each cohort.

	C57 ^{unex}		SEM	*mdx* ^{unex}		SEM	B-PMO ^{unex}		SEM	C57 ^{ex}		SEM	*mdx* ^{ex}		SEM	B-PMO ^{ex}		SEM
Average Mass ^{GH}	3.75	±	0.2	3.43	±	0.08	3.26	±	0.09	4.04	±	0.3	3.60	±	0.1	3.37	±	0.09
End Diastolic Volume^{TU}	1.96	±	0.1	1.77	±	0.05	1.74	±	0.06	2.03	±	0.2	1.80	±	0.1	1.81	±	0.08
End Systolic Volume^{TU}	0.74	±	0.1	0.65	±	0.08	0.72	±	0.03	0.74	±	0.2	0.87	±	0.2	0.72	±	0.07
Stroke Volume^{TU}	1.22 ^{ΔΔooo}	±	0.04	1.12^{o}	±	0.04	1.02$^{**□□□}$	±	0.04	1.29$^{+ΔΔΔoooox}$	±	0.04	0.93$^{***+□□□}$	±	0.05	1.09$^{□}$	±	0.04
Cardiac Output^{TU}	0.52$^{+ΔΔoox}$	±	0.02	0.42$^{*□□}$	±	0.03	0.42$^{**□□}$	±	0.02	0.53$^{++ΔΔoox}$	±	0.02	0.41$^{□□**}$	±	0.02	0.44$^{*□}$	±	0.01
Ejection Fraction ^{GH}	64	±	2.7	64	±	3.6	59	±	0.9	66	±	3.8	54	±	5.1	61	±	2.2
End Diastolic Volume^{TU}	1.64	±	0.04	1.53	±	0.05	1.64	±	0.08	1.66	±	0.05	1.66	±	0.05	1.68	±	0.09
End Systolic Volume ^{GH}	0.45^{ΔΔΔooo}	±	0.02	0.55^{oo}	±	0.03	0.67$^{***□□}$	±	0.03	0.45^{ΔΔooo}	±	0.04	0.74$^{***□□□++}$	±	0.04	0.67	±	0.08
Stroke Volume^{TU}	1.18$^{+Δoo}$	±	0.04	0.98$^{*□}$	±	0.04	0.97$^{*□}$	±	0.06	1.21$^{+Δoox}$	±	0.06	0.92$^{**□□}$	±	0.04	1.01$^{□}$	±	0.04
Cardiac Output^{TU}	0.50$^{+++ΔΔox}$	±	0.02	0.37$^{***□□}$	±	0.03	0.40$^{**□}$	±	0.02	0.50$^{++Δox}$	±	0.02	0.40$^{*□}$	±	0.02	0.40$^{*□}$	±	0.01
Ejection Fraction ^{GH}	72$^{+ΔΔΔooo}$	±	1.0	64^{*o}	±	1.7	59$^{***□□}$	±	1.4	72^{ΔΔoo}	±	2.6	55$^{***+□□}$	±	1.9	61	±	3.4
Heart Rate ^{GH}	427	±	15.4	373	±	20.2	376	±	13.2	410	±	11.0	428	±	12.2	401	±	8.6
Body Weight^{TU}	32.4^{Δo}	±	0.8	32.4^{Δo}	±	1.2	35.9$^{*+□□□}$	±	0.7	29.6^{ΔΔΔooo}	±	0.7	35.9$^{*+□□□}$	±	0.5	32.60	±	0.8

Restoration of dystrophin in the diaphragm did not protect cardiac function with exercise.

The interaction effect between exercise and mouse groups (ie. *mdx*, C57BL/10 and B-PMO treated *mdx*) was significant for a number of cardiac measurements, as determined by 2-way ANOVA (see **Table 3.2**). In particular, it showed the effect of moderate exercise on untreated *mdx* mouse hearts, lowered LV SV and increased RV ESV with consequential decrease in RV EF (see **Table 3.1** for significance between *mdx*^{unex} and *mdx*^{ex}). This suggests that exercise resulted in poor RV contractility in the *mdx*^{ex} mice. In contrast, the C57BL/10 and B-PMO treated cohorts were largely unchanged by exercise (see **Table 3.1** for significance relative to exercised counterpart).

Direct comparison of the *mdx*^{ex} cohort with the C57BL/10^{ex} counterpart revealed significant changes in cardiac parameters namely LV SV and LV CO (**Fig. 3.7 and Table 3.1**). The *mdx*^{ex} group also revealed pronounced changes in multiple right ventricle parameters relative to C57BL/10^{ex} counterpart. Again the B-PMO^{ex} cohort revealed similar cardiac function parameter values to the *mdx*^{ex} cohort. The LV SV and LV CO of B-PMO^{ex} mice were both lower than the C57BL10^{ex} mice. Additionally, the right ventricle SV of the B-PMO^{ex} cohort was lowered, along with CO. It therefore seems that B-PMO treatment of the diaphragm did not protect heart function in the event of exercise.

Table 3.2. Statistical significance of cine-MRI measurements, showing the interaction between exercise and mouse groups (*mdx,* C57BL/10 and B-PMO treated mice) following 2-way ANOVA. N= 10 for each cohort.

	Measurement	**Interaction**
LV/BW	Average Mass	N/S
	End Diastolic Volume	N/S
	End Systolic Volume	N/S
	Stroke Volume	0.002
	Cardiac Output	N/S
LV%	Ejection Fraction	N/S
RV/BW	End Diastolic Volume	N/S
	End Systolic Volume	0.05
	Stroke Volume	N/S
	Cardiac Output	N/S
RV%	Ejection Fraction	0.02
BPM	Heart Rate	0.04
Gram	Body Weight	<0.001

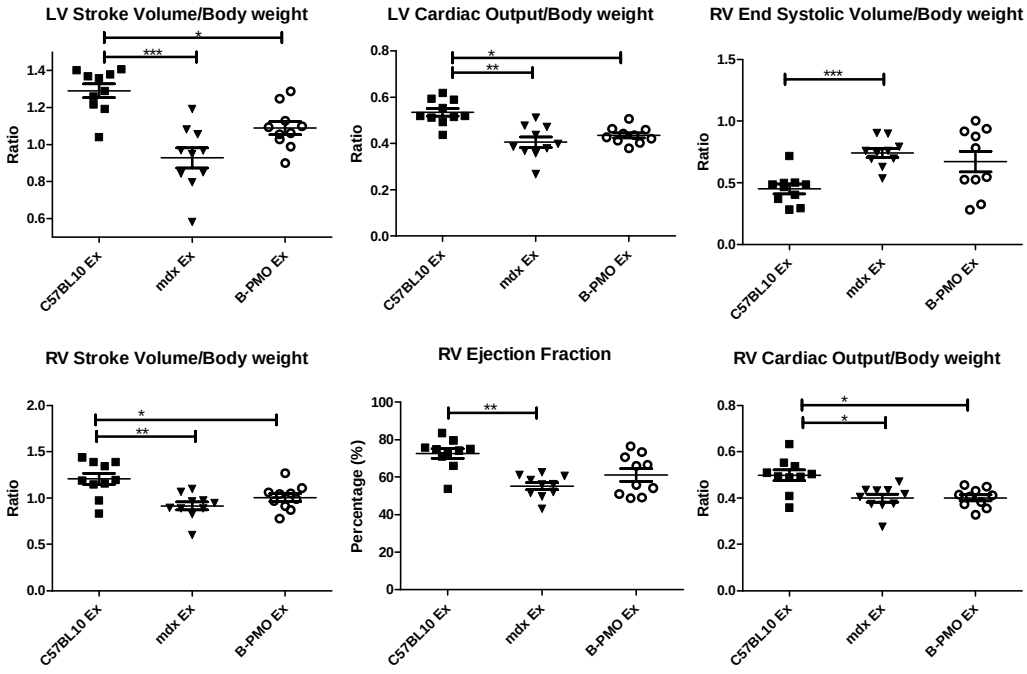

Figure 3.7. Cardiac function parameters measured by cine-MRI in exercised *mdx* and C57BL/10 mouse cohorts. Scatter plot graphs illustrating individual mouse values, mean and standard error of the mean (SEM) for left ventricular(LV) and right ventricular (RV) parameters relative to body weight. Note: The exception to this is the ejection fraction which is represented as a percentage. Cardiac function in B-PMO^{ex} and *mdx*^{ex} was worse than C57BL/10^{ex} mice. Statistical significance was determined using ANOVA followed by Tukey Post-Hoc Test or Games-Howell Post-Hoc Test to correct for variance heterogeneity. (*=p<0.001, **=p<0.01*=p<0.05). N=10 for each cohort.**

Elevated expression of cardiac damage and oxidative stress markers

In addition to MRI analysis, qRT-PCR was performed on heart and diaphragm tissues to assess the expression of genes of cardiac damage and collagen deposition. This was a relatively moderate exercise regimen over a short time course, therefore changes in expression of these markers was not anticipated.

The expression levels of markers for haemodynamic overload and oxidative stress, atrial natriuretic peptide (Nppa) and NADPH oxidase 4 (Nox4) were assessed (**Fig. 3.8**). Nppa is secreted by the atria in response to haemodynamic overload or stress [236] and results in a reduction of blood pressure and cardiac hypertrophy [236]. It has also been used as a diagnostic measure for heart failure [237]. Nox4 is an enzyme involved in superoxide production, thus performing an important role in oxidative stress and dysfunction in the failing heart [238] and associated with cardiac dysfunction in *mdx* mouse [239]. The *mdx*^{unex} and B-PMO^{unex} cohorts had significantly higher Nppa expression than the C57BL/10^{unex} cohort. The Nppa expression level of the *mdx*^{unex} cohort was not significantly different to the B-PMO^{unex} cohort. Nox4 expression was highest in the *mdx*^{ex} cohort closely followed by the *mdx*^{unex} cohort. Interestingly the B-PMO cohorts were not significantly different to the C57BL/10 cohorts, but it is noteworthy that they were approximately 2 fold up regulated. The expression levels of these markers show that dystrophin restoration of the diaphragm did not protect the heart.

Markers for inflammation and collagen deposition, Tgfb1 and Col1a2 respectively, were also assessed in heart samples (**Fig. 3.8**). The expression of Tgfb1 did not fluctuate and Col1a2, an early marker of fibrosis, was only significantly up-regulated in the *mdx*^{unex} cohort. However this did not correlate with Masson's trichrome staining, which revealed extensive collagen deposition and fibrosis in heart samples. **Figure 3.9** demonstrates large fibrotic regions in *mdx*^{unex} and B-PMO^{unex} treated mice hearts. Similarly, **Figure 3.10** demonstrates large areas of fibrosis in the exercised cohorts.

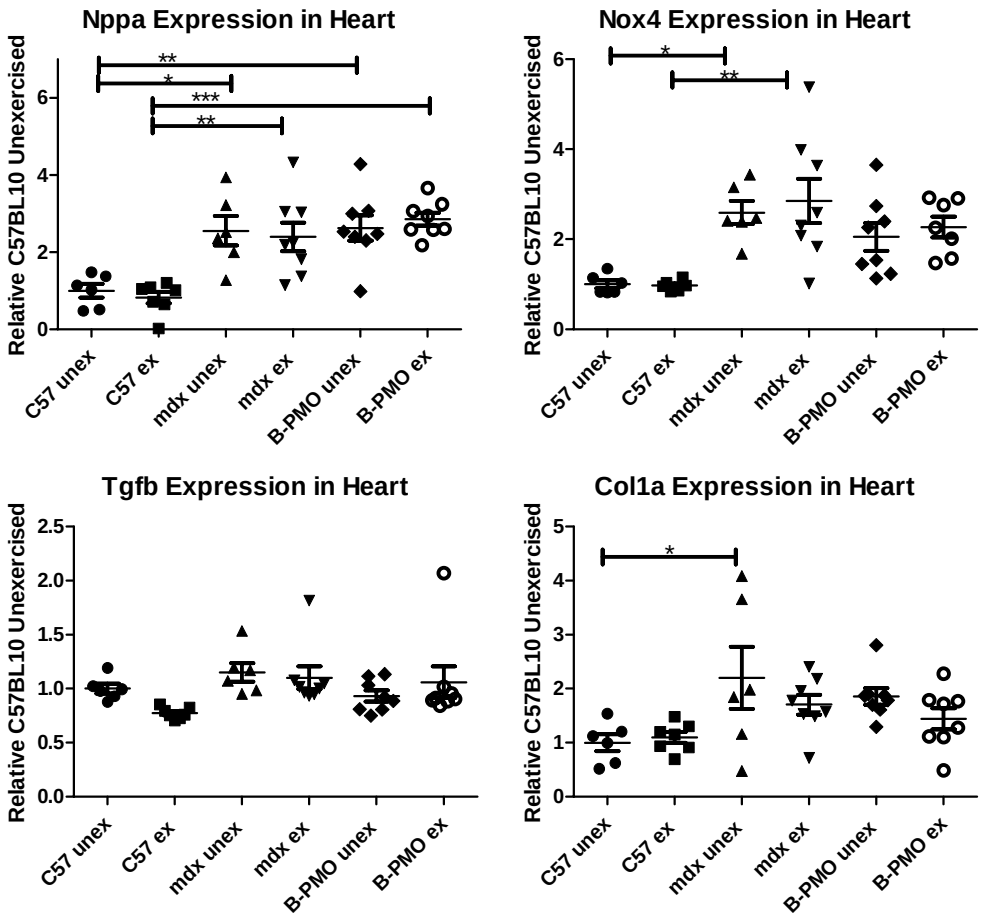

Figure 3.8. Gene expression of markers for injury, inflammation and fibrosis in the hearts of exercised and unexercised mice. Quantitative real time (qRT)-PCR for the expression of Nppa, Nox4, Tgfb and Col1a normalised to C57BL/10 unexercised cohort. Expression of Nppa elevated in B-PMO and *mdx* cohorts, and Nox4 elevated in *mdx* cohorts also. Expression of Tgfb and Col1a relatively stable. Statistical significance was determined using One-way ANOVA, Tukey post-hoc test (*=p<0.001, **=p<0.01*=p<0.05). N=8 for each cohort.**

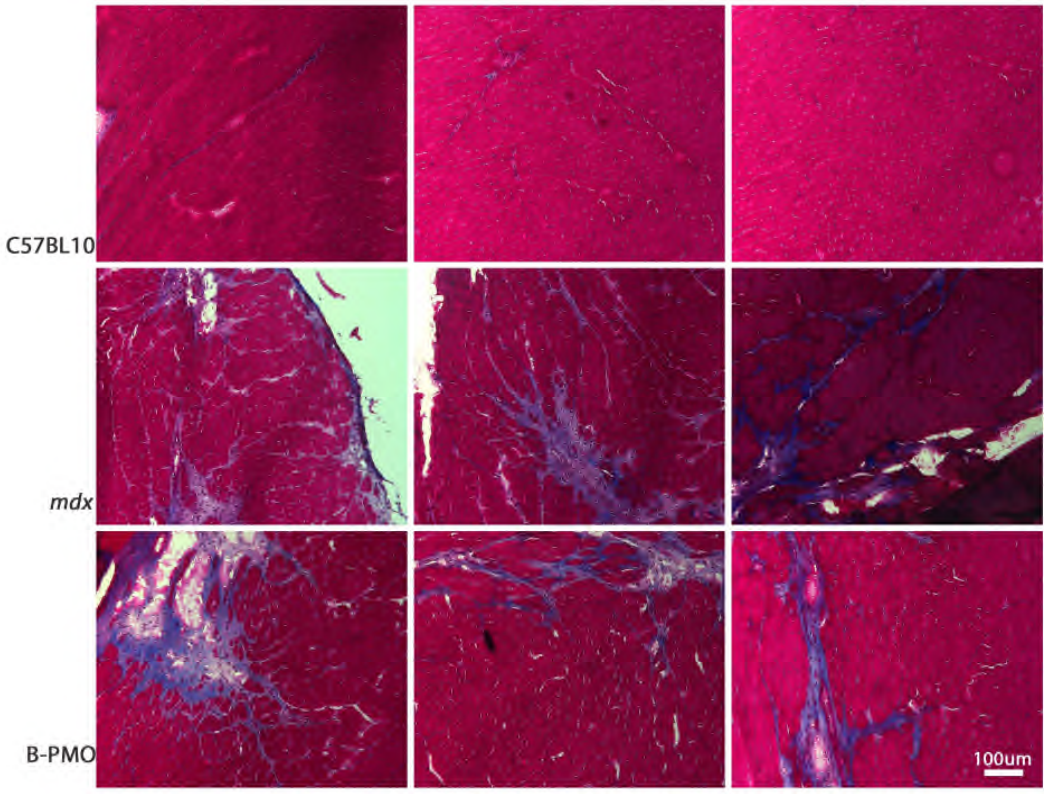

Figure 3.9. Masson's trichrome staining in the hearts of C57BL/10, *mdx* and B-PMO unexercised cohorts. 8 µm sections were taken and stained with Masson's trichrome. Purple areas denote collagen deposition and fibrosis. Extensive fibrosis was observed in the hearts *mdx*^{unex} and B-PMO^{unex} mice. Scale bar: 100 µm.

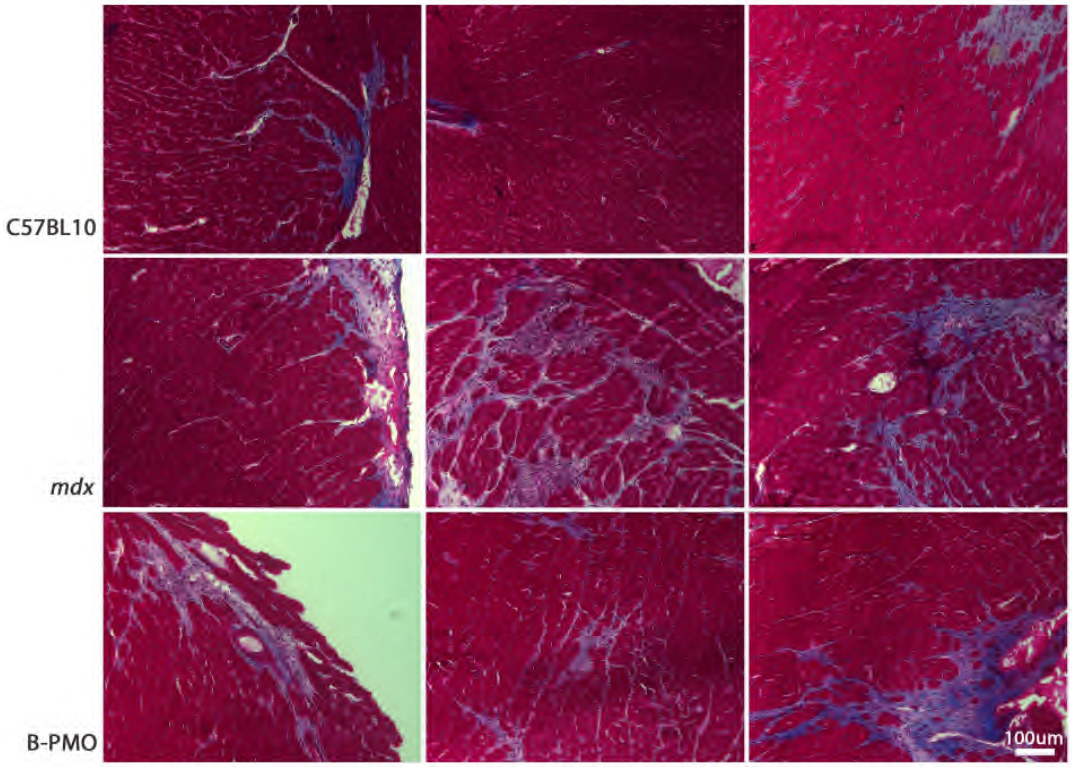

Figure 3.10. Masson's trichrome staining in the hearts of C57BL/10, *mdx* and B-PMO exercised cohorts. 8 µm sections were taken and stained with Masson's trichrome. Purple areas denote collagen deposition and fibrosis. Extensive fibrosis was observed in the hearts *mdx*^{ex} and B-PMO^{ex} mice. Scale bar: 100 µm.

Diaphragm samples were also assessed to determine whether dystrophin restoration in treated cohorts had prevented the onset of fibrosis. Again, expression levels of Col1a2 and Tgfb1 were assessed (**Fig. 3.11**). The expression of Col1a2 was significantly higher in *mdx*^{ex} and *mdx*^{unex} cohorts compared to the C57BL/10s. There was no statistical difference between the *mdx*^{ex} and *mdx*^{unex} cohorts which suggests that the exercise did not result in excessive collagen deposition, possibly due to the short regimen. The B-PMO treated cohorts were not significantly different to the C57BL/10 cohorts, which suggest that dystrophin has prevented the further deposition of collagen. Contrastingly, Tgfb1 was only significantly up regulated in the B-PMO^{ex} group, however the fold change was very low (0.5 fold change higher). Masson's trichrome staining of the diaphragm was also performed to assess collagen deposition. Representative images of this staining indicate some deposition of collagen in the treated mice (**Fig. 3.12**), perhaps due to collagen deposition prior to B-PMO administration (treatment only at 21 weeks of age).

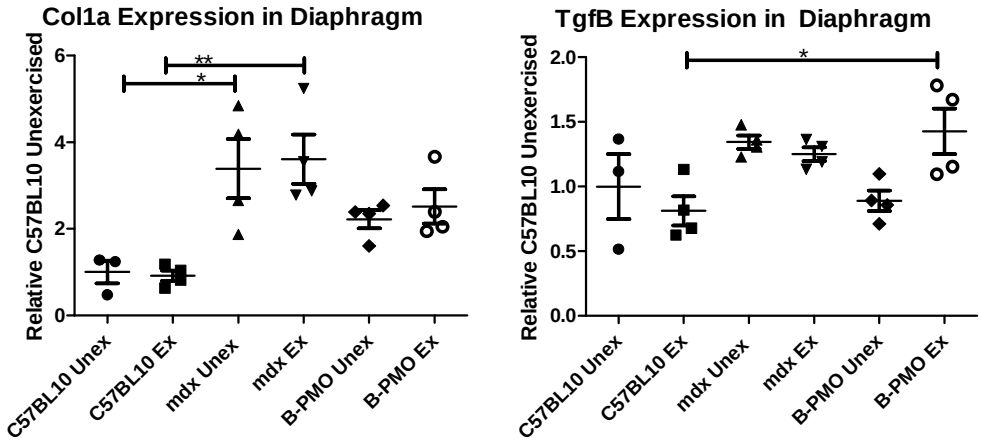

Figure 3.11. Gene expression of markers for inflammation and fibrosis in the diaphragms of exercised and unexercised mice. Quantitative real time (qRT)-PCR for the expression Tgfb and Col1a normalised to C57BL/10 unexercised cohort. Col1a expression elevated for *mdx* cohorts whereas Tgfb slightly elevated in B-PMO^{ex} cohort. Statistical significance was determined using One-way ANOVA, Tukey post-hoc test (*=p<0.001, **=p<0.01*=p<0.05). N=4 for each cohort.**

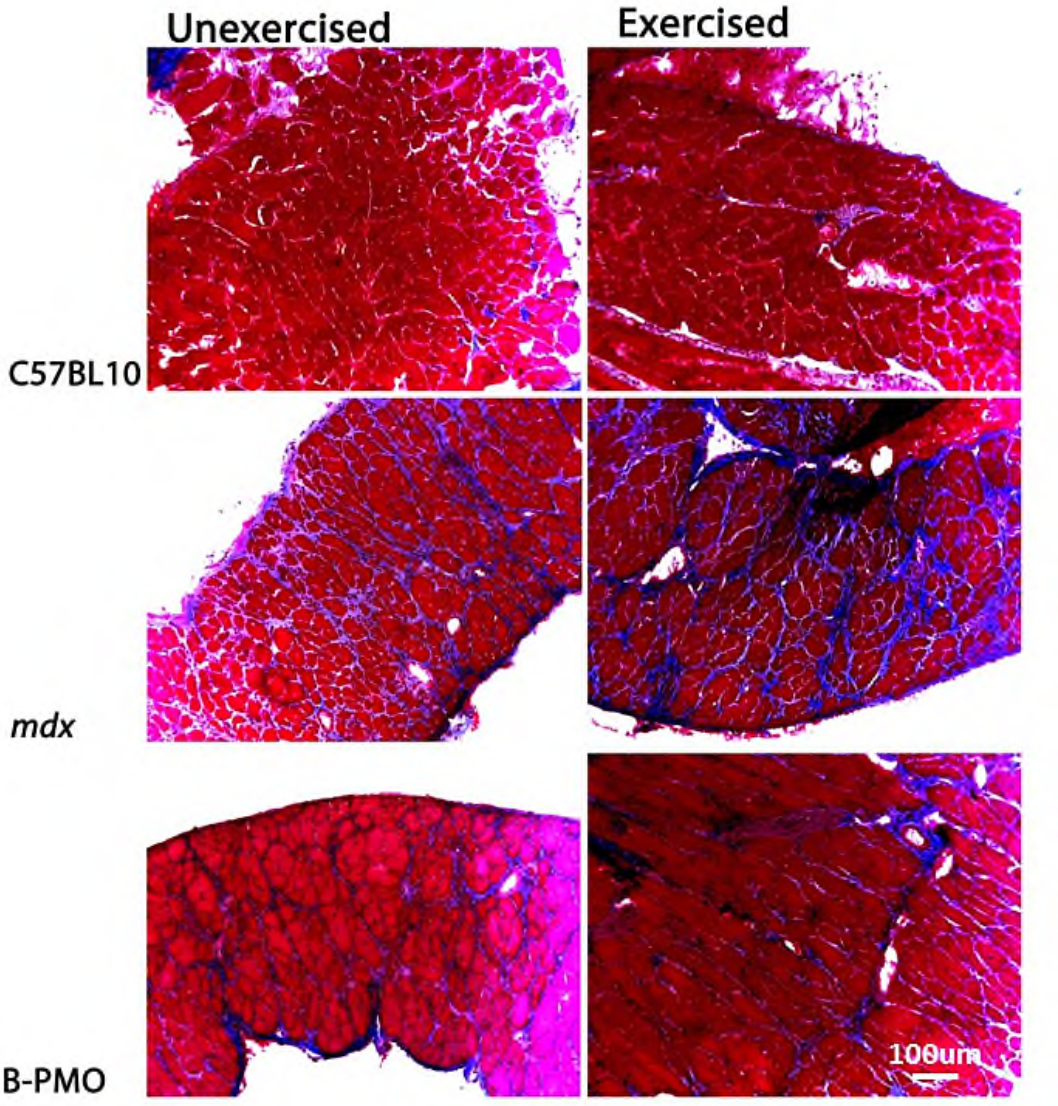

Figure 3.12. Masson's trichrome staining in the diaphragms of unexercised and exercised cohorts of C57BL/10, *mdx* and B-PMO treated mice. Purple areas denote collagen deposition and fibrosis. Extensive areas of fibrosis were apparent in *mdx* and B-PMO cohorts. Scale bar: 100 µm.

Sarcolemmal integrity in unexercised and exercised mice

It is well documented that an increase in workload in dystrophic mouse models leads to a substantial increase in Evans blue dye (EBD) leakage [240]. This event is a direct result of a lack of dystrophin at the sarcolemma, which maintains stability and integrity of the membrane [241] and prevents the infiltration of EBD into tissue. Therefore the extent of EBD leakage was compared in the diaphragm of untreated *mdx* mice with those with corrected dystrophin in the diaphragm. The presence of EBD was also assessed in heart and *tibialis anterior* muscles.

The surface areas of EBD leakage into the diaphragm of the *mdx*^{ex} and *mdx*^{unex} cohorts were markedly greater than the C57BL/10 and B-PMO cohorts (**Fig. 3.13**). The B-PMO treated mice were normalised. This result was anticipated, as a substantial amount of dystrophin was restored in the diaphragm of these mice, thus improving membrane stability and preventing the leakage of EBD into tissue.

Whilst there was no significant EBD leakage in the hearts of any of these cohorts, it should be noted that one of the B-PMO^{ex} mice displayed marked EBD leakage (**Fig. 3.14)**. Substantial sarcolemmal damage in the heart was not anticipated due to the moderate and short exercise regimen.

Leakage of EBD in the *tibialis anterior* of the *mdx*^{ex} cohort was significantly higher than all other cohorts with the exception of the B-PMO^{ex} counterpart (*mdx*^{ex} cohort: average of 8% EBD leakage). This result was anticipated as the exercise would have caused some mechanical damage to dystrophic skeletal muscle cells, such as the *tibialis anterior*, allowing EBD leakage into the tissue. Perhaps the lower EBD surface area of B-PMO^{ex} treated mice was due to the very low levels of dystrophin restored in the *tibialis anterior* (**Fig. 3.2-4**).

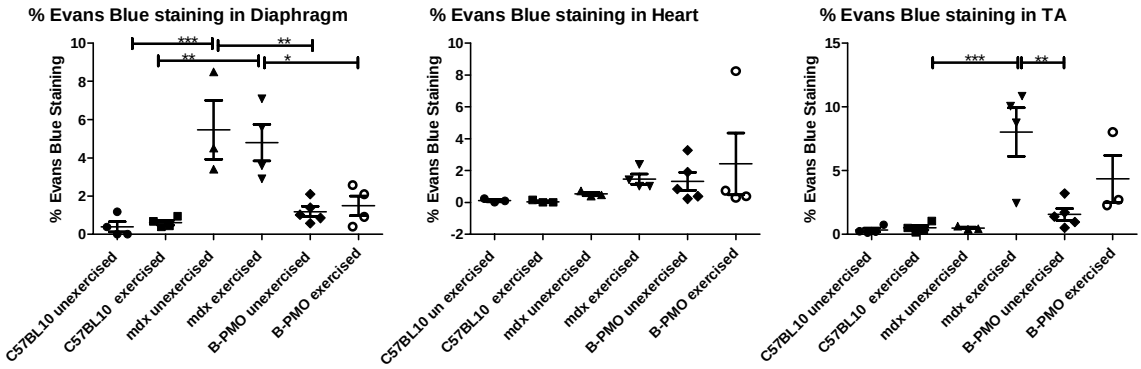

Figure 3.13. Quantification of Evan's blue dye leakage in exercised and unexercised C57BL/10, *mdx* and B-PMO treated *mdx* mice. Evans blue leakage was quantified by calculating the surface area of stained cells relative to total surface area of section. Scatter plot graphs of Evans blue staining illustrating individual mouse values, mean and standard error of the mean (SEM) in diaphragm, heart and *tibialis anterior* muscles (top). Evans blue leakage was pronounced in diaphragm of *mdx* mice, and *tibialis anterior* of *mdx*^{ex} and B-PMO^{ex} mice. No statistical significance between cohorts for heart. Statistical significance was determined using One-way ANOVA, Tukey post-hoc test (*=p<0.001, **=p<0.01*=p<0.05). N=3-4 for each cohort.**

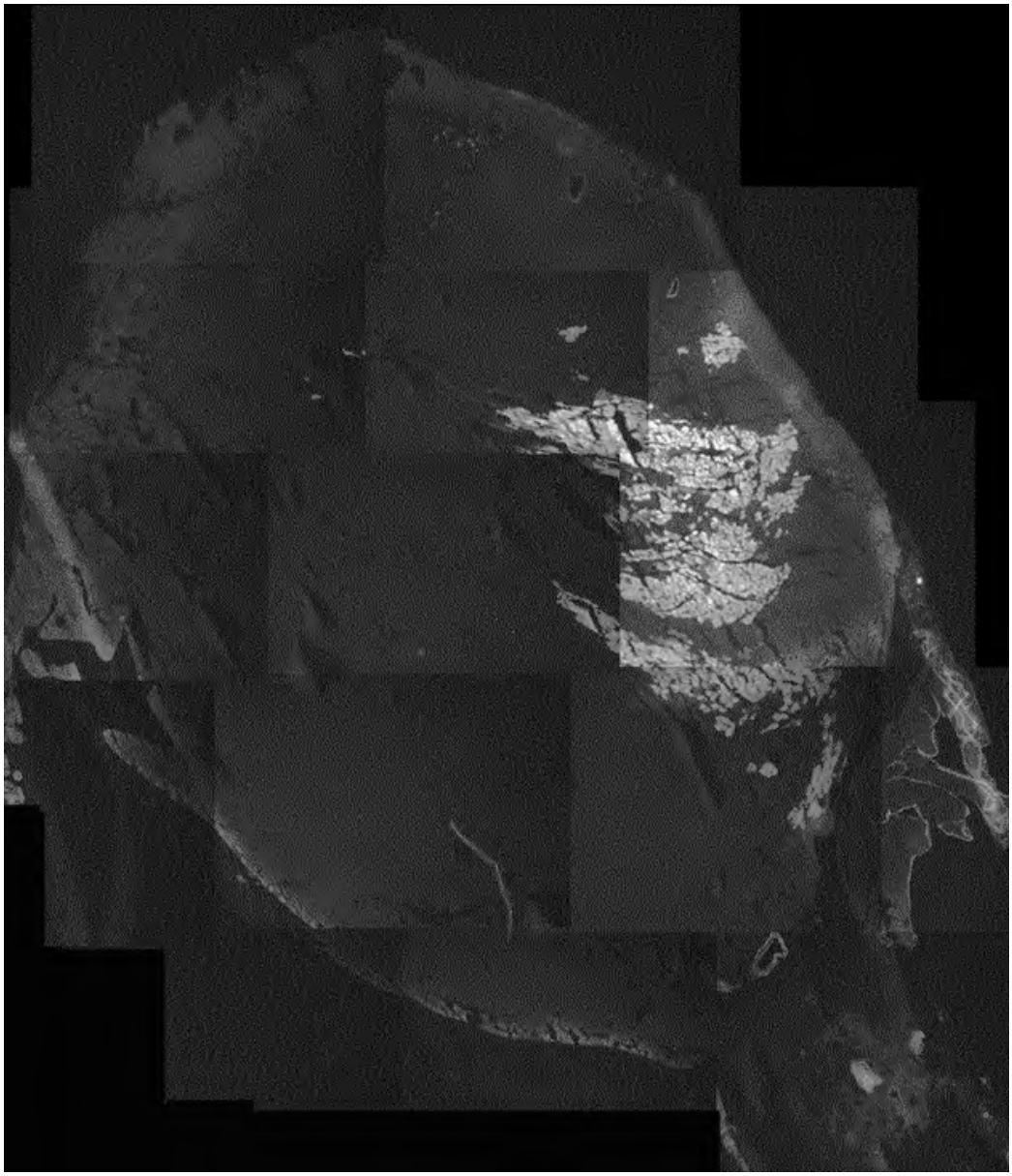

Figure 3.14. Image of the B-PMO^{ex} treated mouse heart which showed extensive dye infiltration. 10X magnification images were taken and manually reconstructed to attain a consolidated image of the section.

Intravenous versus intraperitoneal dystrophin restoration in various tissues

Interestingly, the authors from another study utilising B-PMO observed improved cardiac function following a single IV administration [222]. The single experimental difference between this study and the work presented here in **Chapter 3** is the administration route. Previous studies have revealed the improved delivery capacity of peptide-PMO administered via the IV route, compared to IP administration, which resulted predominantly in diaphragm restoration. The limited dystrophin restoration by IP administration in accessory respiratory muscles has already been demonstrated in **Figure 3.2**. We therefore wanted to assess the extent of dystrophin restoration compared to IV administration (**Fig. 3.15**). A single 19 mg/kg IV administration of B-PMO resulted in widespread and high levels of dystrophin restoration in the intercostal and sternomastoid muscles. In addition there appeared to be low levels of dystrophin restored in both the elastic and smooth muscle layers of the aorta and bronchioles of mice treated IV.

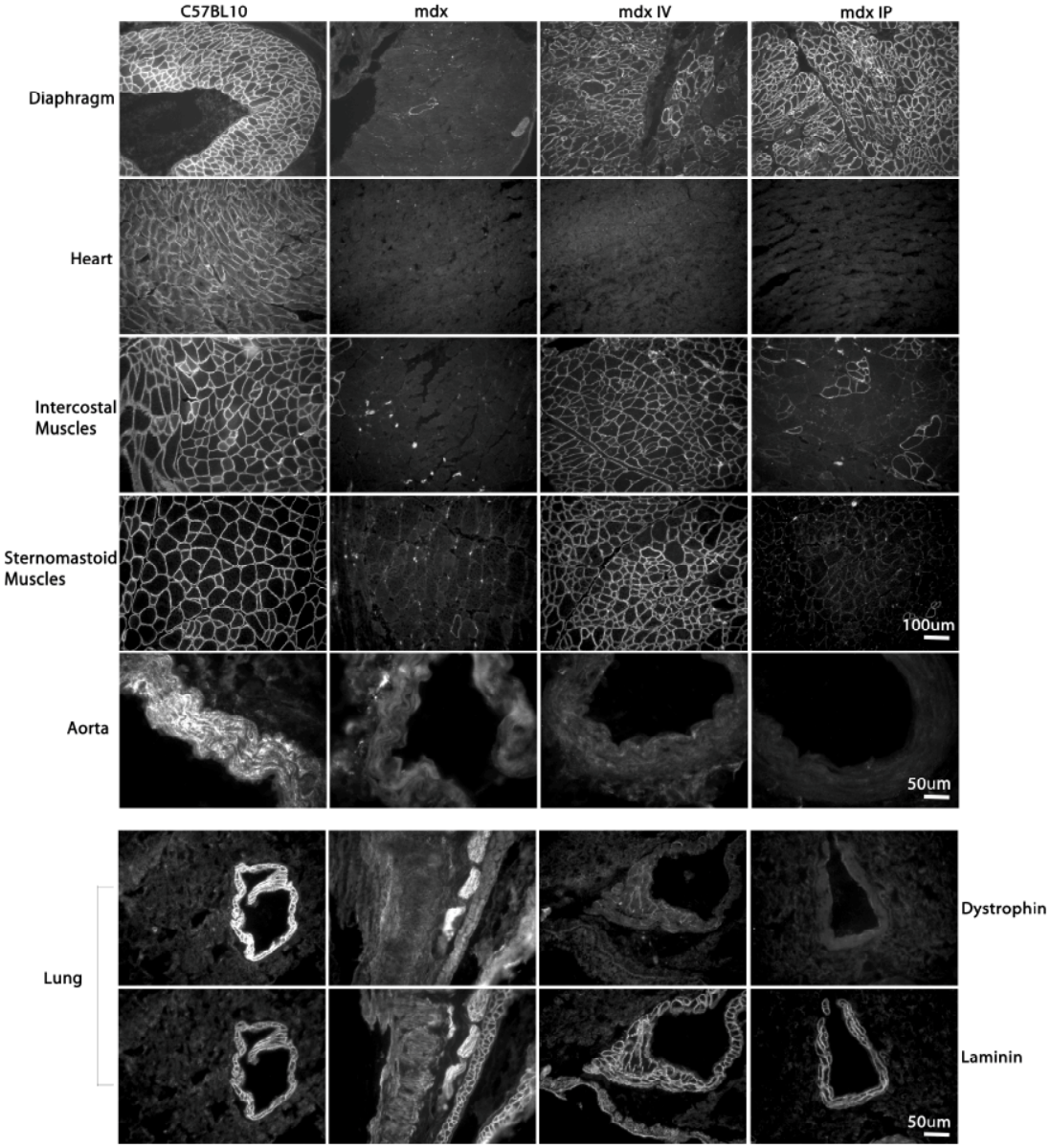

Figure 3.15. Immunohistochemical staining of dystrophin comparing B-PMO treatment following intravenous (IV) and intraperitoneal (IP) administration. Representative images of dystrophin staining for diaphragm, heart, intercostal muscles, sternomastoid muscles, aorta and lung are shown. For lung tissue laminin co-stain was included in order to define the bronchiole wall. Figure illustrates restoration of dystrophin in multiple tissues when B-PMO was administered IV. Dystrophin was only prevalent in diaphragm of IP treated mice. Scale bars for diaphragm, heart, intercostal and sternomastoid muscles: 100 µm; scale bars for aorta and lung: 50 µm.

Discussion

The main objective of this study was to assess the impact of dystrophin restoration in the diaphragm alone on cardiac function in a DMD mouse model, using B-PMO delivered via the IP route. It was anticipated, based on a previous study [222] that dystrophin restoration in the diaphragm would improve cardiac function parameters potentially by improving respiratory function. In short, dystrophin restoration in the diaphragm did not have a beneficial effect on cardiac function, with or without exercise.

In addition to MRI measurement of heart function, markers of cardiac damage, oxidative stress and fibrosis were also utilised to assess the cardiac phenotype in treated mice. Nppa expression in *mdx* and B-PMO treated hearts were significantly higher than C57BL/10 cohorts and Masson's trichrome staining in the hearts of these cohorts revealed extensive collagen deposition. Therefore, it seems that diaphragmatic dystrophin restoration did not reduce or change the pathology of the dystrophic heart. No dramatic changes in Col1a or Tgfb1were observed. As Col1a is an early marker of collagen deposition, perhaps the expression of this gene had largely normalised by the time of sample collection. However, the normalised EBD leakage levels of the dystrophin restored diaphragm suggest some improvement in the pathology of this tissue. This improvement in diaphragm pathology did not however extend to functional improvements in the heart. Perhaps a treatment regimen, or higher doses and earlier administration of B-PMO may have had a beneficial effect on cardiac function.

The MRI results showed no improvement in cardiac function following treatment, which contrasts with results published by Crisp *et al*. These authors observed improved cardiac function following IV administration of B-PMO in *mdx* mice. The distinct difference between these two studies is the delivery route i.e. IV versus IP administration. This suggests that IV administration restored dystrophin in tissues in addition to diaphragm, which were important for improving cardiac function. Indeed a direct comparison of tissues removed from IV and IP treated mice were stained for the presence of dystrophin **(Figure 3.15)** to reveal marked restoration of dystrophin in accessory respiratory muscles (intercostal and sternomastoid) and possibly some dystrophin in major vessels and the bronchioles of the lungs. Whilst it was difficult to determine from this dataset whether it was the restoration of accessory muscles, the microvasculature, the bronchioles or a combination of all these, these mechanisms may explain the improvements in cardiac function. Improvement in diaphragm and accessory muscle function would have resulted in improved respiration and lung capacity [70] which are impaired in *mdx* mice [232].The alternative theory involves the role of dystrophin in vasoregulation. Dystrophin is absent in vascular endothelial cells which are present in microvasculature [242-244] including that of the lung, and in the tunica media of blood vessels of *mdx* mice [245]. The absence of dystrophin in blood vessels contributes to impaired vasodilatory response due to reduced eNOS and impaired NO signalling [246]. Restoration of dystrophin (following IV administration) in the microvasculature and the lungs may have improved NO handling, thus improving vasoregulation

thereby reducing vascular resistance. Reduced vascular resistance would in turn reduce pulmonary hypertension, thus alleviating pressure on the right side of the heart. It has been suggested that *mdx* muscle works under hypoxic conditions, making this hypothesis seem feasible [71, 247]. Conversely, in the present study, dystrophin was not present in accessory respiratory muscles, the microvasculature or the bronchioles in the lung. Therefore expiratory function may have been impaired (lack of dystrophin in accessory respiratory muscles) or the absence of dystrophin in pulmonary vessels may have led to poor vasoregulation, thus aggravating vascular resistance.

Restoration of dystrophin in the diaphragm seemed to improve the pathology of this muscle, but it did not have a beneficial impact on cardiorespiratory function. Although the diaphragm is a major respiratory muscle and a major muscle to target, restoration of dystrophin in the diaphragm is only likely to confer cardiorespiratory benefit when coupled with dystrophin restoration in other tissues, including other accessory respiratory muscles and, of course, the heart itself. In short, this study suggests that targeting a single muscle or organ to treat the systemic disease, DMD, is insufficient. Rather it reinforces the concept that efforts should be focussed on a body-wide treatment, and working to find a therapy that will restore dystrophin in the particularly difficult organ to target, the heart.

Chapter 4. Identification of new peptide-PMO candidates with improved exon skipping capacity in heart

Introduction

Inadequacy of naked antisense oligonucleotides

Chapter 3 demonstrates the importance of a body wide treatment and the requirement for a therapy that targets the heart and corrects cardiac function. Current AOs being utilised in clinical trials, PMO and 2'OMe, have limited capacity to correct dystrophin expression in the hearts of a DMD mouse model, the *mdx* mouse. These AOs required high doses to restore dystrophin to skeletal muscles and were not capable of restoring dystrophin protein in cardiac muscle [173, 174, 182, 183]. The limited potency of these compounds has carried through into clinical trials with a recent report from Prosensa (Drisapersen; 2'OMe) revealing the limited improvement in the gold standard measurement, the 6 minute walk test (announced at Action Duchenne Conference, 2013). Results from the Eteplirsen (PMO) study were slightly more positive, but limited by a small subject group and inappropriate controls. This study did, however, show some improvement in the 6 minute walk test [194] and pulmonary function (Sarepta announcement, February 2014).

The lack of significant functional output measurements from the clinical studies raises concerns regarding the rescue of the skeletal muscle phenotype, resulting in improved locomotor activity with a detrimental impact on cardiac histopathology (following multiple PMO administrations)

[197]. It is therefore imperative that future therapies designed for the treatment of DMD target both skeletal and heart muscle.

The derivation of heart targeting CPPs

The poor bioavailability of AOs has been attributed to their inability to translocate through the lipid membrane due to their size [248] and charge. Cell-penetrating peptides that may be readily conjugated to the charge neutral AO, PMO, possess a unique ability to permeate the plasma membrane [205]. As previously described, motifs and CPPs made for the treatment of DMD, MSP and B peptide, required high or multiple administrations to cause skipping in the heart [213, 222, 223, 225, 249]. The penetratin-derived CPPs, Pip2- and Pip5-PMO, were capable of restoring dystrophin in the heart following a single administration (analysed 2 weeks later). Based on the success of these peptides, additional structure activity studies were undertaken on the Pip5e-sequence. This peptide has a central 5 amino acid (5-aa) hydrophobic core flanked by arginine-rich domains (see **Fig1.8**). B-peptide is an arginine rich sequence which bears homology to the arginine-rich flanking domains of Pip5e [204]. As B-peptide resulted in high dystrophin restoration in skeletal muscle (less efficient in heart than Pip5e [230]), it was assumed that the high arginine content contributed to the efficiency of delivery to skeletal muscle, and the hydrophobic region of Pip5e was essential for heart muscle delivery. However, the rationale behind this latter observation is poorly understood and further examination of the hydrophobic core was required.

Rationale for study

As the heart penetrating capacity of Pip5e has been attributed to the hydrophobic core [230], the work in this Chapter determined whether alterations to the amino acid sequence of the Pip5e core could improve delivery capacity. Derivatives of Pip5e-PMO included serial deletions, scrambled sequences and lengthening of the hydrohobic core. They were assigned a sequential numerical name, Pip6-PMOs. These Pip6-PMO derivatives were developed to firstly identify peptides with improved cardiac splicing activity, and secondly to understand the effect that serial amino acid deletions and additions had on the hydrophobic core. This was determined using techniques designed to assess dystrophin splicing and protein restoration.

Synopsis of findings

All Pip6-PMO conjugates were administered as a single, low dose of 12.5 mg/kg via the tail vein in *mdx* mice. Peptides that maintained 5-aa core caused widespread dystrophin production in all tissues. Pip6a-, Pip6b- and Pip6f-PMO exhibited good cardiac activity, better than the previous lead candidate, Pip5e-PMO. These peptides also resulted in the re-localisation of the dystrophin-associated protein complex proteins to the sarcolemma. Conversely, serial amino acid deletions to the core region (Pip6c- and Pip6d-PMO) and further alterations, including additions to this core (Pip6g-, and Pip6h-PMO), resulted in a reduction of efficacy, specifically dystrophin splicing and protein production, and particularly in the heart.

This study has revealed 3 highly promising Pip6-PMO drug candidates, one of which will be utilised for future experiments designed to better characterise their ability to restore cardiac function.

Methodology

A number of Pip6-PMO AOs were designed and underwent screening in order to understand which components of the central hydrophobic core were integral to efficacy, in particular to restore dystrophin in heart. Four and a half to five and a half month old *mdx* mice were used for this experiment (an 'n' of 3 was used for each peptide; 33 mice used in total). Each Pip6-PMO conjugate was prepared in 0.9% saline solution at a dose of 12.5 mg/kg and administered *via* the tail vein of the mice (**Fig. 4.1**). Two weeks later, mice were sacrificed by CO_2 inhalation, and muscles, and other tissues harvested and snap-frozen. A variety of muscles, namely the *tibialis anterior*, gastrocnemius, quadriceps, bicep, heart, diaphragm and abdomen, were assessed for the presence of dystrophin (and exon splicing) by immunohistochemical staining, RT-PCR, qRT-PCR and western blotting.

In addition, the re-localisation of dystrophin associated proteins was assessed by immunohistochemical staining. Briefly, slides were blocked using a MOM blocking kit (Vector Labs) and probed for α-sarcoglycan and α-dystroglycan (Novocastra) antibodies (1:100 dilution). Staining for nNOS was performed using a goat anti-rabbit antibody (Abcam). Plasma samples were sent to Mary Lyon Centre (MRC, Harwell) to determine levels of ALT, AST, CK and BUN which are indicators of liver and muscle damage.

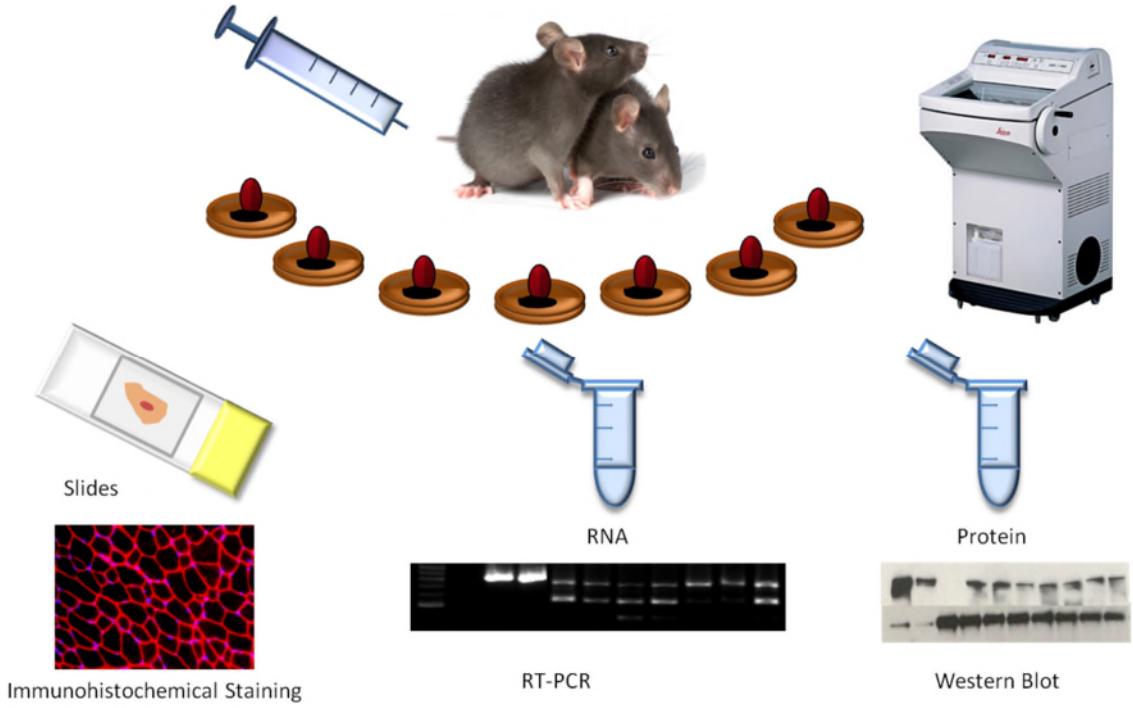

Figure 4.1. Illustration of screening process. From top, mice received a single 12.5 mg/kg intravenous injection. Tissues were harvested and cryosectioned using a cryostat (right). Slides were prepared and tissue was collected into eppendorf tubes for RNA and protein extractions. Representative images of the final experiment are illustrated (bottom from left; Immunohistochemical staining, RT-PCR and western blot).

Results[4]

Derivation of new Pip6-PMO series

The cardiac delivery capacity of Pip5e-PMO has been attributed to the central hydrophobic core; therefore this core was altered while maintaining the 5-aa core in an effort to identify peptides which were more efficient at lower doses. These modifications included the inversion of the hydrophobic region (Pip6a), substitution of tyrosine for iso-leucine (Pip6b), substitution of glutamine for arginine (Pip6e) and a scrambled hydrophobic core sequence (Pip6f; **Table 4.1).** The effect of a shorter hydrophobic core was unknown, so serial deletions to the core by 1 amino acid (removal of tyrosine; Pip6c) and 2 amino acids (removal of isoleucine and tyrosine; Pip6d) were also synthesised.

[4] The results from this Chapter were published by Nature Publishing Group, Aug 2012 (Journal- Molecular Therapy- Nucleic Acids). No permissions required. Images have been reformatted and text re-written.

Table 4.1. List of Pip5e derivatives, Pip6a-h, and their sequences.

Peptide	Sequence
Pip5e-	RXRRBRRXR ILFQY RXRBRXRBC
Pip6a-	RXRRBRRXR YQFLI RXRBRXRB
Pip6b-	RXRRBRRXR IQFLI RXRBRXRB
Pip6c-	RXRRBRRXR QFLI RXRBRXRB
Pip6d-	RXRRBRRXR QFL RXRBRXRB
Pip6e-	RXRRBRRX YRFLI RXRBRXRB
Pip6f-	RXRRBRRXR FQILY RXRBRXRB
Pip6g-	RXRRBRRX YRFRLI XRBRXRB
Pip6h-	RXRRBRRX ILFRY RXRBRXRB

Efficiency of Pip6-PMO derivatives in the *in vivo* production of dystrophin

The efficiency of each peptide was determined as their ability to induce dystrophin splicing and protein restoration. These processes were measured by RT-PCR, qRT-PCR (splicing), immunohistochemical staining and western blotting (protein).

All 5-aa core Pip6-PMO treated mice had widespread dystrophin expression following immunohistochemical staining (Pip6a-, Pip6b-, Pip6e- and Pip6f; **Fig. 4.2**), predominantly in *tibialis anterior*, diaphragm and abdominal muscles. These Pip6-PMO conjugates also revealed dystrophin expression in heart. The shortened core peptides (Pip6c- and Pip6d-PMO) gave good dystrophin restoration in skeletal muscles. These observations were corroborated by the immunohistochemical staining quantification relative to laminin co-stain in quadriceps, diaphragm and heart muscles (**Fig. 4.3**). Quantification revealed the lowest dystrophin restoration in the quadriceps with Pip6d- treatment (%RS- 12%, **Table 4.2**) closely followed by Pip6c-PMO (%RS- 19%). By comparison, the other Pip6-PMOs gave higher, similar dystrophin restoration levels (%RS range between 21-33%). Pip6d-PMO had the lowest dystrophin restoration in the diaphragm (19%) whereas the other Pip6-PMO conjugates gave higher recovery scores with Pip6b-PMO exhibiting the highest expression (%RS range between 39-48%, Pip6b 57%). All 5-aa core Pip6-PMO conjugates exhibited high dystrophin expression in the heart, with the exception of Pip6e. When directly compared to *mdx,* the heart immunohistochemical quantification values for Pip6a-, Pip6b- and Pip6f-PMO were found to be

statistically significant (**Table 4.3**). Pip6a- and Pip6b-PMO conjugates gave the highest recovery (%RS- 38% and 34% respectively), closely followed by Pip6f-PMO (%RS- 26%) and Pip5e-PMO (%RS- 17%). When these peptides were directly compared to Pip5e-PMO treatment, only Pip6a-PMO was significantly higher in the heart (**Table 4.4**). The heart recovery scores for Pip6c- and Pip6d-PMO were very low, indicating their poor cardiac efficacy (Pip6c %RS- 0% and Pip6d 2.50%).

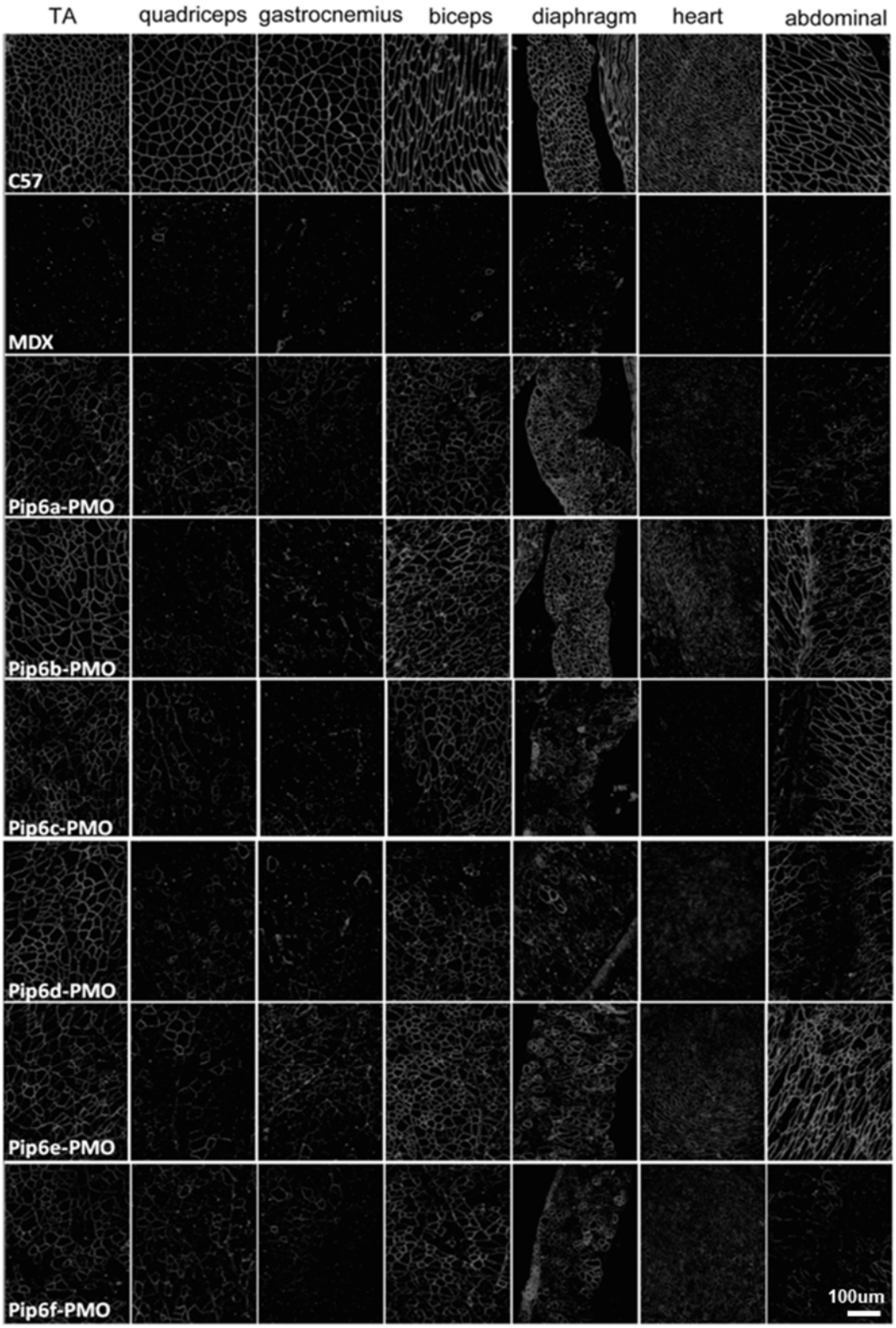

Figure 4.2. Immunohistochemical staining for dystrophin in C57BL/10 control, *mdx* untreated and Pip6-PMO treated mice. A single 12.5mg/kg systemic injection was administered. Tissues were harvested 2 weeks later and dystrophin immunostaining in *tibialis anterior,* quadriceps, gastrocnemius, diaphragm, heart and abdomen muscle groups for C57BL/10, *mdx* treated and *mdx* untreated mice are shown. Scale bar: 100 µm.

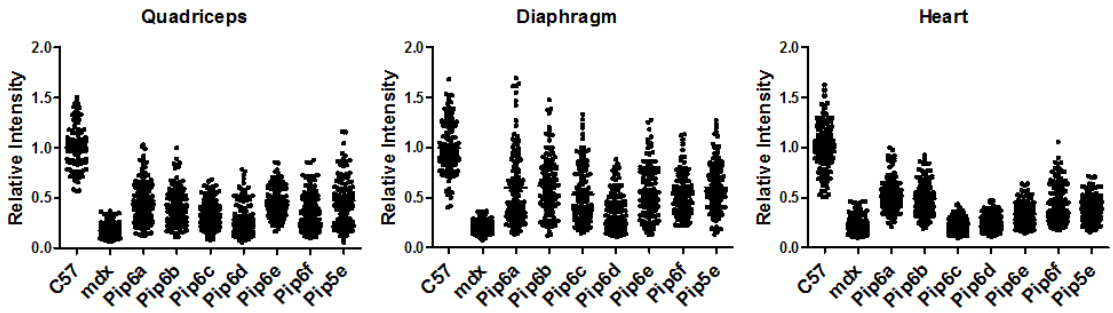

Figure 4.3 Quantification of dystrophin immunohistochemical staining for C57BL/10 control, *mdx* untreated and Pip6a-f-PMO treated mice. Dystrophin expression was calculated relative to laminin co-stain for quadriceps, diaphragm and heart samples. A cross-section of both quadriceps was used. Quantification used 120 regions of interest, calculated as the intensity of dystrophin relative to the corresponding intensity of laminin, normalised to C57BL/10 unexercised. The box plots show the normalised relative intensity values for each region of interest (for statistical significance see Tables 4.3 and 4.4). N= 3 for each cohort.

Table 4.2. Dystrophin recovery scores for immunohistochemical staining of quadriceps, diaphragm and heart in treated cohorts (percentage). N= 3 for each cohort.

Recovery scores for immunohistochemical staining quantification	**Quadriceps**	**Diaphragm**	**Heart**
C57BL/10	100	100	100
Mdx	0	0	0
Pip6a	33	47	38
Pip6b	31	57	34
Pip6c	19	39	0
Pip6d	12	19	3
Pip6e	32	39	12
Pip6f	21	45	26
Pip5e	33	48	17

Table 4.3. Statistical significance table for immunohistochemical staining of Pip6a-f and Pip5e-PMO relative to untreated *mdx* mice. Significance for quadriceps, diaphragm and heart are shown. Statistics were calculated using a repeated measure, multi-level model (**=p<0.0001, ***=p<0.001, **=p<0.01, *=p<0.05). N= 3 for each cohort.**

	Quadriceps		**Diaphragm**		**Heart**	
C57BL/10	****	0.0000	****	0.0000	****	0.0000
Pip6a	****	0.0000	****	0.0000	****	0.0000
Pip6b	****	0.0000	****	0.0000	****	0.0000
Pip6c	**	0.004	****	0.0000	N/S	0.9
Pip6d	N/S	0.06	*	0.016	N/S	0.7
Pip6e	****	0.0000	****	0.0000	N/S	0.1
Pip6f	**	0.02	****	0.0000	**	0.002
Pip5e	****	0.0000	****	0.0000	*	0.03

Table 4.4. Statistical significance table for immunohistochemical staining of Pip6a-f and *mdx* untreated relative to Pip5e-PMO treated mice. Significance for quadriceps, diaphragm and heart are shown. Statistics were calculated using a repeated measure, multi-level model (**=p<0.0001, ***=p<0.001, **=p<0.01, *=p<0.05). N= 3 for each cohort.**

	Quadriceps		**Diaphragm**		**Heart**	
C57BL/10	****	0.0000	****	0.0000	****	0.0000
Mdx	****	0.0000	****	0.0000	*	0.03
Pip6a	N/S	1.0	N/S	1.1	*	0.04
Pip6b	N/S	1.1	N/S	0.5	N/S	0.08
Pip6c	N/S	1.9	N/S	1.6	N/S	2.0
Pip6d	N/S	2.0	N/S	2.0	N/S	1.9
Pip6e	N/S	1.1	N/S	1.6	N/S	1.5
Pip6f	N/S	1.8	N/S	1.2	N/S	0.3

In addition to immunohistochemical staining quantification, Δ23 splicing measured by RT-PCR and qRT-PCR (additional quantitative parameter as multiple treatments compared) and dystrophin protein restoration (western blotting) were also calculated for all Pip6-PMO conjugates. **Figure 4.4** displays representative images of RT-PCRs for each Pip6-PMO compound and is quantitatively represented by qRT-PCR (**Fig. 4.5**). There were no significant differences between treatments using qRT-PCR. Similar levels of Δ23 skipping were observed in the quadriceps of all 5-aa Pip6-PMO treated mice, and Pip6c- and Pip6d-PMO again caused the lowest skipping. Most conjugates resulted in similar Δ23 skipping in the diaphragm with the exception of Pip6f- and Pip5e-PMO, which exhibited the highest exon skipping (13% and 18% respectively, **Table 4.5**). Pip6d-PMO again caused the lowest skipping (5%). Pip6f-PMO caused the highest skipping in the heart (10%) whereas the shortened Pip6-PMOs (Pip6c- and Pip6d-) resulted in negligible exon skipping.

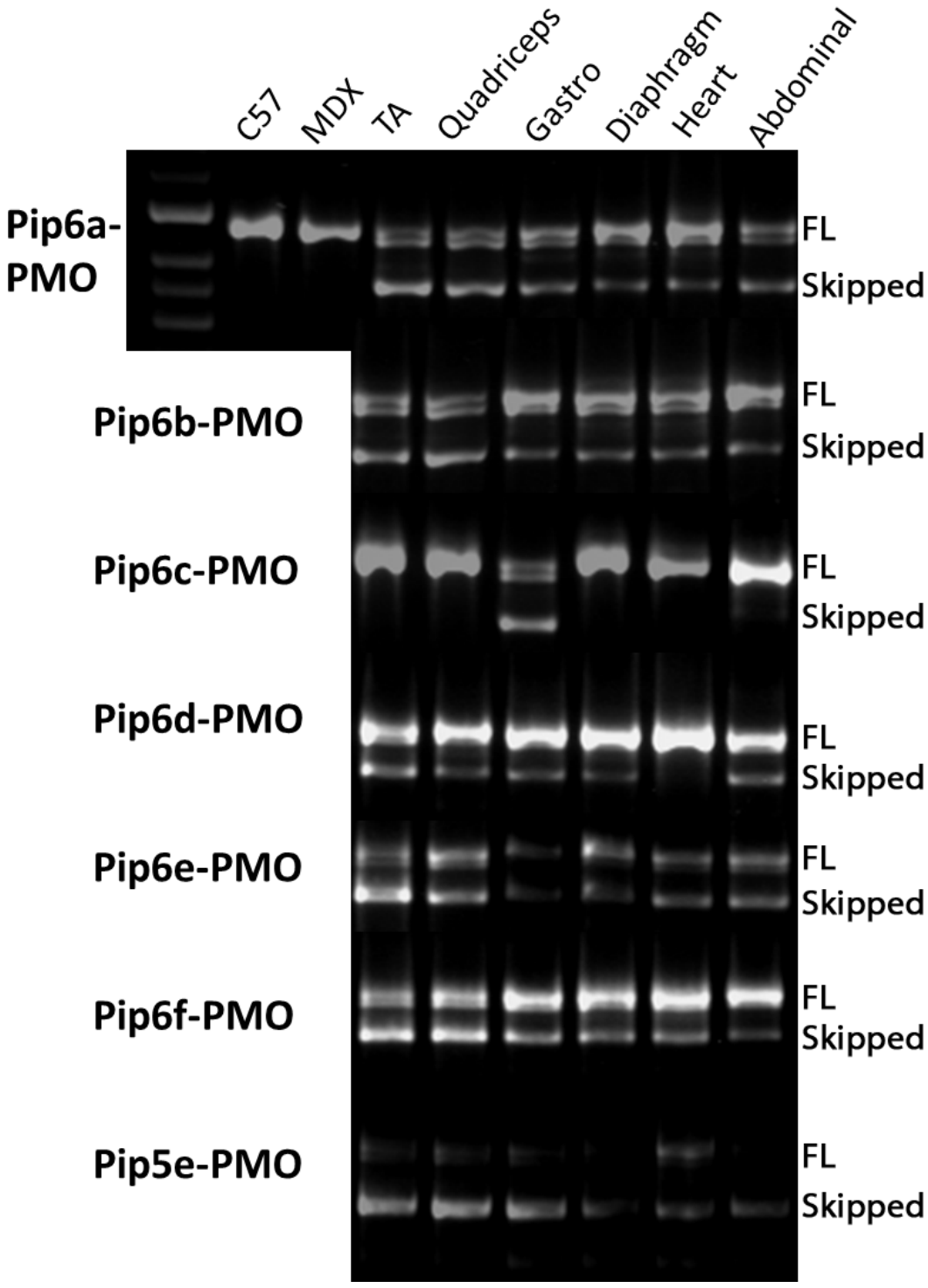

Figure 4.4.Dystrophin splicing in C57BL/10 control, *mdx* untreated and Pip6a-f-PMO treated mice measured by RT-PCR. Representative real time (RT)-PCR. images illustrate skipping of dystrophin transcript in *tibialis anterior*, quadriceps, gastrocnemius, diaphragm, heart and abdominal tissue for each Pip-6-PMO treatment. The top band represents full length dystrophin (FL) and the lower band represents the skipped transcript (Skipped).

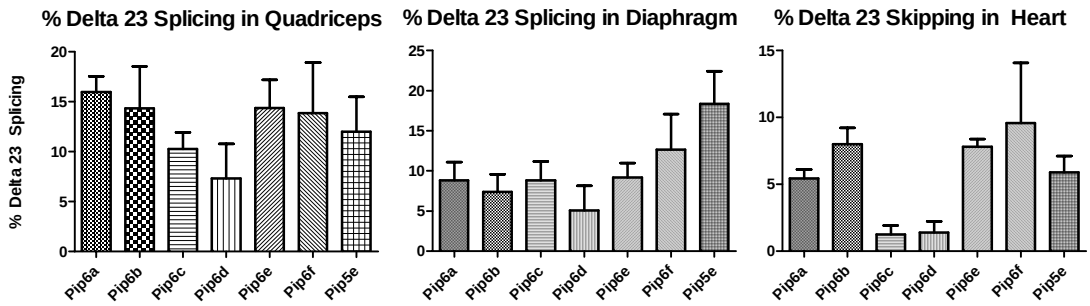

Figure 4.5. Dystrophin splicing in Pip6a-f-PMO treated mice measured by qRT-PCR. Percentage Δ23 exon skipping determined by quantitative real time (q-RT)-PCR in quadriceps, diaphragm and heart muscle. No statistically significant differences between groups (determined using One-way ANOVA, Tukey post-hoc test). N= 3 for each cohort.

Table 4.5. Quantitative real time (q-RT)-PCR mean values of Δ23 exon-skipping in quadriceps, diaphragm and heart of treated cohorts. N= 3 for each cohort.

qRT-PCR mean values	Quadriceps	Diaphragm	Heart
Pip6a	16	9	5
Pip6b	14	7	8
Pip6c	10	9	1
Pip6d	7	5	1
Pip6e	14	9	8
Pip6f	14	13	10
Pip5e	12	18	6

Western blots (**Fig. 4.6a**), performed on the tissues of each mouse, were quantified relative to a 50% and 10% C57BL/10 control (**Fig. 4.6b**). All 5-aa Pip6-PMO conjugates revealed high dystrophin protein restoration in the *tibialis anterior* and quadriceps muscles. Protein restoration in the *tibialis anterior* of Pip6b-PMO treated mice was significantly greater than untreated *mdx* mice. Similarly to immunohistochemical staining and qRT-PCR, the shortened conjugates (Pip6c and Pip6d) gave lower dystrophin protein restoration in the *tibialis anterior* and quadriceps. The levels of dystrophin restoration in the diaphragm were uniform for all treatments, with the exception of Pip5e-PMO which gave greater restoration. Similar to qRT-PCR skipping, Pip6b- and Pip6f-PMO conjugates gave the highest dystrophin protein restoration in the heart. The shortened Pip6-PMO conjugates again gave negligible dystrophin restoration in the heart (**Fig. 4.6**).

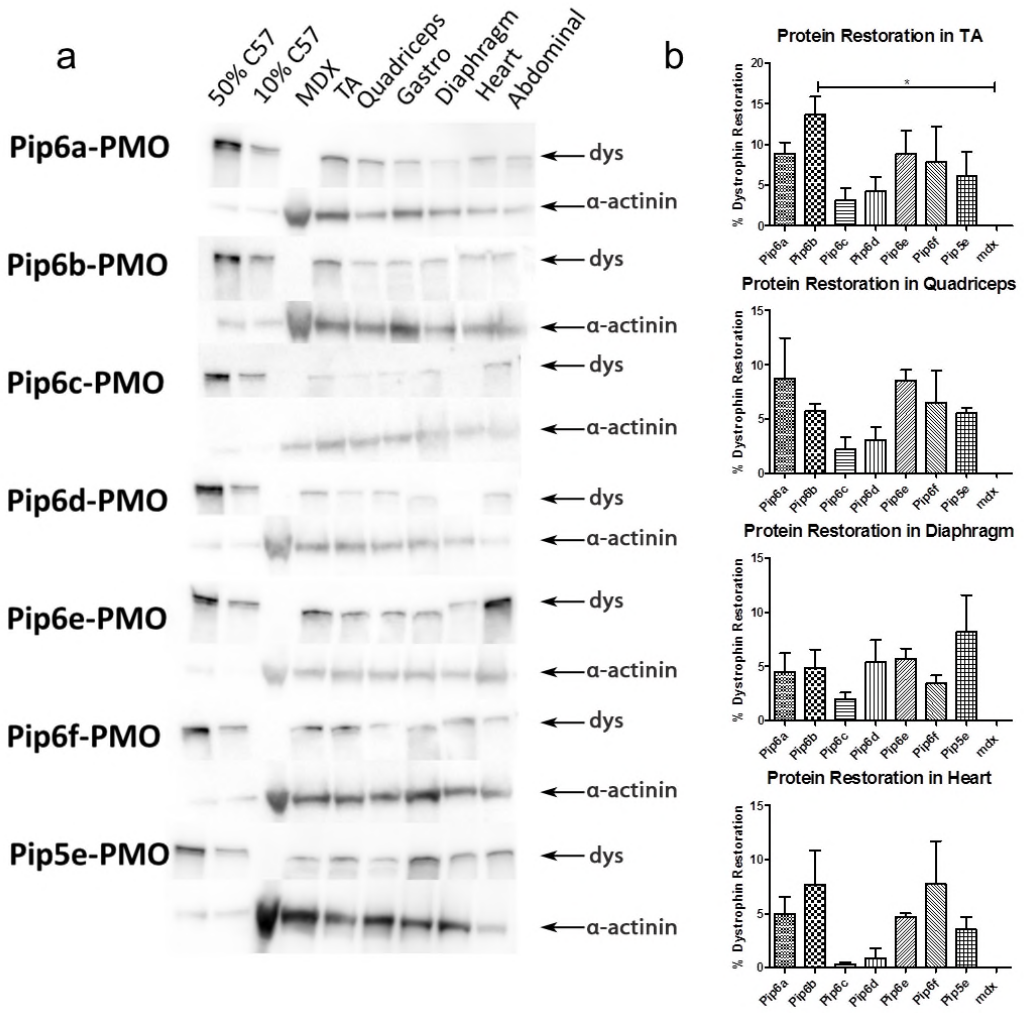

Figure 4.6. Dystrophin protein restoration in C57BL/10 control, *mdx* untreated and Pip6a-f-PMO treated mice. Representative western blot images for each treatment illustrating dystrophin protein restoration in *tibialis anterior*, quadriceps, gastrocnemius, diaphragm, heart and abdominal tissue for each treatment (a). Ten micrograms of total protein was loaded alongside 50% and 10% C57BL/10. Tissues from treated cohorts were quantified relative to C57BL/10 controls, and normalised to α-actinin loading control. Quantification of western blots for the *tibialis anterior*, quadriceps, diaphragm and heart tissues of Pip6a-f treatments (b). Statistical significance determined using One-way ANOVA, Tukey post-hoc test (*=p<0.001, **=p<0.01*=p<0.05). N= 3 for each cohort.**

To summarise, it is clear that *mdx* mice treated with the 5-aa core Pip6-PMOs (Pip6a, Pip6b and Pip6f-PMO) consistently had high dystrophin expression and exon skipping in *tibialis anterior*, quadriceps and heart muscles. Indeed the pattern of restoration was better than produced by the previous lead candidate, Pip5e-PMO. Pip6e-PMO exhibited similar trends to Pip5e-PMO in these tissues. By contrast the shortened Pip6-PMO derivatives revealed diminishing efficacy. These results show that the length of the hydrophobic core was crucial, not only for good heart dystrophin production, but also for skeletal muscle, such as quads and *tibialis anterior*.

Restoration of dystrophin associated protein complex

Dystrophin is an integral component of the DAG complex and comprises multiple binding domains for other DAG proteins; including nNOS and sarcoglycans. The absence of dystrophin at the sarcolemma causes disruption and mis-location of these proteins. It was therefore necessary to ensure that restoration of dystrophin by the successful 5-aa core Pip6's did indeed allow the re-localisation of 3 such DAG proteins, nNOS, α-sarcoglycan and β-sarcoglycan. Immunohistochemical staining was performed in the *tibialis anterior* muscle of C57BL/10, untreated *mdx* and Pip6a- Pip6b- Pip6e- and Pip6f-PMO treated mice. The treated *tibialis anterior* muscles had good expression of these proteins (**Fig. 4.7**) which denotes adequate re-localisation following just a single 12.5mg/kg administration.

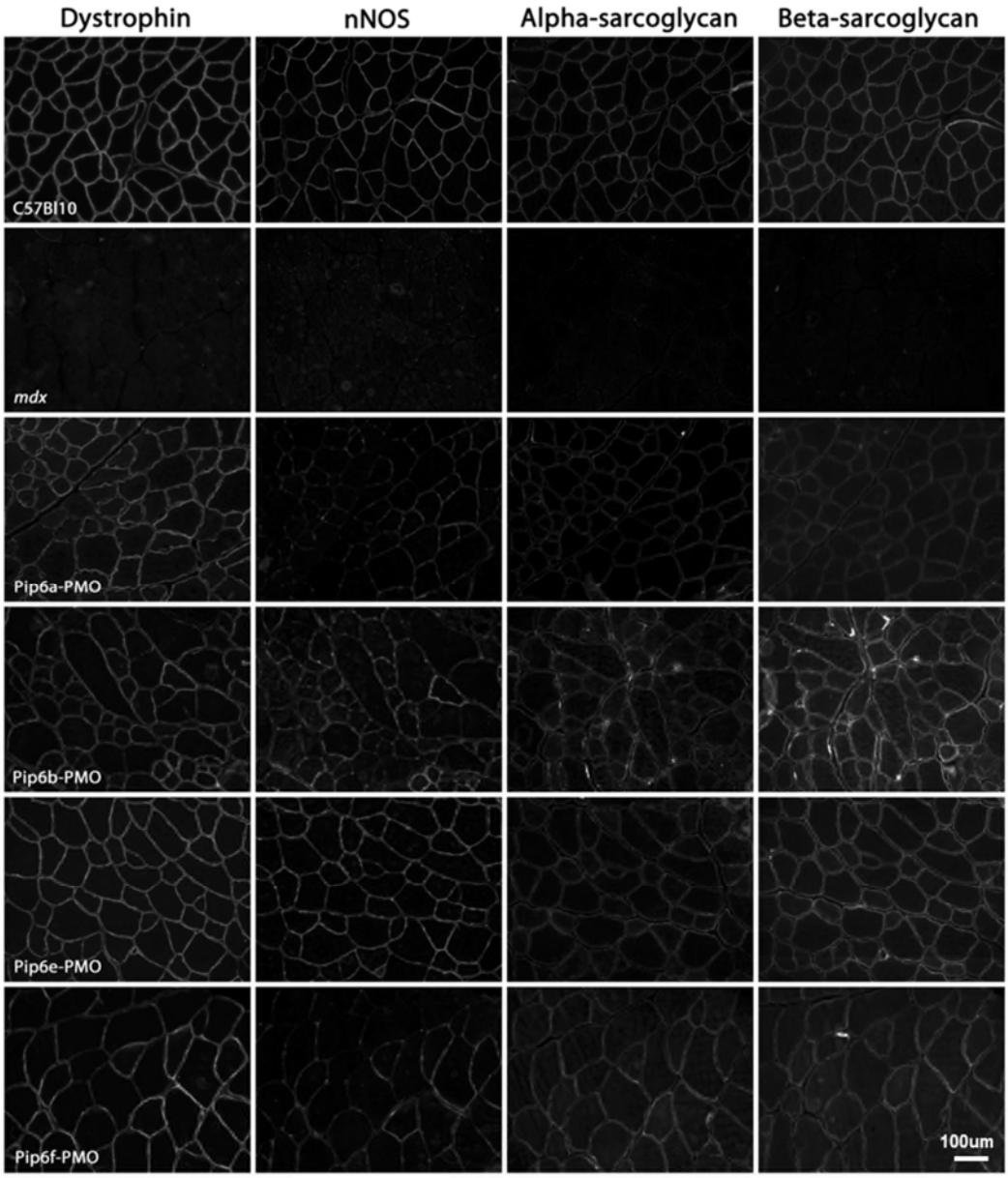

Figure 4.7. Immunohistochemical staining of dystroglycan complex proteins in C57BL/10 control, *mdx* untreated and the 5-aa hydrophobic core Pip6-PMO treated mice. Immunohistochemical staining of dystrophin, nNOS, alpha-sarcoglycan and beta-sarcoglycan in the *tibialis anterior* muscles of C57BL/10 control, untreated *mdx* and 5-aa Pip6-PMO treated *mdx* mice. For treatment, mice were administered a single 12.5 mg/kg tail vein injection of peptide-PMO and tissues were harvested 2 weeks later. The figure illustrates re-localisation of nNOS, alpha-sarcoglycan and beta-sarcoglycan for 5-aa core Pip6-PMOs. Scale bar: 100 µm.

Toxicity profile of Pip6-PMOs

As with any treatment, toxicity was of concern. Plasma samples were collected from treated mice, 2 weeks after the single 12.5 mg/kg administration and were sent, including their respective controls, to MRC Harwell for analysis. ALT and AST are enzymes associated with liver damage and are known to be up-regulated in *mdx* mice [183, 230]. Plasma levels of both ALT and AST for Pip6- and Pip5e-PMO treated mice were normalised to C57BL/10 levels (**Fig. 4.8**). BUN, another liver toxicity marker, remained largely unchanged following treatment (not significantly different to C57BL/10 or *mdx*). CK is a marker routinely used in DMD patients to predict the progression of the disease [250]. Again, CK was normalised to wild type levels following Pip6-PMO treatment. In conclusion these Pip6-PMO conjugates exhibited an exceptional toxicity profile at this dose in *mdx* mice.

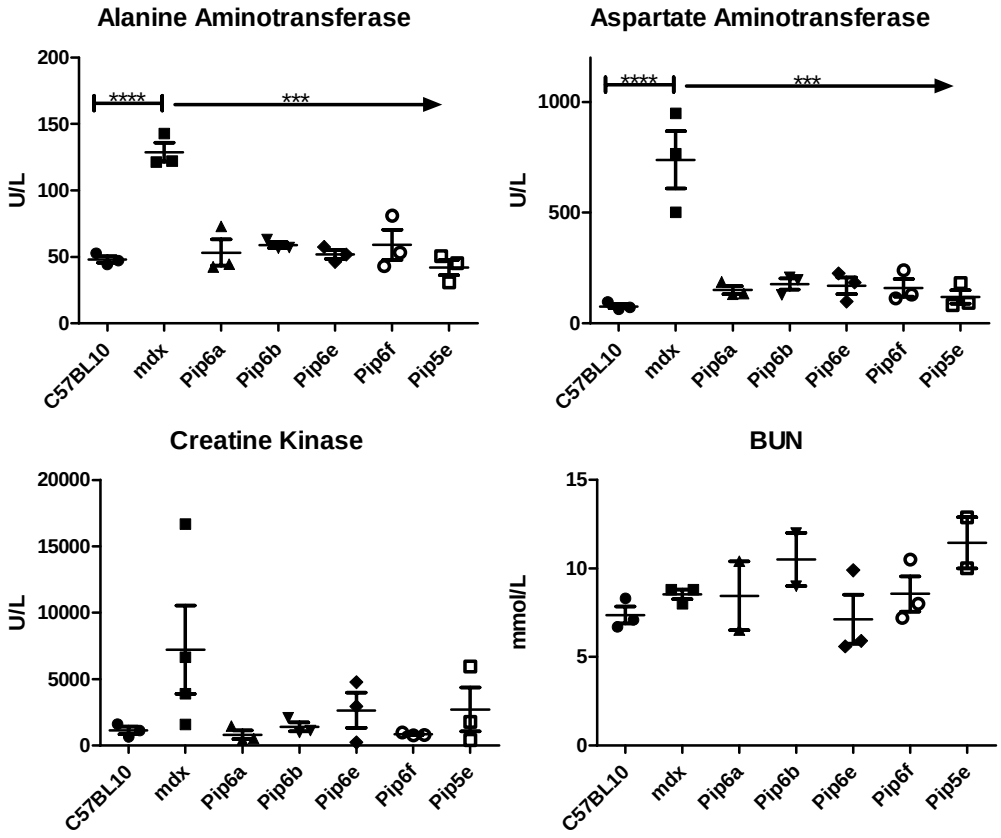

Figure 4.8.Toxicity markers assessed in plasma samples of C57BL/10 control, *mdx* untreated, Pip6-PMO and Pip5e-PMO treated *mdx* mice, following a single 12.5 mg/kg injection. Measurement of plasma alanine aminotransferase (ALT), aspartate aminotransferase (AST), creatine kinase and blood urea nitrogen (BUN) levels in C57BL/10 control mice compared to *mdx* untreated and treated mice. Treatment with Pip6-PMOs results in normalisation if ALT, AST and creatine kinase levels. BUN levels are unchanged. Statistical significance was determined using One-way ANOVA, Tukey post-hoc test (*=p<0.001, **=p<0.01*=p<0.05). N= 3 for each cohort.**

Additional alterations to length and core sequence reduces delivery efficacy

It was assumed from the Pip6a-to Pip6f-PMO analysis that the order of residues in the hydrophobic core did not affect the efficiency of dystrophin production in the heart, but that amino acid deletions to this region were critical. Interestingly, the development of Pip6e-PMO which involves the repositioning of an arginine residue from one of the flanking regions to the core was surprisingly well-tolerated. It was therefore decided that two further Pip6e-PMO derivatives would be synthesized (**Table 4.1**) to determine the effect of additions to the hydrophobic core (Pip6g-PMO), and establish whether the location of the arginine within the hydrophobic core (Pip6h-PMO) is critical to cardiac delivery efficacy. Pip6h-PMO was therefore an inversion of the Pip6e- hydrophobic region, similar in structure to the inversion of Pip5e core to yield Pip6a.

The changes to the hydrophobic core reduced dystrophin expression in all tissues, as observed in the immunohistochemical staining (**Fig. 4.9a**). The immunohistochemical staining quantification revealed very low dystrophin expression levels in the quadriceps (%RS 5%, **Table 4.6, Fig. 4.9b**), diaphragm (%RS- 13%) and heart (%RS- 0%) muscles of Pip6g-PMO treated mice. Dystrophin expression was also very low in heart tissue of the Pip6h-PMO (%RS- 3%) cohort (both conjugates the same as untreated *mdx* mice*,* **Table 4.7)**. Pip6h-PMO dystrophin expression in quadriceps and diaphragm were markedly better than Pip6g-PMO (%RS- 13% and 28% respectively) however were still substantially less efficient than the Pip6e-PMO parent peptide (for significance see **Table 4.8**).

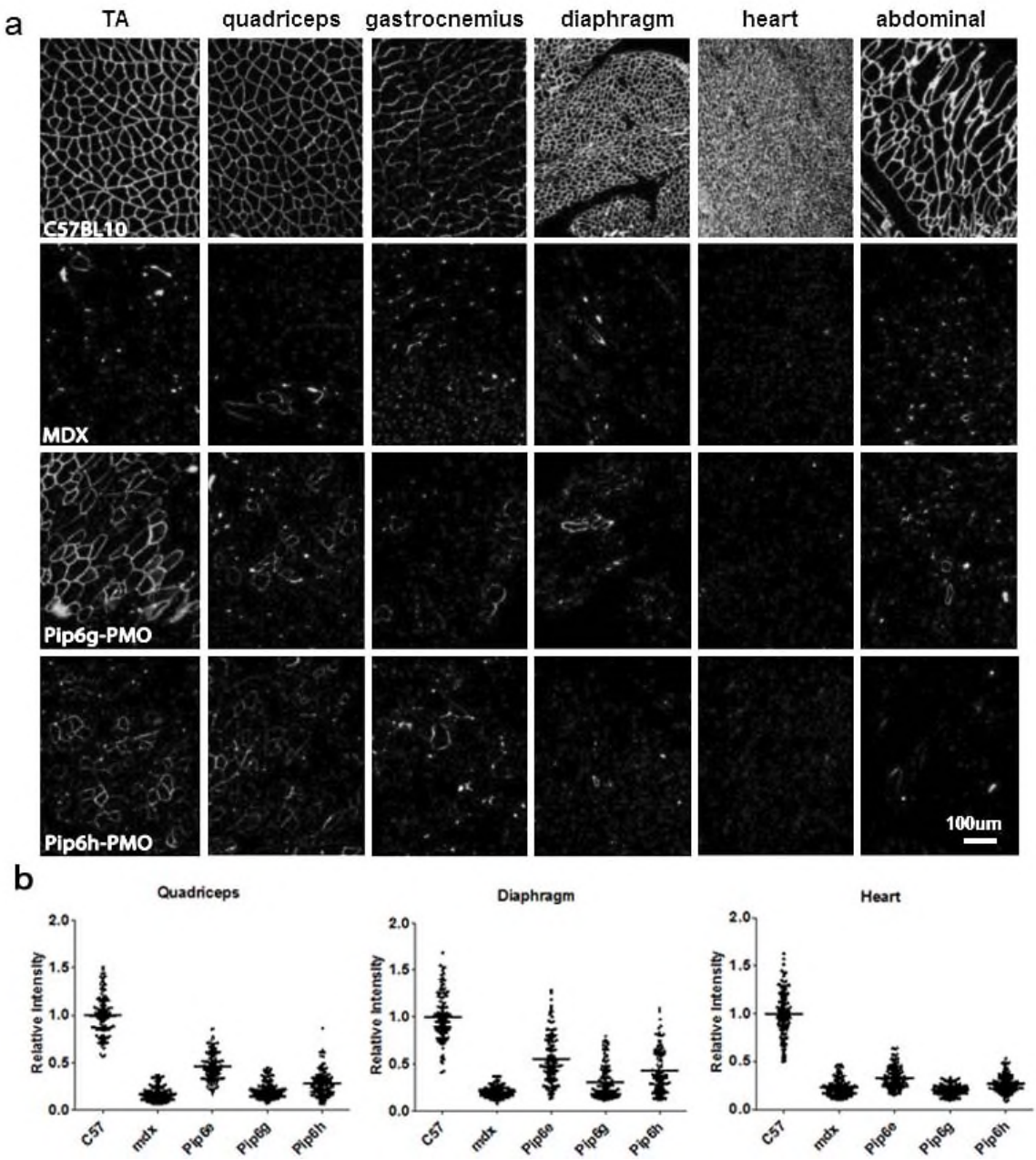

Figure 4.9. Immunohistochemical staining for dystrophin in C57BL/10 control, *mdx* untreated and Pip6g and Pip6h-PMO treated mice. Dystrophin immunostaining in *tibialis anterior*, quadriceps, gastrocnemius, diaphragm, heart and abdominal muscle from C57BL/10, *mdx* untreated and *mdx* treated mice are shown (a). Scale bar: 100 µm. Quantification of dystrophin immunohistochemical staining relative to laminin counter-stain in quadriceps, diaphragm and heart muscles of C57BL/10, *mdx* untreated and *mdx* treated mice (b). Quantification calculated using 120 regions of interest. This is calculated as the intensity of dystrophin relative to the corresponding intensity of laminin, normalised to C57BL/10 unexercised. The box plots show the normalised relative intensity values for each region of interest (for statistical significance see Tables 4.7 and 4.8). N= 3 for each cohort.

Table 4.6. Dystrophin recovery scores for immunohistochemical staining of quadriceps, diaphragm and heart in treated cohorts. N= 3 for each cohort.

Recovery scores	Quadriceps	Diaphragm	Heart
C57BL/10	100	100	100
Mdx	0	0	0
Pip6e	32	39	12
Pip6g	5	13	0
Pip6h	13	28	3

Table 4.7. Statistical significance table for immunohistochemical staining of Pip6e- and derivatives relative to untreated *mdx* mice. Significance for quadriceps, diaphragm and heart are shown. Statistics were calculated using a repeated measure, multi-level model (**=p<0.0001, ***=p<0.001, **=p<0.01, *=p<0.05). N= 3 for each cohort.**

	Quadriceps		**Diaphragm**		**Heart**	
C57BL/10	****	0.0000	****	0.0000	****	0.0000
Pip6e	****	0.0000	****	0.0000	N/S	0.09
Pip6g	N/S	0.4	N/S	0.08	N/S	0.6
Pip6h	*	0.03	***	0.0004	N/S	0.6

Table 4.8. Statistical significance table for immunohistochemical staining of Pip6e- derivatives and controls relative to Pip6e-PMO treated mice. Significance for quadriceps, diaphragm and heart are shown. Statistics were calculated using a repeated measure, multi-level model (**=p<0.0001, ***=p<0.001, **=p<0.01, *=p<0.05). N= 3 for each cohort.**

	Quadriceps		**Diaphragm**		**Heart**	
C57BL/10	****	0.0000	****	0.0000	****	0.0000
Mdx	****	0.0000	****	0.0000	N/S	0.08
Pip6g	****	0.0000	***	0.0003	*	0.03
Pip6h	**	0.008	N/S	0.0630	N/S	0.2

Similarly, the Pip6e-PMO derivatives expressed low dystrophin splicing in all tissues relative to the Pip6e-PMO parent peptide as illustrated in representative RT-PCR images (**Fig. 4.10a**) and qRT-PCR analysis (significantly lower than Pip6e-PMO, **Fig. 4.10b**). Dystrophin protein levels were exceptionally low, significantly in quadriceps and heart relative to Pip6e-PMO treated mice (**Fig. 4.11a&b**). Considering the results from all techniques, the data suggests that increased length of the hydrophobic core, and the location and number of arginine residues in the core were critical to increasing dystrophin restoration in heart.

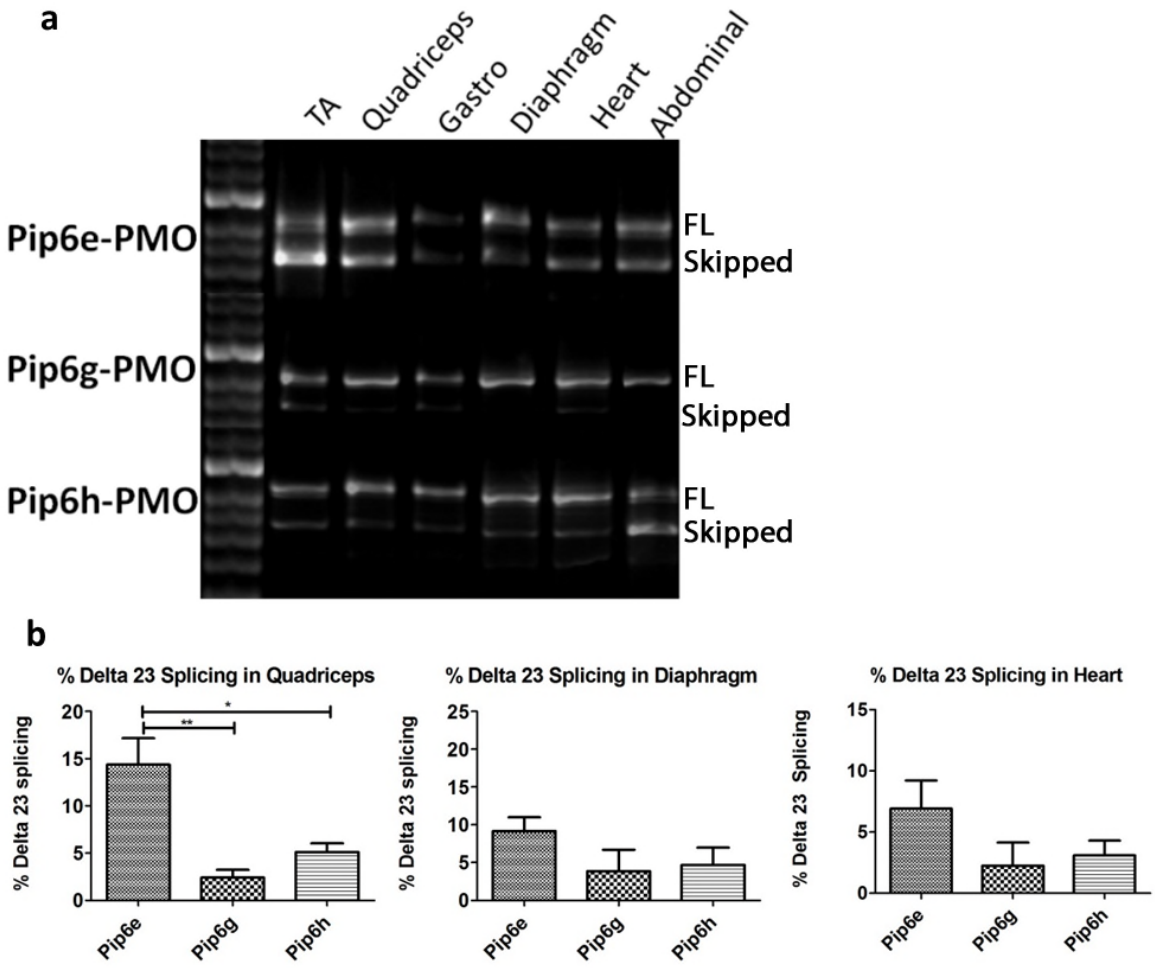

Figure 4.10. Dystrophin splicing in C57BL/10 control, *mdx* untreated and the Pip6e-PMO derivatives, Pip6g and Pip6h. (a) Representative real time (RT)-PCR images demonstrating exon skipping in treated cohorts. The top band represents full length dystrophin (FL) and the lower band represents the skipped transcript (Skipped). (b) Percentage Δ23 exon skipping as determined by quantitative real time (q-RT)-PCR in quadriceps, diaphragm and heart. Statistical significance determined using One-way ANOVA, Tukey post-hoc test (*=p<0.001, **=p<0.01*=p<0.05). N= 3 for each cohort.**

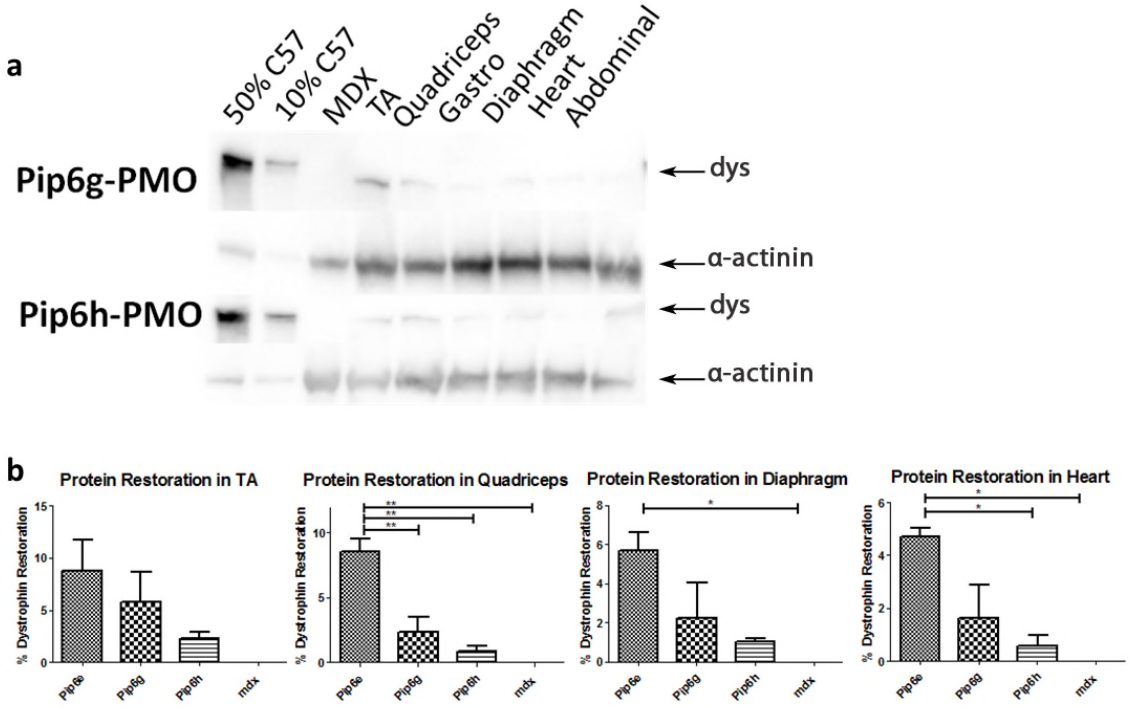

Figure 4.11. Dystrophin protein restoration in C57BL/10 control, *mdx* untreated and the Pip6e-PMO derivatives, Pip6g and Pip6h. (a) Representative western blot images for each treatment showing dystrophin protein restoration. (b) Quantification of western blots for the *tibialis anterior*, quadriceps, diaphragm and heart tissues of Pip6g and Pip6h were calculated. A western blot for each mouse for all treatments (n=3) was performed and quantified against a 50% and 10% C57BL/10 control which was averaged. Statistical significance determined using One-way ANOVA, Tukey post-hoc test (*=p<0.001, **=p<0.01*=p<0.05). N= 3 for each cohort.**

Discussion

In order to better elucidate the integral components of the hydrophobic core within the Pip series peptides, a number of Pip5e-PMO derivatives were designed. These included peptides maintaining the 5 aa hydrophobic core (Pip6a-, Pip6b-, Pip6e- and Pip6f-PMO), shortened peptides in which the core was truncated (Pip6c- and Pip6d-PMO) and additional modifications (Pip6g- and Pip6h-PMO). The 5-aa core modifications included the inversion of the hydrophobic region (Pip6a), substitution of tyrosine for iso-leucine (Pip6b), substitution of glutamine for arginine (Pip6e) and a scrambled hydrophobic core sequence (Pip6f). The shorter hydrophobic core peptides included 1 amino acid (Pip6c) and 2 amino acid removal (isoleucine and tyrosine deleted; Pip6d). Further modifications were made including additions to the hydrophobic core (Pip6g-PMO), and alterations to the location of the arginine (Pip6h-PMO).

In short, *mdx* mice treated with the 5-aa core PMOs (Pip6a, Pip6b, Pip6e and Pip6f-PMO) demonstrated comparable or improved dystrophin production and exon skipping in *tibialis anterior*, quadriceps and heart muscles over the previous lead candidate, Pip5e-PMO. Conversely the shortened core peptides (Pip6c- and Pip6d-PMO) revealed a reduction in activity, as did the modified Pip6e-PMO derivatives (Pip6g- and Pip6h-PMO).

Most importantly, this study demonstrates that the 5-aa core length was essential for improved skeletal muscle activity and cardiac delivery. Consequently, when amino acids were added or removed from this core, it reduced activity in both skeletal and cardiac muscle. As previously mentioned, B-PMO is an arginine rich (RXR) peptide which exhibits highly efficient splicing activity in skeletal muscle, and therefore the arginine rich flanking regions of Pip-PMOs had been attributed to the skeletal muscle activity observed [204]. However, Pip6c- and Pip6d-PMOs, which comprise the exact flanking regions as the 5-aa core peptides, exhibited a decrease in activity and dystrophin production in all muscle groups, thus revealing the significance of the central core. It seems highly logical that serial deletions to the core incrementally reduced splicing efficiency (i.e. Pip6d- was worse than Pip6c-PMO) as this in turn reduced hydrophobicity [251]. It is generally agreed in the CPP field that hydrophobicity facilitates binding to the cell membrane thus enabling the translocation of peptide-conjugated AO into the cell. Many studies support the notion that CPPs are internalised via either clathrin mediated endocytosis or macropinocytosis [252] and indeed, Lehto *et al.* recently demonstrated that Pip6a-PMO is translocated via energy- and caveolae-mediated endocytosis in skeletal muscle and via clathrin mediated endocytosis in cardiomyocytes [253].

From the 5-aa core data, it appeared as though the sequence of the central core was not essential to maintain the heart dystrophin production, since an inverted sequence (Pip6a), a single substitution of an equally

hydrophobic residue (Pip6b), and a scrambled sequence (Pip6f) were at least as active as Pip5e-PMO. However, it does seem that introducing a cationic amino acid such as arginine into the core, and/or the position of the arginine residue was important. Pip6e-PMO, with an arginine residue in the core, was admittedly the least effective 5-aa peptide screened. The relocation of the arginine residue into the core resulted in the alignment of a hydrophobic X residue adjacent to the core (X-YRFLI). Other peptides with similar changes, such as Pip6h-PMO (X-ILFRY core) and the double arginine core conjugate Pip6g-PMO (X-YRFRLI-X core), resulted in further diminution in heart activity. Although the reason behind this observation is unknown, it bears similarities with the structure/activity study performed with oligo-arginines. It was established that spacing A-Hex and/or B-Ala between the arginine residues rendered the CPPs stable in serum and improved splice correction (attributed to an ability to escape the endosome) [217] [206]. Perhaps the hydrophobic core also required flanking between arginine residues, suggesting that the precise spacing of arginines incurred a spatial dynamic that was integral to the activity of these Pip-peptides.

Ultimately, this study has identified 3 Pip6-PMOs with improved delivery capacity over the previous lead peptide, Pip5e-PMO. However, only one could be utilised for future cardiac function studies. When the dystrophin splicing and protein restoration techniques were considered Pip6a-, Pip6b- and Pip6f-PMO all displayed good recovery scores for immunohistochemical staining. However, following closer examination of

the qRT-PCR and western blots, Pip6f-PMO consistently revealed the highest splicing and protein expression thus identifying this peptide-AO as the candidate for future cardiac experimentation.

The work in this **Chapter** focussed on the dystrophin restorative capacity of Pip-PMOs and did not reveal any physiological improvement as a result of restoration. It is well documented that the absence of dystrophin causes the dysregulation of a number of cellular processes [254], as well as progressive LV dysfunction, leading to dilated cardiomyopathy [73, 74]. It was therefore important to measure whether dystrophin improved the dystrophic heart at a molecular and physiological level, as assessed by qRT-PCR, EBD infiltration, Masson's trichrome staining and MRI. The experiments will be presented in the following **Chapter 5**.

Chapter 5. Long-term administration of Pip6f-PMO prevents exercised induced deterioration in heart function

Introduction

DMD patients require heart targeting therapy

The onset of cardiomyopathy manifests at about 10 years of age and is found in most patients by 20 years of age [8]. Although respiratory complications are the major cause of death amongst DMD patients, cardiomyopathy is the next contributor to mortality [20]. Thus a treatment that targets both skeletal and cardiac muscle is required in order to treat this disorder. The ability to restore dystrophin in skeletal muscle and the heart is made possible with the advent of CPPs and the further development of the Pip series which are capable of infiltrating the heart. Following on from **Chapter 4,** which revealed the dystrophin restorative capacity of Pip-PMOs, the objective of this work was to assess their physiological effect on heart function.

Exercise progresses the cardiac phenotype

It has been postulated that improvements in skeletal muscle function (following dystrophin restoration) in the absence of cardiac dystrophin may worsen the cardiac disease progression owing to increased exercise capacity. Two independent studies, the first utilising naked PMO [197] and the second whereby the skeletal muscle phenotype was transgenically corrected [255], documented increased locomotor activity. They further observed the onset of severe cardiac histopathology, a fivefold increase in

cardiac injury and dilated cardiomyopathy. In addition, the results in **Chapter 3** indicated that dystrophin restoration of the diaphragm alone did not improve cardiac function. Thus treatment of DMD requires the correction of dystrophin in both skeletal and cardiac muscle in order to prevent and/or stabilise cardiac function, particularly in the event of exercise.

Understanding the effect of exercise on the dystrophic heart is clinically relevant due to studies advocating physical exercise in the 'use it or lose it' campaign, to prevent the onset of skeletal muscle deterioration [256-258]. Whilst this idea is relevant for the skeletal muscle aspect of the disease, the cardiac aspect has only recently been investigated in the *mdx* model [259]. The specific effect of inactivity/activity on skeletal muscle and the consequential cardiac involvement was investigated and revealed that inactivity worsened muscle weakness and increased susceptibility to contraction induced injury in *mdx* mice but was improved with voluntary exercise. More importantly however, it was found that the increased activity decreased LV function (ejection fraction and shortening fraction) indicating deterioration in the cardiac phenotype. These observations are concerning as the majority of new drugs in clinical trials, including 'naked' AO chemistries, do not restore dystrophin in the heart.

Rationale for study

Results in **Chapter 4** revealed three candidate Pip6-PMO conjugates with improved cardiac dystrophin restoration over the previous lead peptide, Pip5e-PMO, of which Pip6f-PMO displayed the greatest dystrophin expression. This structure-activity study was limited to dystrophin restoration, DAG re-localisation and toxicity and did not include an assessment of physiological improvement, such as cardiac function and phenotype. Therefore a repeated, low dose administration regimen was used to assess the maximal level of dystrophin restoration achievable in heart, and to determine whether this was sufficient to maintain or improve cardiac function and sarcolemmal integrity. As improvements in the skeletal muscle phenotype results in an increase in locomotor activity, which has a detrimental knock-on effect on cardiac pathology, an exercise regimen aimed at moderately increasing the cardiac workload was implemented. This would firstly reveal the impact of exercise on the untreated dystrophic heart and secondly indicate whether the Pip6f-PMO treatment would restore a sufficient amount of dystrophin in the heart to enable it to withstand increased cardiac workload.

Synopsis of findings

The repeat, low dose administration regimen resulted in considerable restoration of total dystrophin protein in skeletal muscle (between 58-101%) and 28% protein restoration in heart. In addition, the moderate exercise in the untreated *mdx* mice resulted in reduced contractility and larger hearts, which denote dilated ventricles and cardiac hypertrophy.

Treatment with Pip6f-PMO preserved these cardiac parameters and prevented deterioration of the cardiac phenotype even with exercise. Furthermore, gene expression levels of markers of oxidative stress and injury indicated a stabilised cardiac phenotype in the Pip6f-PMO treated cohort.

These findings have direct clinical relevance as they suggest that increased activity in DMD patients may be detrimental to the heart, further heightening the importance of cardiac dystrophin restoration in DMD patients.

Methodology

Five different cohorts were required for this study, all of which utilised male mice; untreated unexercised *mdx* (*mdx*^{unex}; n=10), untreated exercised *mdx* (*mdx*^{ex}; n=9), C57BL0 unexercised (C57BL/10^{unex}; n=10), C57BL/10 exercised (C57BL/10^{ex}; n=10) and Pip6f-PMO treated exercised *mdx* mice (Pip6f-PMO^{ex}; n=10). For the treated cohort, 12 week old mice were injected (via the tail vein) with Pip6f-PMO prepared in 0.9% saline solution at a dose of 10 mg/kg (**Fig. 5.1**, bottom). These mice received 4 daily IV administrations (just prior to first exercise bout) followed by 5 bi-weekly doses. The exercise regimen commenced at 12 weeks of age and mice were exercised 3 times every 2 weeks for a 12 week period (**Fig. 5.1**, top). Mice were allowed 2 minutes for familiarisation. For the first 2 exercise days, mice were run at a speed of 5 m/min which was increased in 1 m/min increments to 10 m/min. For the following 6 exercise sessions, the speed was incrementally increased to 12 m/min over a 45 minute period. A speed of 12 m/min for 45 minutes was adhered to for the remaining exercise sessions. Mice were monitored closely for behavioural changes and also to ensure the welfare of the animals. All mice underwent cardiac cine-MRI at 24 weeks of age. Following MRI, mice were sacrificed by CO_2 inhalation, and tissues harvested and snap-frozen in dry-ice cooled isopentane before storage at -80^{0}C. Three to 4 mice from each cohort were injected IP with 1% EBD (10 µl/gram of mouse; 300 µl per 30 g mouse) and the *tibialis anterior*, diaphragm and heart tissues were harvested 20 hours later.

The diaphragm, heart, *tibialis anterior*, intercostal and sternomastoid muscles were analysed for dystrophin using standardised techniques; immunohistochemical staining, RT-PCR and western blot. The expression of cardiac injury and oxidative stress markers were assessed by qRT-PCR. Heart samples were also cryosectioned and stained with Masson's trichrome to assess the deposition of collagen/fibrosis. Sequential images of the section were taken at 10x magnification and manually reconstructed using Adobe Photoshop CS5 so that a consolidated image of the entire section could be viewed. The surface area of Masson's trichrome staining was quantified relative to the total surface area of the section using ImageJ. Tissues from EBD injected mice were cryosectioned washed and mounted. Similarly to Masson's trichrome staining, images of the entire section of EBD-stained tissues were taken, manually reconstructed and quantified. Plasma samples from each cohort were sent to the Mary Lyon Centre Clinical Pathology Lab (MRC, Harwell, UK) for toxicological analysis.

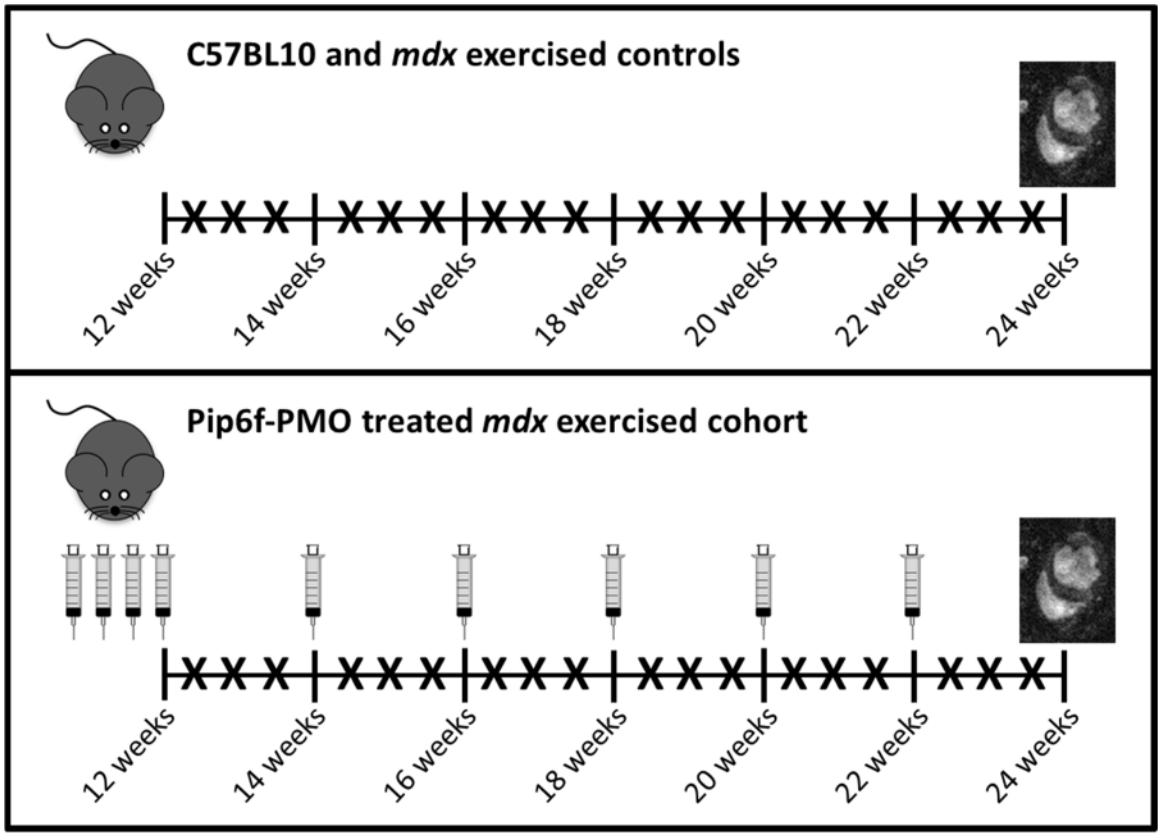

Figure 5.1. Schematic illustrating the administration and exercise regimen. The exercise regime for the *mdx* and C57BL/10 cohorts (top) commenced at 12 weeks of age and continued for a further 12 weeks; 3 bouts of 45 minute exercise every 2 weeks. At 12 weeks of age the Pip6f-treated cohort received 4 daily administrations of 10 mg/kg Pip6f-PMO followed by biweekly administrations. This cohort was exercised at the same time intervals as the untreated cohorts. All mice underwent cine-MRI at 24 weeks of age. X symbolises exercise bouts, image of syringe symbolises administration of peptide-PMO

Results

Pip6f-PMO treatment restored dystrophin in skeletal muscle and heart

Dystrophin splicing and protein expression in the Pip6f-PMO^{ex} cohort was determined. Immunohistochemical staining of the diaphragm, heart, *tibialis anterior*, intercostal muscles and sternomastoid muscles demonstrated widespread and high levels of dystrophin restoration **(Fig. 5.2)**. **Figure 5.3** shows the full extent of restoration and distribution in the hearts of treated mice. This was confirmed by quantification of dystrophin fluorescence relative to laminin co-stain **(Fig. 5.4)**. Dystrophin recovery scores showed pronounced dystrophin restoration in skeletal muscles (between 74-104%) and 46% in cardiac muscle.

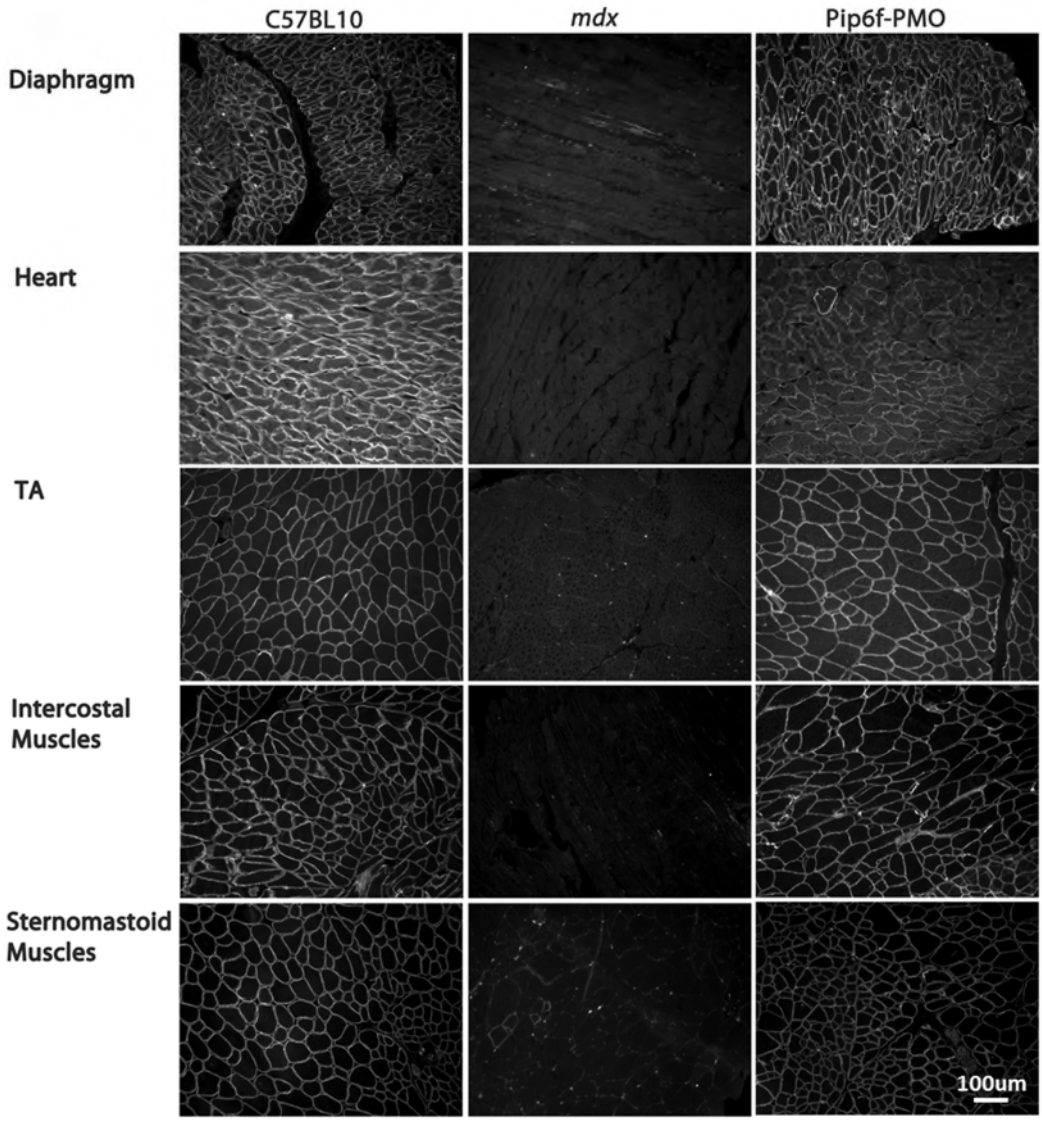

Figure 5.2. Immunohistochemical staining of dystrophin following Pip6f-PMO treatment. Dystrophin immunohistochemical staining of dystrophin protein in C57BL/10^{ex}, *mdx*^{ex} and Pip6f-PMO^{ex} *mdx* mice in the diaphragm, heart, *tibialis anterior*, intercostal and sternomastoid muscles. Pip6f-PMO treatment resulted in widespread and high expression of dystrophin in all tissues. Scale bar: 100 µm.

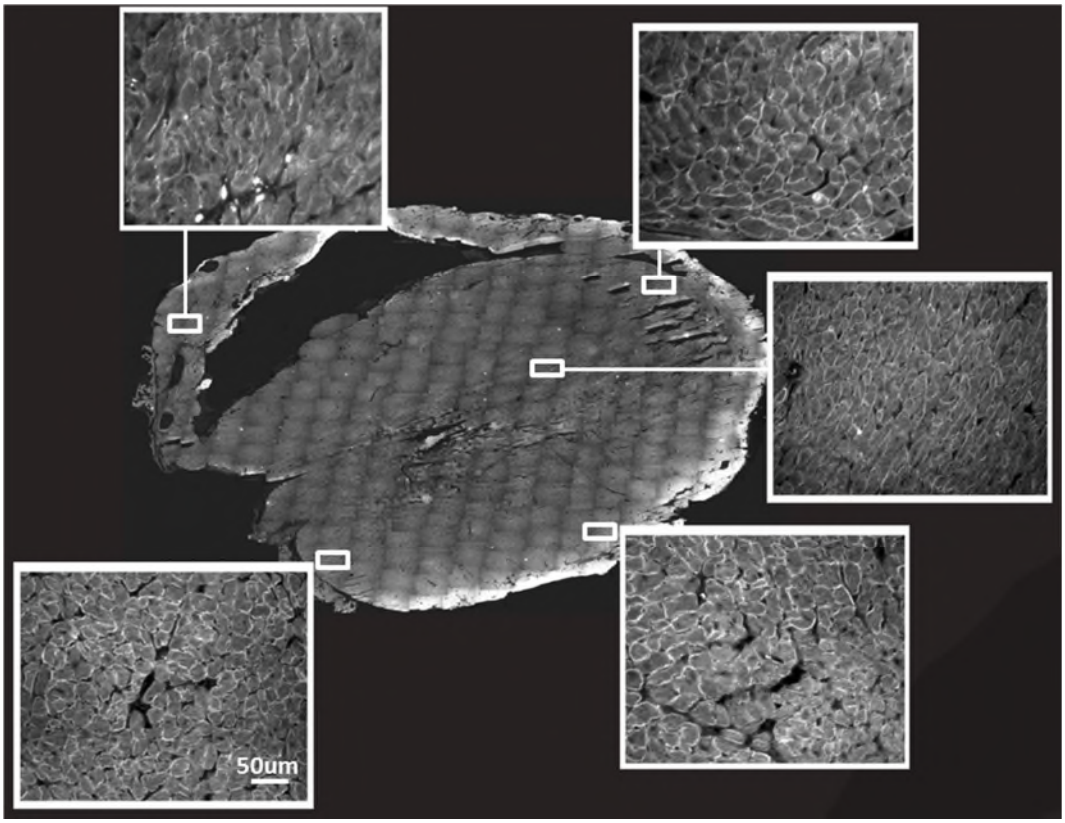

Figure 5.3. Immunohistochemical staining of Pip6f-PMO treated heart. The centre image illustrates macro-histology with inserts which display higher magnification of the designated areas. The inserts were taken from random areas of the heart to display the extent of dystrophin restoration. For the macro-histology image, 20X magnification images were taken and manually reconstructed to attain a consolidated image of the entire section. Scale bar for zoomed areas: 50 µm.

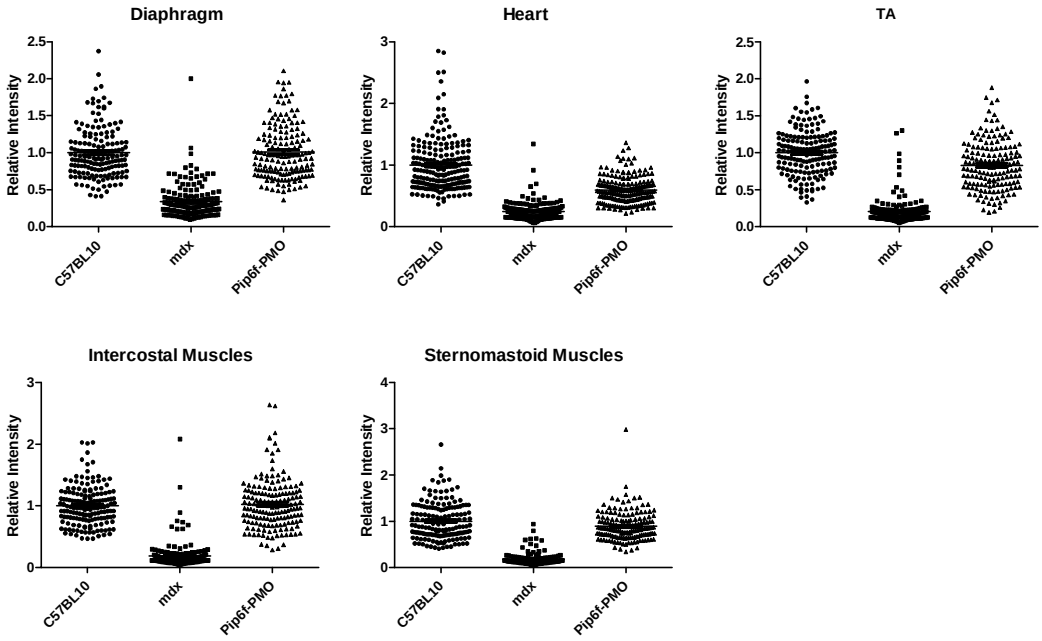

Figure 5.4. Immunohistochemical staining quantification of dystrophin following Pip6f-PMO treatment. Dystrophin immunohistochemical staining quantification of dystrophin protein in C57BL/10^{ex}, *mdx*^{ex} and Pip6f-PMO^{ex} *mdx* mice in the diaphragm, heart, *tibialis anterior*, intercostal and sternomastoid muscles. Dystrophin expression was calculated relative to laminin co-stain for diaphragm, heart, *tibialis anterior*, intercostal and sternomastoid muscle. Quantification used 120 regions of interest, calculated as the intensity of dystrophin relative to the corresponding intensity of laminin, normalised to C57BL/10 unexercised. The box plots show the normalised relative intensity values for each region of interest.Pip6f-PMO treatment resulted in widespread and high expression of dystrophin in all tissues. N= 4 for each cohort.

The RT-PCR **(Fig. 5.5**) and western blot **(Fig. 5.6**) analyses for the Pip6f-PMO^{ex} cohort exhibited similar results, with complete skipping of the full-length transcript for the diaphragm, *tibialis anterior*, intercostal and sternomastoid muscles and approximately 50% skipping in heart. Quantification of western blots revealed between 58-100% restoration in skeletal muscles and 28% dystrophin protein restoration in heart. This low-dose repeat administration protocol was therefore capable of successfully restoring a considerable amount of dystrophin in a variety of muscles, most remarkably in the heart.

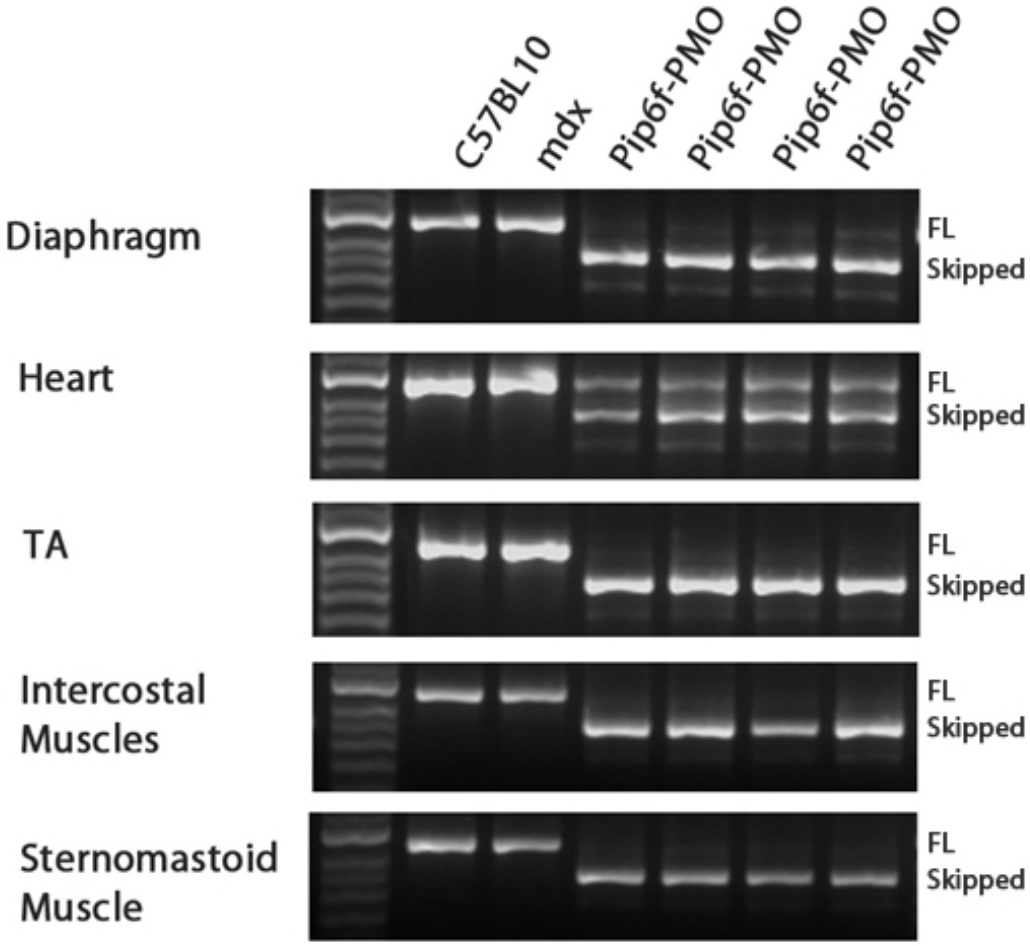

Figure 5.5. Dystrophin splicing in Pip6f-PMO treated mice relative to *mdx* untreated and C57BL/10 control groups. Representative images of reverse-transcriptase (RT) PCR illustrating Δ23 splicing in diaphragm, heart, *tibialis anterior*, intercostal and sternomastoid muscles of Pip6f-PMO treated cohort. The top band represents full length dystrophin (FL) and the lower band represents the skipped transcript (Skipped). Figure shows complete Δ23 splicing in diaphragm, *tibialis anterior*, intercostal and sternomastoid muscles, and approximately 50% splicing in heart. N= 4 for each cohort.

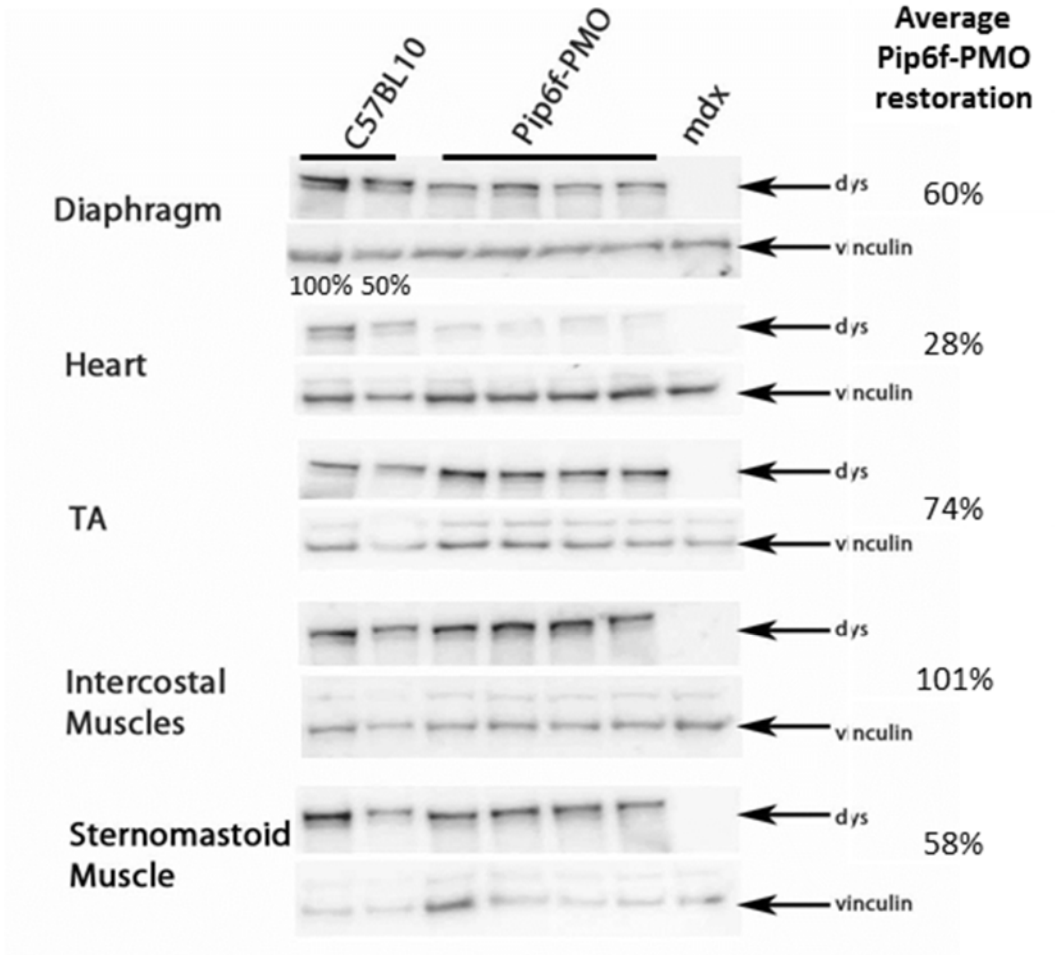

Figure 5.6. Dystrophin protein restoration in Pip6f-PMO treated mice relative to *mdx* untreated and C57BL/10 control groups. Representative images of western blots splicing in diaphragm, heart, *tibialis anterior*, intercostal and sternomastoid muscles of Pip6f-PMO treated mice. Ten-15 µg of protein was loaded and quantified relative to vinculin loading control. Average dystrophin restoration levels in treated mice shown relative to C57BL/10 cohorts. N= 4 for each cohort.

Exercise caused deterioration in cardiac function in untreated *mdx*^{ex} mice

The exercise regime moderately increased the workload on the heart. Mice underwent cine-MRI at 24 weeks of age (5 days following their last exercise bout for exercised cohorts). All cardiac parameters were normalised to body weight with the exception of EF. The interaction effect between exercise and mouse groups (*mdx* and C57BL/10) was significant for the majority of cardiac measurements, as determined by 2-way ANOVA (see **Table 5.1**). In short, the exercise in the *mdx* cohort resulted in an increase in average mass, EDV and ESV with consequential decrease if EF (**Table 5.2**). These events suggest the onset hypertrophy (visually illustrated in **Fig. 5.7**) and reduced contractility of the heart (ventricles dilated). The heart rate was also higher (with resultant increase in CO), which possibly indicates a compensatory mechanism to deal with the increased work load. Conversely, exercise had the opposite effect on C57BL/10 mice, whereby the EDV and ESV were smaller denoting a slight improvement in contractility.

This is complimented by the One-way ANOVA whereby the *mdx*^{ex} and C57BL/10^{ex} mice were directly compared (*mdx*^{ex} mice: LV ESV larger, with reduced LV EF, RV EDV and ESV larger with consequential decrease in EF; **Table 5.2** and **Fig 5.8**).

Table 5.1. Statistical significance of cine-MRI measurements, showing the interaction between exercise and mouse groups (*mdx,* C57BL/10 and B-PMO treated mice) following 2-way ANOVA. N= 10 for each cohort.

	Measurements	**Interaction**
LV/BW	Average Mass	0.002
	End Diastolic Volume	0.007
	End Systolic Volume	0.02
	Stroke Volume	N/S
	Cardiac Output	0.003
LV%	Ejection Fraction	0.04
RV/BW	End Diastolic Volume	0.004
	End Systolic Volume	0.009
	Stroke Volume	0.05
	Cardiac Output	0.001
RV%	Ejection Fraction	N/S
BPM	Heart Rate	0.03
Gram	Body Weight	N/S

Table 5.2. Values for all left (LV) and right ventricle (RV) cardiac measurements for Pip6f-PMO study. All parameters are normalised to body weight (BW). The ejection fraction is represented as a percentage and heart rate calculated as beats per minute (BPM). Weights are in grams. Statistical significance was determined using ANOVA followed by Tukey Post-Hoc Test (^{TU}ANOVA). Games-Howell Post-Hoc Test was also performed to correct for variance heterogeneity (^{GH}ANOVA). Each cohort is compared to all other cohorts. (* significantly different to C57^{unex}, + significantly different to C57^{ex}, # significantly different to *mdx*^{unex}, / significantly different to *mdx*^{ex} and ~ significantly different to Pip6f-PMO^{ex}. Number of symbols denotes significance i.e. ***=p<0.001, **=p<0.01*=p<0.05). Means ± SEM. N= 9-10 for each cohort.

		C57 Unex	SEM	C57 Ex	SEM	*mdx* Unex	SEM	*mdx* Ex	SEM	Pip6f-PMO Ex	SEM
Left ventricle/ body weight	Average Mass^{GH}	3.75	± 0.2	3.45$^{/}$	± 0.07	3.43 $^{/}$	± 0.08	3.91 $^{\sim\#+}$	± 0.1	3.45 $^{/}$	± 0.05
	End Diastolic Volume^{TU}	1.96	± 0.1	1.67	± 0.06	1.77	± 0.05	2.10	± 0.2	1.88	± 0.03
	End Systolic Volume^{TU}	0.74	± 0.1	0.50 $^{/}$	± 0.04	0.65	± 0.08	0.90 $^{+}$	± 0.2	0.71	± 0.04
	Stroke Volume^{GH}	1.22	± 0.04	1.17	± 0.05	1.12	± 0.04	1.20	± 0.06	1.17	± 0.03
	Cardiac output^{TU}	0.52$^{\#}$	± 0.02	0.48	± 0.02	0.42$^{/*}$	± 0.03	0.52 $^{\#}$	± 0.02	0.44	± 0.01
Left ventricle%	Ejection Fraction^{TU}	64	± 2.7	70$^{/}$	± 2.3	64	± 3.6	59^{+}	± 2.5	62	± 1.9
Right ventricle/ body weight	End Diastolic Volume^{TU}	1.64	± 0.04	1.52 $^{/}$	± 0.08	1.53$^{/}$	± 0.05	1.79 $^{+\#}$	± 0.08	1.68	± 0.06
	End Systolic Volume^{TU}	0.45$^{//}$	± 0.02	0.38 $^{\#\#///\sim}$	± 0.03	0.55 $^{++}$	± 0.03	0.66 $^{**+++}$	± 0.05	0.54 $^{+}$	± 0.04
	Stroke Volume^{GH}	1.18$^{\#}$	± 0.04	1.14	± 0.07	0.98*	± 0.04	1.13	± 0.05	1.14	± 0.03
	Cardiac output^{TU}	0.50 $^{\#\#\#}$	± 0.02	0.47 $^{\#}$	± 0.03	0.37 $^{***//+}$	± 0.03	0.49 $^{\#\#}$	± 0.02	0.43	± 0.01
Right ventricle %	Ejection Fraction^{TU}	72 $^{\#\#//}$	± 1	75$^{\#\#\#///\sim}$	± 1.7	64 $^{**+++}$	± 1.7	63 $^{**+++}$	± 1.7	68 $^{+}$	± 1.2
BPM	Heart Rate^{TU}	427	± 15.4	410	± 11	374	± 20.2	433	± 12.4	377	± 13.2
Gram	Body weight^{GH}	32.40	± 0.8	31.00$^{/\sim\sim}$	± 0.3	32.40	± 1.2	33.33^{+}	± 0.6	33.90^{++}	± 0.5

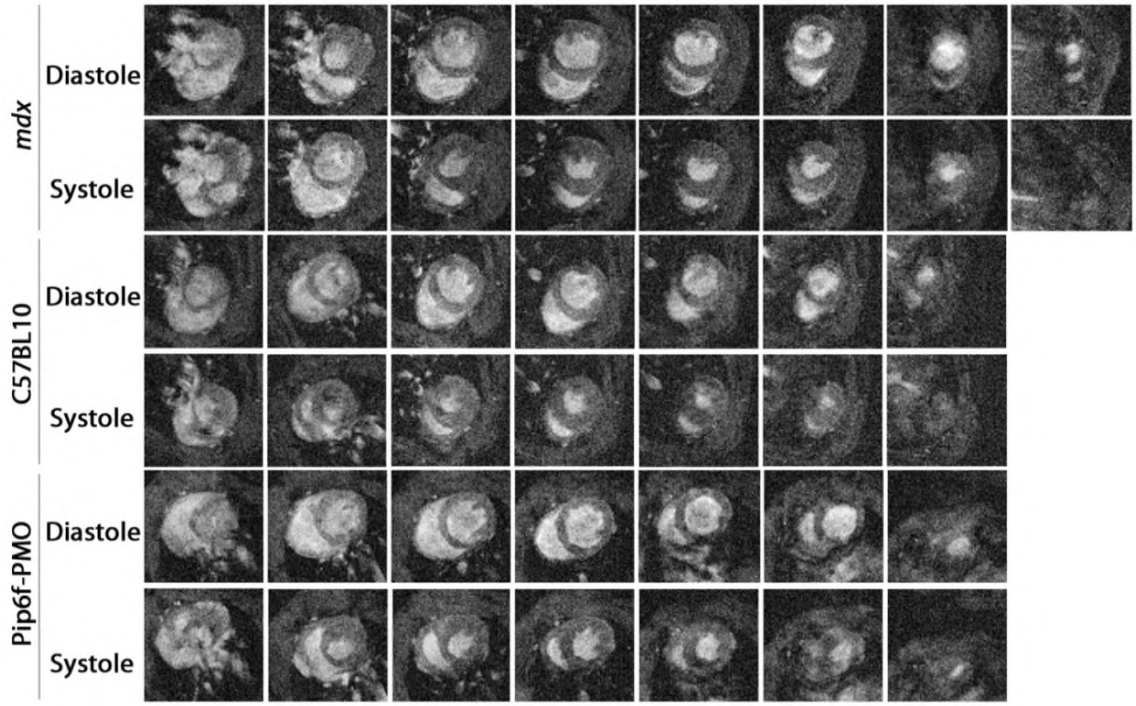

Figure 5.7. Cine-MRI heart images from scans of *mdx*^{ex}, C57BL/10^{ex} and Pip6f-PMO ^{ex} treated mice during diastole and systole. *Mdx* ^{ex} images revealed larger hearts compared to C57BL/10 ^{ex} and Pip6f-PMO ^{ex} hearts as observed in scans 4-6. In addition, more scans were required to image the entire hearts of the *mdx*^{ex} mice.

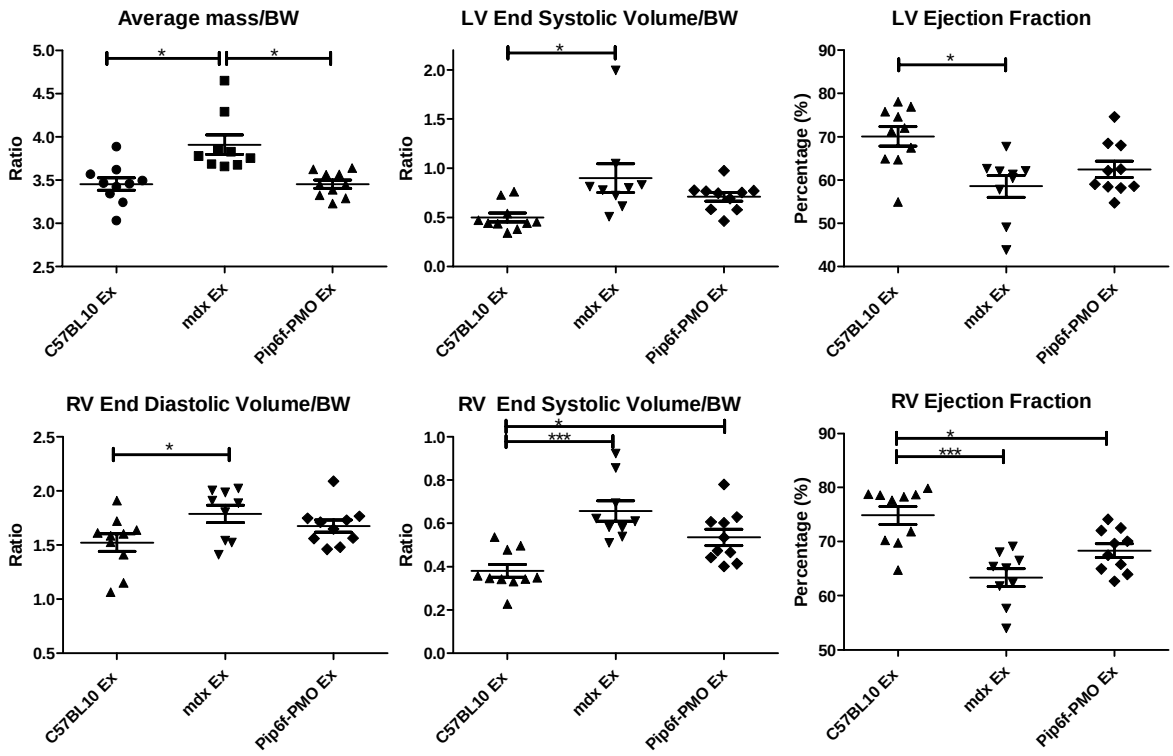

Figure 5.8. Cardiac function measured by cine-MRI in exercised C57BL/10, *mdx* and Pip6f-PMO treated cohorts. Scatter plot graphs illustrating individual mouse values, mean and standard error of the mean (SEM) for left ventricular (LV) average mass and end diastolic volume (relative to body weight- BW), and ejection fraction (top). Right ventricle (RV) parameters including end diastolic volume and end systolic volume (relative to body weights), and ejection fraction were also calculated (bottom). *Mdx*^{ex} mice indicated deterioration in function compared to C57^{unex} and Pip6f-PMO^{ex}. Statistical significance was determined by Students T-test (*=p<0.001, **=p<0.01*=p<0.05). N= 9-10 for each cohort.**

Pip6f-PMO treatment protected the *mdx* mouse heart from exercise induced deterioration

In contrast, the Pip6f-PMO^{ex} treated hearts did not exhibit impaired contractility or undergo LV hypertrophy to cope with the increased workload. This was confirmed by the similar average heart mass between C57BL/10^{ex} and Pip6f-PMO^{ex} groups (**Table 5.2, Fig 5.7** and **Fig 5.8**). In fact, all left ventricle measurements showed normalisation/partial normalisation of the Pip6f-PMO^{ex} cohort relative to C57BL/10^{ex}. The RV ESV of the Pip6f-PMO^{ex} cohort was significantly elevated relative to C57BL/10 **(Fig 5.8)**, however it should be noted that this parameter was not significantly different from the *mdx*^{unex} cohort **(Table 5.2)**. Most of the Pip6f-PMO^{ex} RV parameter values were similar to the *mdx*^{unex} group, which suggests that the treatment halted the progression of the cardiomyopathy and stabilised function **(Table 5.2)**.

Elevated Nox4 and Nppa expression in *mdx*^{ex} hearts

It was predicted that the increase in workload caused by exercise on the *mdx* mouse heart would cause in an increase in biomarkers of injury or damage. Muscles were collected 5 days following the last exercise bout therefore the observed changes denote a delay in recovery or prolonged/permanent damage. Two markers that are up-regulated following damage or oxidative stress were measured, Nppa and Nox4. Nppa is released in response to haemodynamic overload or stress [236] and Nox4 has been associated with increases in oxidative stress [260]. These markers did not change with exercise in C57BL/10 mice.

Quantitative-RT-PCR expression of Nppa revealed elevated expression in the hearts of *mdx*^{ex} mice over C57BL/10^{ex} cohort **(Fig. 5.9)**. The box plot graph for the *mdx*^{ex} cohort (**Fig. 5.9)** reveals the variability between the individual mice. This could be due to inconsistencies from the exercise regimen (some mice ran better than others) or with their individual ability to deal with the increased workload and adapt over the 5 day rest interim. Nppa expressions for Pip6f-PMO^{ex} and *mdx*^{unex} cohorts were not significantly different to C57BL/10 cohorts. Nox4 was also markedly elevated in the *mdx*^{ex} hearts compared to the C57BL/10^{ex} cohort **(Fig. 5.9)**. Nox4 levels in the Pip6f-PMO^{ex} and *mdx*^{unex} cohorts were also significantly elevated. The expression levels of Nppa and Nox4 were similar for both the Pip6f-treated^{ex} and the *mdx*^{unex} mouse hearts which suggest that the treatment regimen stabilised the cardiac pathology and prevented the deterioration of cardiac muscle with exercise.

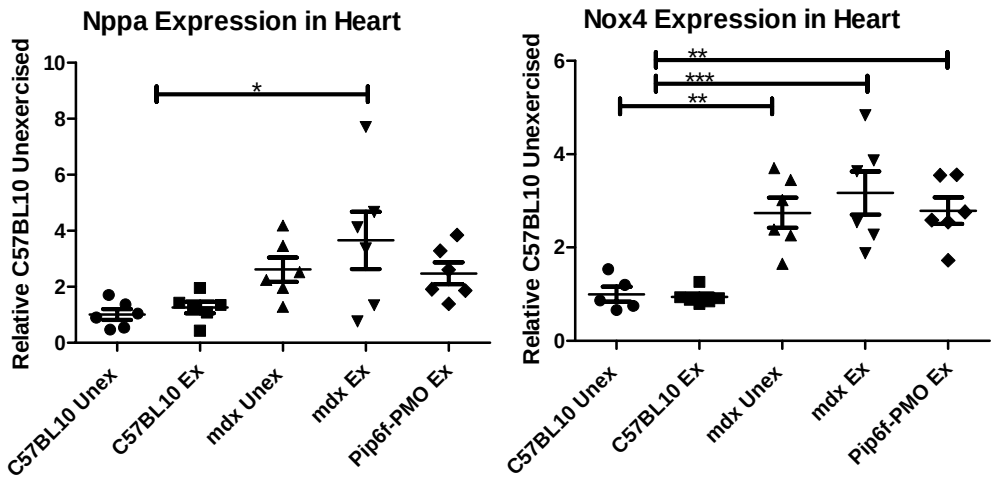

Figure 5.9. Gene expression of markers for injury and oxidative stress in the hearts of exercised and unexercised mice. Quantitative real time (qRT)-PCR for the expression of Nppa and Nox4 were normalised to C57BL/10 unexercised cohort. Expression of Nppa in *mdx*^{ex} was significantly up-regulated. Nox4 expression was also up-regulated in *mdx* and the Pip6f-PMOex cohorts (*mdx*^{unex} and Pip6f-PMO^{ex} to a lesser extent). Statistical significance determined using One-way ANOVA, Tukey post-hoc test (*=p<0.001, **=p<0.01*=p<0.05). N= 8 for each cohort.**

Pip6f-PMO^{ex} prevented fibrosis in *mdx* mouse hearts

Myocardial fibrosis manifests from about 6 months of age in *mdx* mice [73]. Collagen deposition is an indicator of fibrosis or scarring and can be visualised with Masson's trichrome staining. **Figure 5.10** displays the areas with the greatest collagen deposition. *Mdx*^{ex} hearts had substantially larger fibrotic lesions than C57BL/10^{ex} and Pip6f-PMO^{ex} hearts. Collagen deposition was quantified by calculating the surface area of collagen staining relative to total surface area of section (**Fig. 5.11**). Quantification of collagen deposition in *mdx*^{ex} hearts was significantly greater than both the C57BL/10^{ex} and Pip6f-PMO^{ex} cohorts.

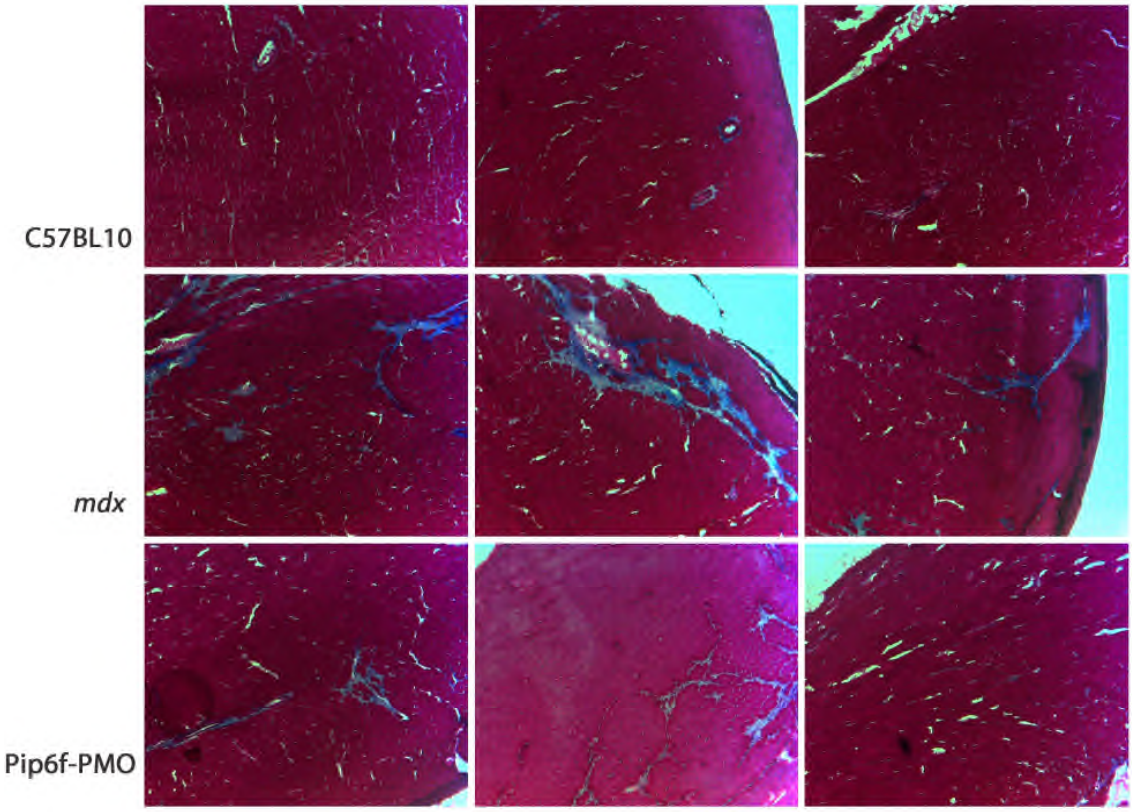

Figure 5.10. Masson's trichrome staining and quantification in the hearts of exercised C57BL0, *mdx* and Pip6f-PMO treated cohorts. (a) Staining illustrates substantial fibrotic lesions in *mdx* cohort. 10X magnification images were taken and manually reconstructed.

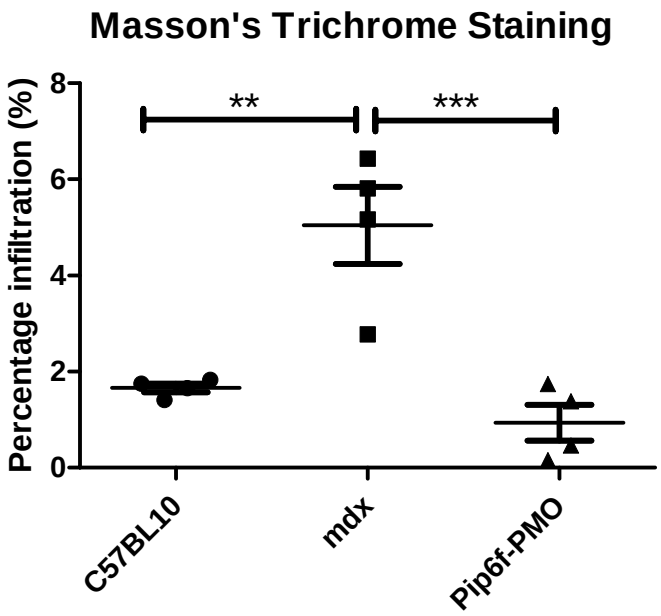

Figure 5.11. Percentage surface area stained with Masson's trichrome. This was determined as the surface area of collagen staining relative to total surface are of section. Statistical significance determined using One-way ANOVA, Tukey post-hoc test (*=p<0.001, **=p<0.01*=p<0.05).**

Exercise increased sarcolemmal fragility in *mdx* cardiac muscle

The role of dystrophin in skeletal and cardiac muscle is to stabilise the sarcolemma and protect myocytes/cardiomyocytes from mechanical damage [31, 85]. Therefore the absence of dystrophin in *mdx* mice results in elevated EBD leakage. The leakage of EBD into cardiac and skeletal muscle is an indicator of damage induced by the stress of exercise [240]. Thus the sarcolemmal integrity of the *tibialis anterior*, diaphragm and heart were assessed using EBD. The surface area of EBD stained cells was quantified relative to the total surface area of the section **(Fig. 5.12)** and revealed significantly higher leakage in *mdx*^{ex} mice in diaphragm and heart muscle. The levels of EBD leakage were low in these tissues, possibly due to the 3-4 day delay between the last exercise time-point and the EBD administration. Over the course of this delay the muscles may have had time to repair and could therefore account for less EBD leakage. Most importantly the leakage of dye in the tissues of Pip6f-PMO^{ex} treated mice was normalised to C57BL/10^{ex} levels which shows that the treatment regimen was capable of restoring sarcolemmal integrity.

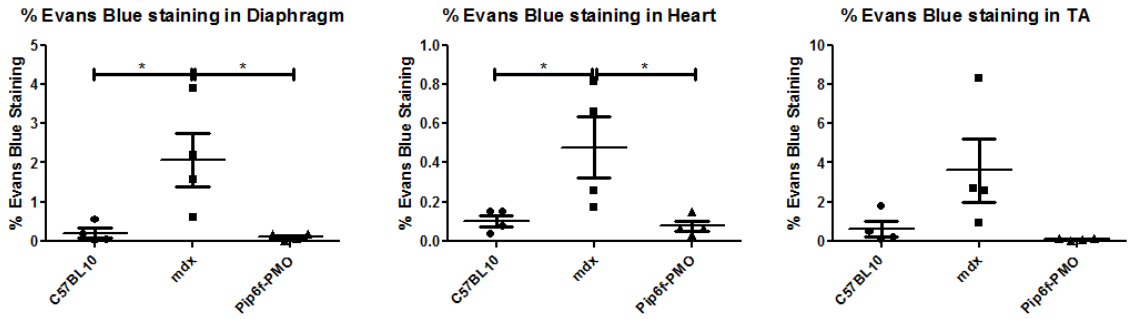

Figure 5.12. Quantification of Evan's blue leakage in exercised C57BL/10, *mdx* and Pip6f-treated *mdx* mice. Evans blue leakage was quantified by calculating the surface area of stained cells relative to total surface area of section. Scatter plot graphs of Evans blue staining illustrating individual mouse values, mean and standard error of the mean (SEM) in diaphragm, heart and *tibialis anterior* muscles. Pip6f-PMO treatment prevents leakage of Evans blue dye in diaphragm, heart and *tibialis anterior* (normalised to C57BL/10). Statistical significance was determined using One-way ANOVA, Tukey post-hoc test (*=p<0.001, **=p<0.01*=p<0.05). N= 4 for each cohort.**

Altered behaviour of untreated, exercised *mdx* mice

The *mdx*^{ex} cohort also exhibited some interesting behavioural changes that were recorded whilst mice were being exercised. It was very difficult to encourage this cohort to run consistently, as they would run intermittently and required constant encouragement. Generally the *mdx*^{ex} mice would rest as often as possible and were largely inactive, possibly due to a damaged muscle. Conversely, the C57BL/10^{ex} mice were very active and inquisitive. Similarly the Pip6-PMO^{ex} cohort ran very well and required very little encouragement.

In addition, 3 mice from *mdx*^{ex} group were removed from the study due to a severe aversion to running and erratic/uncharacteristic behaviour. We attempted to increase the sample number (12) for this cohort however it could not have been anticipated that 25% would need to be removed. This exercise regimen was considered to be moderate compared to previous studies [240, 261], but was certainly a contributory stress factor which impacted the behaviour of these animals.

Toxicological profile of Pip6f-PMO cohort

Toxicological analysis on plasma samples was performed to ensure the safety of Pip6f-PMO administration. Toxicity markers, ALT and AST were completely normal in the Pip6f-PMO^{ex} mice **(Fig. 5.13)**. Albumin, bilirubin and urea levels were consistent between all cohorts. In conclusion, the toxicity profile for this treatment regimen was normal.

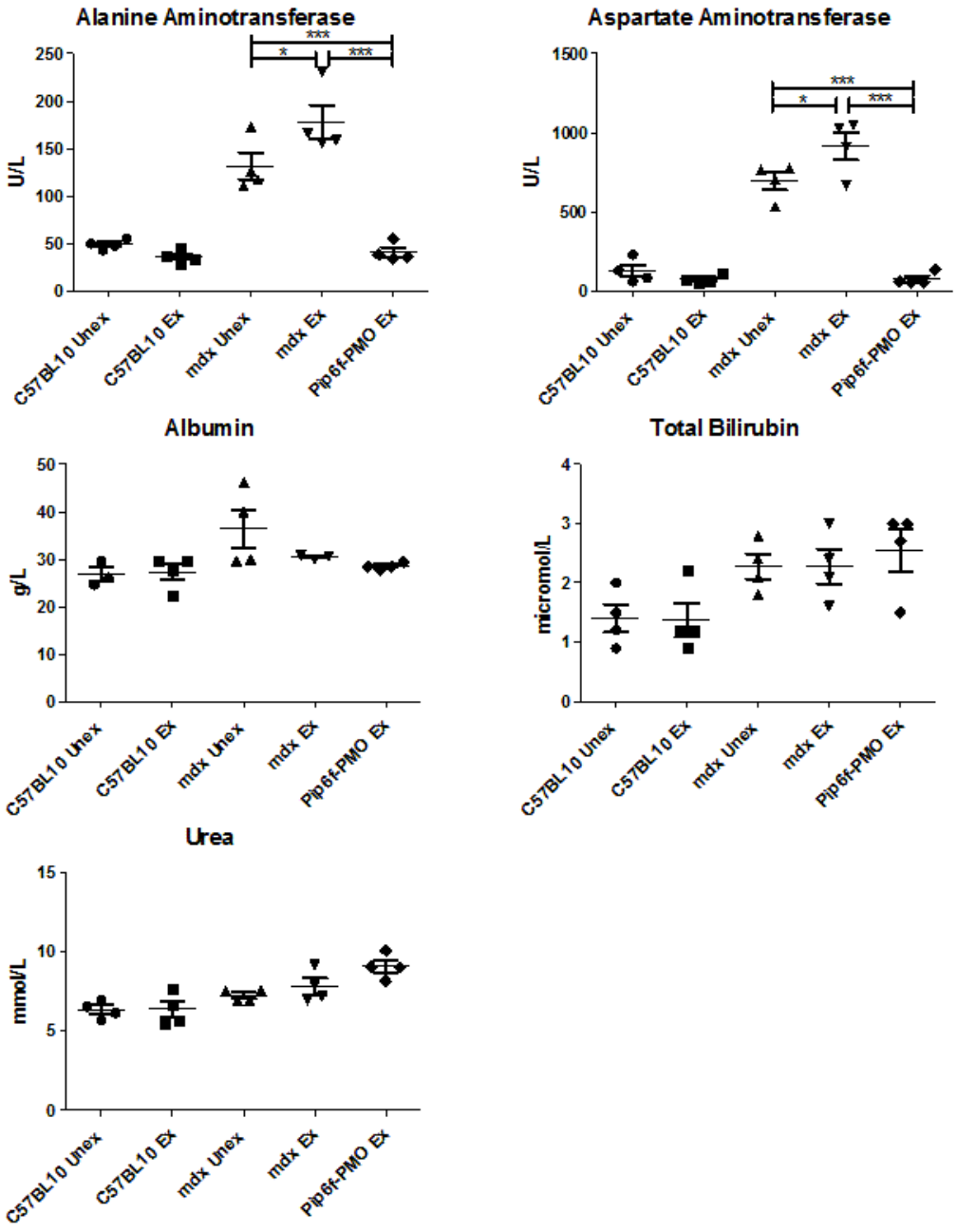

Figure 5.13. Profile of liver and kidney toxicity markers in plasma samples. Graphs show plasma alanine aminotransferase (ALT), aspartate aminotransferase (AST), albumin, total bilirubin and urea between all 5 cohorts in this study. Treatment reduced ALT and AST to C57BL/10 levels while albumin, bilirubin and urea stayed within normal range. Statistical significance determined using One-way ANOVA, Tukey post-hoc test (*=p<0.001, **=p<0.01*=p<0.05). N= 4 for each cohort.**

Two other markers for muscle tissue damage are CK and LDH. CK is another marker often used to predict the progression of the disease in DMD patients [250]. This biomarker was markedly elevated in both the *mdx*^{unex} *and mdx*^{ex} mice, but was normalised by Pip6f-PMO treatment (**Fig. 5.14**). Similarly, LDH which denotes tissue breakdown/damage, was substantially elevated in both *mdx* groups. LDH was completely normalised by Pip6f-PMO treatment indicating the improved skeletal muscle phenotype of these *mdx* mice.

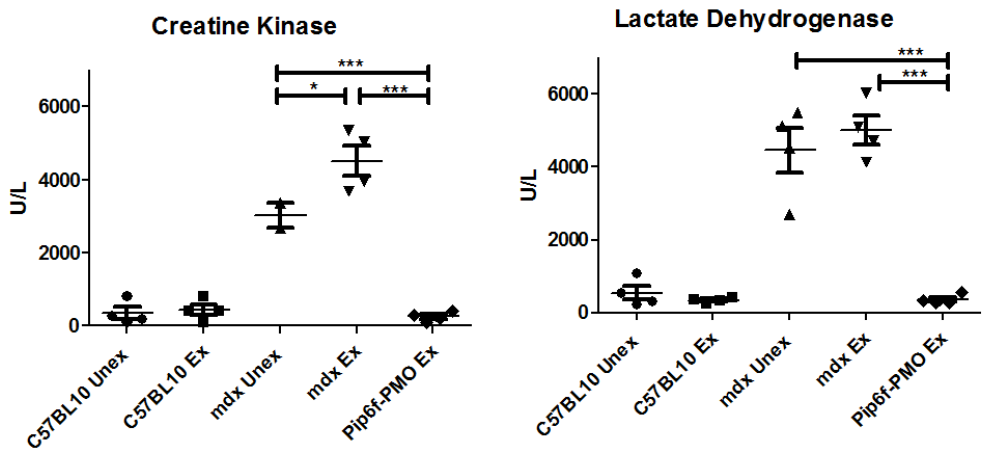

Figure 5.14. Plasma biomarkers of muscle integrity in exercised and unexercised cohorts. Graphs showing creatine kinase (CK) and lactate dehydrogenase (LDH) levels in C57BL/10 control mice compared to *mdx* untreated and treated mice. CK and LDH were elevated in both *mdx* cohorts but Pip6f-PMO treatment resulted in normalisation of these markers. Statistical significance determined using One-way ANOVA, Tukey post-hoc test (*=p<0.001, **=p<0.01*=p<0.05). N= 4 for each cohort.**

Discussion

Chapter 4 described three Pip6-PMOs with the capacity to induce widespread dystrophin expression, including in the heart, following a single administration of 12.5 mg/kg [262]. Due to the nature of this study, molecular and physiological improvement as a direct result of the restoration of dystrophin in the heart could not be performed, and so a thorough investigation of one of these candidate peptides, Pip6f-PMO, was run. A repeated, low dose regimen was employed to assess whether the gradual increase in dystrophin restoration could stabilise or reverse the dystrophic cardiac phenotype.

An exercise component was also included in this study as several previous studies have indicated that the rescue of the skeletal dystrophic phenotype in *mdx* mice increased activity with subsequent acceleration in cardiomyopathic progression [197, 235, 255]. In an effort to determine whether Pip6f-PMO was capable of rescuing the dystrophic phenotype (skeletal and cardiac muscle), even in the event of an increase in workload, an exercise regimen was developed and integrated into the treatment protocol. Treadmill exercise was specifically selected over voluntary running as wild-type mice are known to run further distances than *mdx* mice under voluntary running conditions [235, 263, 264], which may have led to anomalies that would have been difficult to control. Treadmill exercise was therefore deemed to be more consistent and intervals between breaks could be tightly regulated. This exercise regimen was designed to moderately increase the workload on the heart and not

deliberately cause damage. This was in contrast to another study which implemented a regimen with a higher speed and longer running intervals [261]. Instead this exercise regimen was predominantly based on the 'Treat NMD protocol and guidelines' for exercising *mdx* mice (may be accessed: http://www.treat-nmd.eu). Investigators had previously only used this protocol for skeletal muscle studies, therefore the running time for the mice was increased from 30 minutes to 45 minutes. A short preliminary study confirmed the efficacy of this protocol, showing significant changes in the untreated *mdx* heart. These changes included an enlarged heart and reduced contractility measured by cine-MRI, analogous to a phenotype exhibited in most DMD patients by their late teens [19, 265]. These MRI results indicated that the untreated dystrophic heart could not contract sufficiently to sustain the increased blood volume, and therefore underwent hypertrophy and other compensatory changes (dilation and increased CO) in order to answer the contractile demand. Other changes observed in *mdx*^{ex} mice included the increased expression of oxidative damage (Nox4) and injury markers (Nppa) and compromised sarcolemmal integrity (EBD leakage) which showed a decline in phenotype.

The Pip6f-PMO treatment regimen revealed that a low dose, bi-weekly administration regimen could induce high dystrophin restoration in skeletal muscle and approximately 28% dystrophin protein restoration in the heart. It is apparent from previous studies that 20% dystrophin restoration is sufficient to show improvement in skeletal muscle function and resistance

to contraction-induced damage [266], however the amount of dystrophin required by the heart to sustain an increased workload had not yet been determined. This study indicates that 28% dystrophin restoration was sufficient to maintain cardiac function and prevented deterioration in heart function with increased cardiac workload. The treatment regimen also prevented oxidative changes (Nox4) and injury (Nppa) in the exercised *mdx* mouse heart. This is based on the similar expression levels of these biomarkers to *mdx*^{unex} mice. In addition, the level of EBD leakage in the hearts of treated mice was normalised and collagen deposition (Masson's trichrome staining) was reduced. The skeletal muscle phenotype was also improved. There was minimal leakage of EBD in the *tibialis anterior* and diaphragm, and blood circulating levels of CK and LDH were both reduced.

Had this administration-exercise regime continued, it is anticipated that the cardiac function of the *mdx* unexercised cohort would have deteriorated further with age, but that the Pip6f-treated cohort would have remained stable. This is supported by the improvement in behavioural activity observed in the treated cohort in comparison to the *mdx*^{ex} group i.e. Pip6f-PMO^{ex} mice ran well and did not require encouragement. These results illustrate the protective capacity of the treatment protocol, although additional studies investigating longer term and/or higher doses may be required to elucidate whether treatment with Pip6f-PMO also has a regenerative capacity.

This treatment regimen was initiated at 12 weeks of age, at which stage *mdx* mice would have undergone multiple rounds of degeneration and regeneration in skeletal muscle, which starts at 3-8 weeks of age [267]. Cardiac metabolic alterations may occur as early as 10-12 weeks of age [268, 269], therefore other changes that may have damaged the heart may also have occurred by this age. Perhaps the treatment regimen was implemented too late and this may explain why the effect of administration of the Pip6f-PMO at 12 weeks age was limited to stabilising the heart and not correcting cardiac function. This suggests that such treatment alone may not completely restore cardiac function in patients with advanced cardiomyopathy, but based on the data, may prevent its progression. It is predicted this treatment would likely slow the development of the pathology and stabilise cardiac function.

This study has shown that a repeat, low dose administration regimen induced between 58-100% expression of dystrophin protein in skeletal muscle and 28% protein restoration in heart. It further revealed that a moderate exercise regime resulted in significant deterioration of cardiac function in untreated *mdx* mice, characterised by hypertrophied hearts and reduced contractility. However, most importantly the Pip6f-PMO treatment normalised these cardiac parameters and prevented the deterioration of the cardiac phenotype, even with increased cardiac workload of exercise.

Chapter 6. Discussion

Summary of Findings

Cardiorespiratory complications contribute significantly to death amongst DMD boys. Two studies have proposed the restoration of dystrophin in the diaphragm as a potential therapy for DMD. Researchers used a helper-dependent adenovirus vector containing the full-length dystrophin expression cassette to restore dystrophin in the diaphragm and noted increased tidal volume and improved compensatory hyperpnea [70]. They did not, however, look at the impact of this therapy on heart function or pathology. Another study, considered controversial at the time, reported that restoring dystrophin in the diaphragm improved cardiac function. If this were indeed the case, it would mean that further attempts at optimising AO delivery to restore dystrophin in the heart were no longer required. This sparked an interest in determining the contribution of the diaphragm to cardiac function. A study was therefore conducted (**Chapter 3**) to predominantly restore dystrophin in diaphragm with residual/negligible quantities in skeletal tissue and accessory respiratory muscles, and then determine the effect on the heart. It was noted that cardiac function in treated mice was not restored to normal levels. In addition, the treatment did not have any beneficial impact on heart function with exercise, as cardiac function remained significantly worse than C57BL/10 controls. The absence of dystrophin in the microvasculature may contribute to vasoregulatory defects, which increase vascular resistance and pulmonary hypertension and account for the RV dysfunction observed in the B-PMO treated cohorts. A further systemic

approach to restore dystrophin in multiple muscles improved cardiac function, which may be due to the restoration of accessory respiratory muscles and the microvasculature (including in the lung).

Chapter 3 revealed that the restoration of dystrophin in the diaphragm alone is insufficient to improve cardiac function, which combined with concerns that an increase in activity may be detrimental to cardiac pathology, highlight the importance of a treatment that targets the heart. Many in the DMD field maintain that CPP-AO treatment is currently the best therapy for DMD, of which Pip-PMOs readily target the heart. In collaboration with the Gait lab, a new series of peptides, Pip6-PMOs, were designed.

Chapter 4 describes the screening of multiple Pip6-PMOs, from which three promising 5-aa peptides had improved heart delivery. This structure-activity study revealed that shortening the hydrophobic core reduced cardiac and skeletal muscle localisation which was attributed to the diminished hydrophobicity. Additional modifications, whereby the position of arginine was altered, also changed activity, which may possibly be due to spacing of A-Hex amino acids. Thus this study revealed the importance of maintaining the 5-aa hydrophobic core, and indicated that the position of arginine and the cationic/hydrophobic balance may be important considerations in designing future CPPs.

To elaborate on this structure-activity study, further molecular and physiological studies were instigated employing Pip6f-PMO for a multiple, low dose study to assess heart function *in vivo* (described in **Chapter 5**). As there is evidence that increased workload may be detrimental to DMD heart, a moderate exercise regimen was employed in the study. It was determined that a very low dose of 10 mg/kg administered multiple times induced between 58-100% dystrophin protein expression in skeletal muscles and 28% in heart. This degree of restoration was capable of stabilising cardiac function and phenotype, as evidenced by qRT-PCR, EBD staining and Masson's trichrome staining. This study also revealed that the untreated dystrophic heart could not withstand minor increases in exercise induced workload, evidenced by structural and functional deterioration in the heart.

Relevance of studies

The structural-activity screening study (**Chapter 4**) and cardiac function study (**Chapter 5**) both illustrated the utility of Pip-PMOs for possible treatment of DMD patients. The work described in **Chapter 5** further revealed the potency of the Pip-PMOs and how a low dose regimen was sufficient to maintain cardiac function over a long time course. Indeed it is anticipated that a derivative of one of these Pip6-PMOs will progress to clinical trial. Of course a major obstacle to overcome in the clinical field is the issue of toxicity associated with cationic peptides and therefore efforts are focussed on alleviating this concern whilst retaining activity. It is hypothesised that reducing the number of arginine residues in the flanking

regions may incrementally reduce toxicity, an approach actively being pursued by colleagues.

The exercise studies, **Chapter 3** and **Chapter 5**, are both relevant and topical in the clinical realm as they complement other studies that raised concerns regarding increased physical activity being detrimental to the heart. This is of interest as studies applying the 'use it or lose it' rationale for physical training to prevent the onset of skeletal muscle deterioration, are actively being pursued [256, 257]. This approach may be applicable to the skeletal muscle aspect of the disease, however the cardiac aspect has only recently been investigated in the *mdx* mouse model. It appears as though voluntary physical exercise may be beneficial to skeletal muscle, but causes cardiac deterioration [259]. There is a study underway collating information of the cardiomyopathic progression in DMD patients, therefore physicians and health care workers must rely on mouse studies for their treatment strategy, until this work is published. Based on the work in **Chapter 3** and **Chapter 5**, it was apparent that even a moderate increase in physical activity in *mdx* mice, a mouse model which is considered to exhibit a very mild phenotype, is detrimental to heart function. We therefore propose that physical exercise, which increases cardiac workload, is avoided by DMD patients. These studies also continue to emphasise the importance of developing a drug therapy that targets both cardiac and skeletal muscle in DMD patients.

Future Plans

There are a few additional experiments that would complement the research described in this thesis. From **Chapter 3** it may be that restoration of dystrophin in the diaphragm alone does not improve cardiac function due to poor vasoregulation (NO); however this has not been validated. Whole body plethysmography of treated *mdx* mice to assess lung function is required. The panel of tests conducted during routine plethysmography would also allow the assessment of hypercapnic response. Additional experiments would further provide an opportunity to isolate the carotid body, a vital chemoreceptor responsible for hypoxia sensing, which is known to be impaired in *mdx* mice [71]. Whole body plethysmography could directly compare lung function and hypercapnic response in IV versus IP treated mice (with B-PMO). The carotid body can be dissected and studied for the presence of dystrophin and pathology

As discussed, further derivatives of Pip6's are currently being assessed for toxicity and will soon enter clinical trials. There are however, many cardiac studies that would contribute to the understanding of these peptides and their potential therapeutic effects.

Firstly, these peptides may be investigated in other, more severe DMD models, such as the *mdx*/CMAH, to assess whether these Pip-PMOs are still capable of rescuing/stabilising cardiac function. Chandrasekharan *et al.* generated a new *mdx* model that better mimics the human disease

course by introducing an inactivating deletion in the CMAH (cytidine monophosphate-sialic acid hydroxylase) gene [270]. This evolutionary deletion is present in humans, but not mice, therefore the CMAH/*mdx* mouse model has a more advanced disease; early impaired ambulation, earlier onset dilated cardiomyopathy and increased mortality (50% by 11 months of age). Whilst this model is still undergoing phenotyping, the CMAH model appears to exhibit a more severe cardiomyopathy then *mdx* mice. It would thus be an interesting model to utilise for future studies.

Secondly, to directly address a suggestion in **Chapter 5** that it was the late administration (12 weeks of age) of Pip6f-PMO which only stabilised the cardiac function (did not prevent it), this study should start with an earlier treatment regimen i.e. 3-4 weeks of age. A 6-9 month treatment regimen, in which heart structure and function are directly compared with the wild-type, would be sufficient. It is anticipated that the changes in RV function (see **Chapter 5**) would not develop and, if translated to a patient study, early diagnosis and administration of Pip-PMO may prevent cardiomyopathic progression.

However, for older DMD patients, a regenerative approach is required to evade cardiac complications. Therefore, a third avenue which may be pursued would be to investigate a dual therapy, whereby one aspect of treatment would be on the regeneration of cardiac cells and the other to correct heart dystrophin using AOs. Indeed, one such credible approach

revolves around an actin-binding peptide, Thymosin-beta 4, which activates quiescent adult epicardial cells, facilitating neovascularisation and cardiomyocyte production, thereby regenerating the myocardium [271, 272]. This collaborative approach may provide hope for older DMD boys with advancing cardiomyopathy.

Concluding Remarks

The lack of dystrophin in DMD patients has a devastating effect throughout the human body. One of the most important systems that contribute significantly to death amongst patients is cardiorespiratory dysfunction. The cardiorespiratory system is complicated, involving the diaphragm, accessory respiratory muscles, lungs and heart. This work highlighted the importance of identifying a therapy that restored dystrophin in many muscles types and illustrated the utility of Pip-PMOs for the restoration of skeletal and cardiac muscle dystrophin. These conjugates further stabilised cardiac function and pathology, even with increased workload of exercise.

Research into therapies for this debilitating disease is ongoing. Indeed, Pip-PMO derivatives are rapidly progressing through pre-clinical trials, which have shown great potential. It is hoped that this therapy will reach patients with DMD in the near future.

References

1. Klabunde, R.E., *Cardiovascular Physiology Concepts.* 2012.
2. Chen, Y.K., et al., *Neuroimaging indicators of the performance of instrumental activities of daily living in Alzheimer's disease combined with cerebrovascular disease.* Geriatr Gerontol Int, 2014.
3. Gold, G., et al., *Advances in musculoskeletal magnetic resonance imaging.* Top Magn Reson Imaging, 2010. **21**(5): p. 335-8.
4. Maltz, R., D.J. Podberesky, and S.A. Saeed, *Imaging modalities in pediatric inflammatory bowel disease.* Curr Opin Pediatr, 2014.
5. Allen, B.C. and J.R. Leyendecker, *MR enterography for assessment and management of small bowel Crohn disease.* Radiol Clin North Am, 2014. **52**(4): p. 799-810.
6. Partovi, S., et al., *Clinical oncologic applications of PET/MRI: a new horizon.* Am J Nucl Med Mol Imaging, 2014. **4**(2): p. 202-12.
7. Willcocks, R.J., et al., *Longitudinal measurements of MRI-T2 in boys with Duchenne muscular dystrophy: effects of age and disease progression.* Neuromuscul Disord, 2014. **24**(5): p. 393-401.
8. Mazur, W., et al., *Patterns of left ventricular remodeling in patients with Duchenne Muscular Dystrophy: a cardiac MRI study of ventricular geometry, global function, and strain.* Int J Cardiovasc Imaging, 2012. **28**(1): p. 99-107.
9. Imhof, H., et al., *[Basics of MRI technique and MRI image interpretation].* Orthopade, 1994. **23**(5): p. 300-5.
10. Azarisman, S.M., et al., *Role of cardiovascular magnetic resonance in assessment of acute coronary syndrome.* World J Cardiol, 2014. **6**(6): p. 405-14.
11. Kim, R.J., et al., *Relationship of MRI delayed contrast enhancement to irreversible injury, infarct age, and contractile function.* Circulation, 1999. **100**(19): p. 1992-2002.
12. Muntoni, F. and M.J. Wood, *Targeting RNA to treat neuromuscular disease.* Nat Rev Drug Discov, 2011. **10**(8): p. 621-37.
13. Davies, K.E. and K.J. Nowak, *Molecular mechanisms of muscular dystrophies: old and new players.* Nat Rev Mol Cell Biol, 2006. **7**(10): p. 762-73.
14. Emery, A.E., *Population frequencies of inherited neuromuscular diseases--a world survey.* Neuromuscul Disord, 1991. **1**(1): p. 19-29.
15. Dooley, J., et al., *Duchenne muscular dystrophy: a 30-year population-based incidence study.* Clin Pediatr (Phila), 2010. **49**(2): p. 177-9.
16. Brooke, M.H., et al., *Clinical investigation in Duchenne dystrophy: 2. Determination of the "power" of therapeutic trials based on the natural history.* Muscle Nerve, 1983. **6**(2): p. 91-103.
17. Chang, R.F. and S.J. Mubarak, *Pathomechanics of Gowers' sign: a video analysis of a spectrum of Gowers' maneuvers.* Clin Orthop Relat Res, 2012. **470**(7): p. 1987-91.
18. Kirchmann, C., et al., *Echocardiographic and electrocardiographic findings of cardiomyopathy in Duchenne and Becker-Kiener muscular dystrophies.* Pediatr Cardiol, 2005. **26**(1): p. 66-72.
19. Nigro, G., et al., *The incidence and evolution of cardiomyopathy in Duchenne muscular dystrophy.* Int J Cardiol, 1990. **26**(3): p. 271-7.
20. Connuck, D.M., et al., *Characteristics and outcomes of cardiomyopathy in children with Duchenne or Becker muscular dystrophy: a comparative study from the Pediatric Cardiomyopathy Registry.* Am Heart J, 2008. **155**(6): p. 998-1005.

21. Davies, K.E., et al., *Linkage analysis of two cloned DNA sequences flanking the Duchenne muscular dystrophy locus on the short arm of the human X chromosome.* Nucleic Acids Res, 1983. **11**(8): p. 2303-12.
22. Muntoni, F., S. Torelli, and A. Ferlini, *Dystrophin and mutations: one gene, several proteins, multiple phenotypes.* Lancet Neurol, 2003. **2**(12): p. 731-40.
23. Kaspar, R.W., et al., *Analysis of dystrophin deletion mutations predicts age of cardiomyopathy onset in becker muscular dystrophy.* Circ Cardiovasc Genet, 2009. **2**(6): p. 544-51.
24. Sakthivel Murugan, S.M., et al., *Carrier detection in Duchenne muscular dystrophy using molecular methods.* Indian J Med Res, 2013. **137**(6): p. 1102-10.
25. Taylor, P.J., et al., *Measurement of the clinical utility of a combined mutation detection protocol in carriers of Duchenne and Becker muscular dystrophy.* J Med Genet, 2007. **44**(6): p. 368-72.
26. Dunckley, M.G., et al., *Modification of splicing in the dystrophin gene in cultured Mdx muscle cells by antisense oligoribonucleotides.* Hum Mol Genet, 1998. **7**(7): p. 1083-90.
27. Wilton, S.D., et al., *Specific removal of the nonsense mutation from the mdx dystrophin mRNA using antisense oligonucleotides.* Neuromuscul Disord, 1999. **9**(5): p. 330-8.
28. Dickson, G., V. Hill, and I.R. Graham, *Screening for antisense modulation of dystrophin pre-mRNA splicing.* Neuromuscul Disord, 2002. **12 Suppl 1**: p. S67-70.
29. Monaco, A.P., et al., *An explanation for the phenotypic differences between patients bearing partial deletions of the DMD locus.* Genomics, 1988. **2**(1): p. 90-5.
30. Gumerson, J.D. and D.E. Michele, *The dystrophin-glycoprotein complex in the prevention of muscle damage.* J Biomed Biotechnol, 2011. **2011**: p. 210797.
31. Ohlendieck, K., et al., *Dystrophin-glycoprotein complex is highly enriched in isolated skeletal muscle sarcolemma.* J Cell Biol, 1991. **112**(1): p. 135-48.
32. Mosqueira, M., et al., *Cardiac and respiratory dysfunction in Duchenne muscular dystrophy and the role of second messengers.* Med Res Rev, 2013. **33**(5): p. 1174-213.
33. Schmitz, F. and D. Drenckhahn, *Dystrophin in the retina.* Prog Neurobiol, 1997. **53**(5): p. 547-60.
34. Felisari, G., et al., *Loss of Dp140 dystrophin isoform and intellectual impairment in Duchenne dystrophy.* Neurology, 2000. **55**(4): p. 559-64.
35. Tadayoni, R., et al., *Dystrophin Dp71: the smallest but multifunctional product of the Duchenne muscular dystrophy gene.* Mol Neurobiol, 2012. **45**(1): p. 43-60.
36. Masubuchi, N., et al., *Subcellular localization of dystrophin isoforms in cardiomyocytes and phenotypic analysis of dystrophin-deficient mice reveal cardiac myopathy is predominantly caused by a deficiency in full-length dystrophin.* Exp Anim, 2013. **62**(3): p. 211-7.
37. Bushby, K., F. Muntoni, and J.P. Bourke, *107th ENMC international workshop: the management of cardiac involvement in muscular dystrophy and myotonic dystrophy. 7th-9th June 2002, Naarden, the Netherlands.* Neuromuscul Disord, 2003. **13**(2): p. 166-72.
38. Hsu, J.D. and J. Furumasu, *Gait and posture changes in the Duchenne muscular dystrophy child.* Clin Orthop Relat Res, 1993(288): p. 122-5.
39. Shimada, T., *Factors affecting appearance patterns of hip-flexion contractures and their effects on postural and gait abnormalities.* Kobe J Med Sci, 1996. **42**(4): p. 271-90.
40. Gaudreault, N., D. Gravel, and S. Nadeau, *Evaluation of plantar flexion contracture contribution during the gait of children with Duchenne muscular dystrophy.* J Electromyogr Kinesiol, 2009. **19**(3): p. e180-6.

41. Rideau, Y., et al., *The treatment of scoliosis in Duchenne muscular dystrophy.* Muscle Nerve, 1984. **7**(4): p. 281-6.
42. Morrison, J., et al., *T-cell-dependent fibrosis in the mdx dystrophic mouse.* Lab Invest, 2000. **80**(6): p. 881-91.
43. Carnwath, J.W. and D.M. Shotton, *Muscular dystrophy in the mdx mouse: histopathology of the soleus and extensor digitorum longus muscles.* J Neurol Sci, 1987. **80**(1): p. 39-54.
44. Sander, M., et al., *Functional muscle ischemia in neuronal nitric oxide synthase-deficient skeletal muscle of children with Duchenne muscular dystrophy.* Proc Natl Acad Sci U S A, 2000. **97**(25): p. 13818-23.
45. Billard, C., et al., *Cognitive functions in Duchenne muscular dystrophy: a reappraisal and comparison with spinal muscular atrophy.* Neuromuscul Disord, 1992. **2**(5-6): p. 371-8.
46. Cyrulnik, S.E. and V.J. Hinton, *Duchenne muscular dystrophy: a cerebellar disorder?* Neurosci Biobehav Rev, 2008. **32**(3): p. 486-96.
47. Salam, E.A., et al., *Evaluation of neural damage in Duchenne muscular dystrophy patients.* Acta Myol, 2014. **33**(1): p. 13-18.
48. Bianchi, M.L., et al., *Bone mineral density and bone metabolism in Duchenne muscular dystrophy.* Osteoporos Int, 2003. **14**(9): p. 761-7.
49. King, W.M., et al., *Orthopedic outcomes of long-term daily corticosteroid treatment in Duchenne muscular dystrophy.* Neurology, 2007. **68**(19): p. 1607-13.
50. McDonald, D.G., et al., *Fracture prevalence in Duchenne muscular dystrophy.* Dev Med Child Neurol, 2002. **44**(10): p. 695-8.
51. Jaffe, K.M., et al., *Symptoms of upper gastrointestinal dysfunction in Duchenne muscular dystrophy: case-control study.* Arch Phys Med Rehabil, 1990. **71**(10): p. 742-4.
52. Benditt, J.O. and L. Boitano, *Respiratory support of individuals with Duchenne muscular dystrophy: toward a standard of care.* Phys Med Rehabil Clin N Am, 2005. **16**(4): p. 1125-39, xii.
53. Gayraud, J., et al., *Ventilatory parameters and maximal respiratory pressure changes with age in Duchenne muscular dystrophy patients.* Pediatr Pulmonol, 2010. **45**(6): p. 552-9.
54. Melacini, P., et al., *Cardiac and respiratory involvement in advanced stage Duchenne muscular dystrophy.* Neuromuscul Disord, 1996. **6**(5): p. 367-76.
55. Yotsukura, M., et al., *Pulmonary hypertension in progressive muscular dystrophy of the Duchenne type.* Jpn Circ J, 1988. **52**(4): p. 321-6.
56. Sultan, A. and M. Fayaz, *Prevalence of cardiomyopathy in Duchenne and Becker's muscular dystrophy.* J Ayub Med Coll Abbottabad, 2008. **20**(2): p. 7-13.
57. Takami, Y., et al., *High incidence of electrocardiogram abnormalities in young patients with duchenne muscular dystrophy.* Pediatr Neurol, 2008. **39**(6): p. 399-403.
58. Sanyal, S.K., et al., *An ultrastructural basis for electrocardiographic alterations associated with Duchenne's progressive muscular dystrophy.* Circulation, 1978. **57**(6): p. 1122-9.
59. Sanyal, S.K. and W.W. Johnson, *Cardiac conduction abnormalities in children with Duchenne's progressive muscular dystrophy: electrocardiographic features and morphologic correlates.* Circulation, 1982. **66**(4): p. 853-63.
60. Perloff, J.K., et al., *The distinctive electrocardiogram of Duchenne's progressive muscular dystrophy. An electrocardiographic-pathologic correlative study.* Am J Med, 1967. **42**(2): p. 179-88.
61. Hor, K.N., et al., *Circumferential strain analysis identifies strata of cardiomyopathy in Duchenne muscular dystrophy: a cardiac magnetic resonance tagging study.* J Am Coll Cardiol, 2009. **53**(14): p. 1204-10.

62. Hagenbuch, S.C., et al., *Detection of progressive cardiac dysfunction by serial evaluation of circumferential strain in patients with Duchenne muscular dystrophy.* Am J Cardiol, 2010. **105**(10): p. 1451-5.
63. Hor, K.N., et al., *Prevalence and distribution of late gadolinium enhancement in a large population of patients with Duchenne muscular dystrophy: effect of age and left ventricular systolic function.* J Cardiovasc Magn Reson, 2013. **15**: p. 107.
64. Nishimura, T., et al., *Thallium-201 single photon emission computed tomography (SPECT) in patients with duchenne's progressive muscular dystrophy: a histopathologic correlation study.* Jpn Circ J, 2001. **65**(2): p. 99-105.
65. Bulfield, G., et al., *X chromosome-linked muscular dystrophy (mdx) in the mouse.* Proc Natl Acad Sci U S A, 1984. **81**(4): p. 1189-92.
66. Sicinski, P., et al., *The molecular basis of muscular dystrophy in the mdx mouse: a point mutation.* Science, 1989. **244**(4912): p. 1578-80.
67. DiMario, J.X., A. Uzman, and R.C. Strohman, *Fiber regeneration is not persistent in dystrophic (MDX) mouse skeletal muscle.* Dev Biol, 1991. **148**(1): p. 314-21.
68. Lynch, G.S., et al., *Force and power output of fast and slow skeletal muscles from mdx mice 6-28 months old.* J Physiol, 2001. **535**(Pt 2): p. 591-600.
69. Pastoret, C. and A. Sebille, *mdx mice show progressive weakness and muscle deterioration with age.* J Neurol Sci, 1995. **129**(2): p. 97-105.
70. Ishizaki, M., et al., *Rescue from respiratory dysfunction by transduction of full-length dystrophin to diaphragm via the peritoneal cavity in utrophin/dystrophin double knockout mice.* Mol Ther, 2011. **19**(7): p. 1230-5.
71. Mosqueira, M., et al., *Ventilatory chemosensory drive is blunted in the mdx mouse model of Duchenne Muscular Dystrophy (DMD).* PLoS One, 2013. **8**(7): p. e69567.
72. Bia, B.L., et al., *Decreased myocardial nNOS, increased iNOS and abnormal ECGs in mouse models of Duchenne muscular dystrophy.* J Mol Cell Cardiol, 1999. **31**(10): p. 1857-62.
73. Stuckey, D.J., et al., *In vivo MRI characterization of progressive cardiac dysfunction in the mdx mouse model of muscular dystrophy.* PLoS One, 2012. **7**(1): p. e28569.
74. Verhaart, I.E., et al., *Assessment of cardiac function in three mouse dystrophinopathies by magnetic resonance imaging.* Neuromuscul Disord, 2011.
75. Chu, V., et al., *Electrocardiographic findings in mdx mice: a cardiac phenotype of Duchenne muscular dystrophy.* Muscle Nerve, 2002. **26**(4): p. 513-9.
76. Wehling-Henricks, M., et al., *Cardiomyopathy in dystrophin-deficient hearts is prevented by expression of a neuronal nitric oxide synthase transgene in the myocardium.* Hum Mol Genet, 2005. **14**(14): p. 1921-33.
77. Li, W., et al., *Early manifestation of alteration in cardiac function in dystrophin deficient mdx mouse using 3D CMR tagging.* J Cardiovasc Magn Reson, 2009. **11**: p. 40.
78. Williams, I.A. and D.G. Allen, *Intracellular calcium handling in ventricular myocytes from mdx mice.* Am J Physiol Heart Circ Physiol, 2007. **292**(2): p. H846-55.
79. Gervasio, O.L., et al., *TRPC1 binds to caveolin-3 and is regulated by Src kinase - role in Duchenne muscular dystrophy.* J Cell Sci, 2008. **121**(Pt 13): p. 2246-55.
80. Jung, C., et al., *Dystrophic cardiomyopathy: amplification of cellular damage by Ca2+ signalling and reactive oxygen species-generating pathways.* Cardiovasc Res, 2008. **77**(4): p. 766-73.
81. Bellinger, A.M., et al., *Hypernitrosylated ryanodine receptor calcium release channels are leaky in dystrophic muscle.* Nat Med, 2009. **15**(3): p. 325-30.
82. Lai, Y., et al., *Dystrophins carrying spectrin-like repeats 16 and 17 anchor nNOS to the sarcolemma and enhance exercise performance in a mouse model of muscular dystrophy.* J Clin Invest, 2009. **119**(3): p. 624-35.

83. Thomas, G.D., et al., *Impaired metabolic modulation of alpha-adrenergic vasoconstriction in dystrophin-deficient skeletal muscle.* Proc Natl Acad Sci U S A, 1998. **95**(25): p. 15090-5.
84. Mendell, J.R., W.K. Engel, and E.C. Derrer, *Duchenne muscular dystrophy: functional ischemia reproduces its characteristic lesions.* Science, 1971. **172**(3988): p. 1143-5.
85. Danialou, G., et al., *Dystrophin-deficient cardiomyocytes are abnormally vulnerable to mechanical stress-induced contractile failure and injury.* FASEB J, 2001. **15**(9): p. 1655-7.
86. Finsterer, J. and C. Stollberger, *The heart in human dystrophinopathies.* Cardiology, 2003. **99**(1): p. 1-19.
87. Sadeghi, A., A.D. Doyle, and B.D. Johnson, *Regulation of the cardiac L-type Ca2+ channel by the actin-binding proteins alpha-actinin and dystrophin.* Am J Physiol Cell Physiol, 2002. **282**(6): p. C1502-11.
88. Viola, H.M., et al., *L-type Ca(2+) channel contributes to alterations in mitochondrial calcium handling in the mdx ventricular myocyte.* Am J Physiol Heart Circ Physiol, 2013. **304**(6): p. H767-75.
89. Koenig, X., et al., *Enhanced currents through L-type calcium channels in cardiomyocytes disturb the electrophysiology of the dystrophic heart.* Am J Physiol Heart Circ Physiol, 2014. **306**(4): p. H564-73.
90. Shin, J.H., et al., *SERCA2a gene transfer improves electrocardiographic performance in aged mdx mice.* J Transl Med, 2011. **9**: p. 132.
91. Fauconnier, J., et al., *Leaky RyR2 trigger ventricular arrhythmias in Duchenne muscular dystrophy.* Proc Natl Acad Sci U S A, 2010. **107**(4): p. 1559-64.
92. Gavillet, B., et al., *Cardiac sodium channel Nav1.5 is regulated by a multiprotein complex composed of syntrophins and dystrophin.* Circ Res, 2006. **99**(4): p. 407-14.
93. Thomas, G.D., *Functional muscle ischemia in Duchenne and Becker muscular dystrophy.* Front Physiol, 2013. **4**: p. 381.
94. Griggs, R.C., et al., *Prednisone in Duchenne dystrophy. A randomized, controlled trial defining the time course and dose response. Clinical Investigation of Duchenne Dystrophy Group.* Arch Neurol, 1991. **48**(4): p. 383-8.
95. Biggar, W.D., et al., *Long-term benefits of deflazacort treatment for boys with Duchenne muscular dystrophy in their second decade.* Neuromuscul Disord, 2006. **16**(4): p. 249-55.
96. Barber, B.J., et al., *Oral corticosteroids and onset of cardiomyopathy in Duchenne muscular dystrophy.* J Pediatr, 2013. **163**(4): p. 1080-4 e1.
97. Wagner, K.R., N. Lechtzin, and D.P. Judge, *Current treatment of adult Duchenne muscular dystrophy.* Biochim Biophys Acta, 2007. **1772**(2): p. 229-37.
98. Finsterer, J., *Cardiopulmonary support in duchenne muscular dystrophy.* Lung, 2006. **184**(4): p. 205-15.
99. Toussaint, M., M. Chatwin, and P. Soudon, *Mechanical ventilation in Duchenne patients with chronic respiratory insufficiency: clinical implications of 20 years published experience.* Chron Respir Dis, 2007. **4**(3): p. 167-77.
100. Goemans, N. and G. Buyse, *Current treatment and management of dystrophinopathies.* Curr Treat Options Neurol, 2014. **16**(5): p. 287.
101. Fayssoil, A., et al., *Cardiomyopathy in Duchenne muscular dystrophy: pathogenesis and therapeutics.* Heart Fail Rev, 2010. **15**(1): p. 103-7.
102. Viollet, L., et al., *Effects of angiotensin-converting enzyme inhibitors and/or beta blockers on the cardiomyopathy in Duchenne muscular dystrophy.* Am J Cardiol, 2012. **110**(1): p. 98-102.
103. Ogata, H., et al., *Beneficial effects of beta-blockers and angiotensin-converting enzyme inhibitors in Duchenne muscular dystrophy.* J Cardiol, 2009. **53**(1): p. 72-8.

104. Blain, A., et al., *Beta-blockers, left and right ventricular function, and in-vivo calcium influx in muscular dystrophy cardiomyopathy.* PLoS One, 2013. **8**(2): p. e57260.
105. Fayssoil, A., et al., *Successful cardiac resynchronisation therapy in Duchenne muscular dystrophy: a 5-year follow-up.* Presse Med, 2014. **43**(3): p. 330-1.
106. Spurney, C.F., et al., *Membrane sealant Poloxamer P188 protects against isoproterenol induced cardiomyopathy in dystrophin deficient mice.* BMC Cardiovasc Disord, 2011. **11**: p. 20.
107. Yasuda, S., et al., *Dystrophic heart failure blocked by membrane sealant poloxamer.* Nature, 2005. **436**(7053): p. 1025-9.
108. Khairallah, M., et al., *Sildenafil and cardiomyocyte-specific cGMP signaling prevent cardiomyopathic changes associated with dystrophin deficiency.* Proc Natl Acad Sci U S A, 2008. **105**(19): p. 7028-33.
109. Adamo, C.M., et al., *Sildenafil reverses cardiac dysfunction in the mdx mouse model of Duchenne muscular dystrophy.* Proc Natl Acad Sci U S A, 2010. **107**(44): p. 19079-83.
110. Percival, J.M., et al., *Sildenafil reduces respiratory muscle weakness and fibrosis in the mdx mouse model of Duchenne muscular dystrophy.* J Pathol, 2012. **228**(1): p. 77-87.
111. Spurney, C.F., et al., *Losartan decreases cardiac muscle fibrosis and improves cardiac function in dystrophin-deficient mdx mice.* J Cardiovasc Pharmacol Ther, 2011. **16**(1): p. 87-95.
112. Van Erp, C., N.G. Irwin, and A.J. Hoey, *Long-term administration of pirfenidone improves cardiac function in mdx mice.* Muscle Nerve, 2006. **34**(3): p. 327-34.
113. Finkel, R.S., *Read-through strategies for suppression of nonsense mutations in Duchenne/ Becker muscular dystrophy: aminoglycosides and ataluren (PTC124).* J Child Neurol, 2010. **25**(9): p. 1158-64.
114. Fan-Minogue, H. and D.M. Bedwell, *Eukaryotic ribosomal RNA determinants of aminoglycoside resistance and their role in translational fidelity.* RNA, 2008. **14**(1): p. 148-57.
115. Fourmy, D., et al., *Structure of the A site of Escherichia coli 16S ribosomal RNA complexed with an aminoglycoside antibiotic.* Science, 1996. **274**(5291): p. 1367-71.
116. Barton-Davis, E.R., et al., *Aminoglycoside antibiotics restore dystrophin function to skeletal muscles of mdx mice.* J Clin Invest, 1999. **104**(4): p. 375-81.
117. Wagner, K.R., et al., *Gentamicin treatment of Duchenne and Becker muscular dystrophy due to nonsense mutations.* Ann Neurol, 2001. **49**(6): p. 706-11.
118. Politano, L., et al., *Gentamicin administration in Duchenne patients with premature stop codon. Preliminary results.* Acta Myol, 2003. **22**(1): p. 15-21.
119. Malik, V., et al., *Gentamicin-induced readthrough of stop codons in Duchenne muscular dystrophy.* Ann Neurol, 2010. **67**(6): p. 771-80.
120. Welch, E.M., et al., *PTC124 targets genetic disorders caused by nonsense mutations.* Nature, 2007. **447**(7140): p. 87-91.
121. Peltz, S.W., et al., *Nonsense suppression activity of PTC124 (ataluren).* Proc Natl Acad Sci U S A, 2009. **106**(25): p. E64; author reply E65.
122. Finkel, R.S., et al., *Phase 2a study of ataluren-mediated dystrophin production in patients with nonsense mutation duchenne muscular dystrophy.* PLoS One, 2013. **8**(12): p. e81302.
123. Kayali, R., et al., *Read-through compound 13 restores dystrophin expression and improves muscle function in the mdx mouse model for Duchenne muscular dystrophy.* Hum Mol Genet, 2012. **21**(18): p. 4007-20.
124. Arakawa, M., et al., *Negamycin restores dystrophin expression in skeletal and cardiac muscles of mdx mice.* J Biochem, 2003. **134**(5): p. 751-8.

125. Shiozuka, M. and R. Matsuda, *[Therapeutic readthrough strategy for suppression of nonsense mutations in duchenne muscular dystrophy].* Brain Nerve, 2011. **63**(11): p. 1253-60.
126. Yuasa, K., et al., *Injection of a recombinant AAV serotype 2 into canine skeletal muscles evokes strong immune responses against transgene products.* Gene Ther, 2007. **14**(17): p. 1249-60.
127. Wang, Z., et al., *Immunity to adeno-associated virus-mediated gene transfer in a random-bred canine model of Duchenne muscular dystrophy.* Hum Gene Ther, 2007. **18**(1): p. 18-26.
128. Ohshima, S., et al., *Transduction efficiency and immune response associated with the administration of AAV8 vector into dog skeletal muscle.* Mol Ther, 2009. **17**(1): p. 73-80.
129. Rodino-Klapac, L.R., et al., *Persistent expression of FLAG-tagged micro dystrophin in nonhuman primates following intramuscular and vascular delivery.* Mol Ther, 2010. **18**(1): p. 109-17.
130. Yin, H., Q. Lu, and M. Wood, *Effective exon skipping and restoration of dystrophin expression by peptide nucleic acid antisense oligonucleotides in mdx mice.* Mol Ther, 2008. **16**(1): p. 38-45.
131. Goyenvalle, A., et al., *Rescue of severely affected dystrophin/utrophin-deficient mice through scAAV-U7snRNA-mediated exon skipping.* Hum Mol Genet, 2012. **21**(11): p. 2559-71.
132. Bostick, B., et al., *Adeno-associated virus serotype-9 microdystrophin gene therapy ameliorates electrocardiographic abnormalities in mdx mice.* Hum Gene Ther, 2008. **19**(8): p. 851-6.
133. Ghosh, A., et al., *Systemic Trans-splicing adeno-associated viral delivery efficiently transduces the heart of adult mdx mouse, a model for duchenne muscular dystrophy.* Hum Gene Ther, 2009. **20**(11): p. 1319-28.
134. Grieger, J.C. and R.J. Samulski, *Packaging capacity of adeno-associated virus serotypes: impact of larger genomes on infectivity and postentry steps.* J Virol, 2005. **79**(15): p. 9933-44.
135. Harper, S.Q., et al., *Modular flexibility of dystrophin: implications for gene therapy of Duchenne muscular dystrophy.* Nat Med, 2002. **8**(3): p. 253-61.
136. Bostick, B., et al., *AAV micro-dystrophin gene therapy alleviates stress-induced cardiac death but not myocardial fibrosis in >21-m-old mdx mice, an end-stage model of Duchenne muscular dystrophy cardiomyopathy.* J Mol Cell Cardiol, 2012. **53**(2): p. 217-22.
137. Shin, J.H., et al., *A simplified immune suppression scheme leads to persistent micro-dystrophin expression in duchenne muscular dystrophy dogs.* Hum Gene Ther, 2012. **23**(2): p. 202-9.
138. Qiao, C., et al., *Myostatin propeptide gene delivery by adeno-associated virus serotype 8 vectors enhances muscle growth and ameliorates dystrophic phenotypes in mdx mice.* Hum Gene Ther, 2008. **19**(3): p. 241-54.
139. Odom, G.L., et al., *Microutrophin delivery through rAAV6 increases lifespan and improves muscle function in dystrophic dystrophin/utrophin-deficient mice.* Mol Ther, 2008. **16**(9): p. 1539-45.
140. Tang, Y., et al., *Inhibition of the IKK/NF-kappaB pathway by AAV gene transfer improves muscle regeneration in older mdx mice.* Gene Ther, 2010. **17**(12): p. 1476-83.
141. Partridge, T.A., et al., *Conversion of mdx myofibres from dystrophin-negative to -positive by injection of normal myoblasts.* Nature, 1989. **337**(6203): p. 176-9.
142. Mendell, J.R., et al., *Myoblast transfer in the treatment of Duchenne's muscular dystrophy.* N Engl J Med, 1995. **333**(13): p. 832-8.

143. Skuk, D., et al., *Dystrophin expression in muscles of duchenne muscular dystrophy patients after high-density injections of normal myogenic cells.* J Neuropathol Exp Neurol, 2006. **65**(4): p. 371-86.
144. Montarras, D., et al., *Direct isolation of satellite cells for skeletal muscle regeneration.* Science, 2005. **309**(5743): p. 2064-7.
145. Farini, A., et al., *Cell based therapy for Duchenne muscular dystrophy.* J Cell Physiol, 2009. **221**(3): p. 526-34.
146. Peault, B., et al., *Stem and progenitor cells in skeletal muscle development, maintenance, and therapy.* Mol Ther, 2007. **15**(5): p. 867-77.
147. Ferrari, G., et al., *Muscle regeneration by bone marrow-derived myogenic progenitors.* Science, 1998. **279**(5356): p. 1528-30.
148. Goodell, M.A., et al., *Isolation and functional properties of murine hematopoietic stem cells that are replicating in vivo.* J Exp Med, 1996. **183**(4): p. 1797-806.
149. Dezawa, M., et al., *Bone marrow stromal cells generate muscle cells and repair muscle degeneration.* Science, 2005. **309**(5732): p. 314-7.
150. Torrente, Y., et al., *Human circulating AC133(+) stem cells restore dystrophin expression and ameliorate function in dystrophic skeletal muscle.* J Clin Invest, 2004. **114**(2): p. 182-95.
151. Benchaouir, R., et al., *Restoration of human dystrophin following transplantation of exon-skipping-engineered DMD patient stem cells into dystrophic mice.* Cell Stem Cell, 2007. **1**(6): p. 646-57.
152. Torrente, Y., et al., *Autologous transplantation of muscle-derived CD133+ stem cells in Duchenne muscle patients.* Cell Transplant, 2007. **16**(6): p. 563-77.
153. Sampaolesi, M., et al., *Mesoangioblast stem cells ameliorate muscle function in dystrophic dogs.* Nature, 2006. **444**(7119): p. 574-9.
154. Bretag, A.H., *Stem cell treatment of dystrophic dogs.* Nature, 2007. **450**(7173): p. E23; discussion E23-5.
155. Davies, K.E. and M.D. Grounds, *Treating muscular dystrophy with stem cells?* Cell, 2006. **127**(7): p. 1304-6.
156. Darabi, R., et al., *Functional skeletal muscle regeneration from differentiating embryonic stem cells.* Nat Med, 2008. **14**(2): p. 134-43.
157. Nishiyama, T. and S. Takeda, *[Induced pluripotent stem (iPS) cell-based cell therapy for muscular dystrophy: current progress and future prospects].* Brain Nerve, 2012. **64**(1): p. 39-46.
158. Darabi, R., et al., *Human ES- and iPS-derived myogenic progenitors restore DYSTROPHIN and improve contractility upon transplantation in dystrophic mice.* Cell Stem Cell, 2012. **10**(5): p. 610-9.
159. Huard, C., et al., *Transplantation of dermal fibroblasts expressing MyoD1 in mouse muscles.* Biochem Biophys Res Commun, 1998. **248**(3): p. 648-54.
160. Love, D.R., et al., *An autosomal transcript in skeletal muscle with homology to dystrophin.* Nature, 1989. **339**(6219): p. 55-8.
161. Buckle, V.J., et al., *Localisation of a dystrophin-related autosomal gene to 6q24 in man, and to mouse chromosome 10 in the region of the dystrophia muscularis (dy) locus.* Hum Genet, 1990. **85**(3): p. 324-6.
162. Blake, D.J., et al., *Characterization of a 4.8kb transcript from the Duchenne muscular dystrophy locus expressed in Schwannoma cells.* Hum Mol Genet, 1992. **1**(2): p. 103-9.
163. Ohlendieck, K., et al., *Dystrophin-related protein is localized to neuromuscular junctions of adult skeletal muscle.* Neuron, 1991. **7**(3): p. 499-508.
164. Nguyen, T.M., et al., *Localization of the DMDL gene-encoded dystrophin-related protein using a panel of nineteen monoclonal antibodies: presence at neuromuscular junctions, in the sarcolemma of dystrophic skeletal muscle, in vascular and other smooth muscles, and in proliferating brain cell lines.* J Cell Biol, 1991. **115**(6): p. 1695-700.

165. Matsumura, K., et al., *Association of dystrophin-related protein with dystrophin-associated proteins in mdx mouse muscle.* Nature, 1992. **360**(6404): p. 588-91.
166. Mattei, E., et al., *Utrophin up-regulation by an artificial transcription factor in transgenic mice.* PLoS One, 2007. **2**(8): p. e774.
167. Tinsley, J., et al., *Expression of full-length utrophin prevents muscular dystrophy in mdx mice.* Nat Med, 1998. **4**(12): p. 1441-4.
168. Tinsley, J.M., et al., *Daily treatment with SMTC1100, a novel small molecule utrophin upregulator, dramatically reduces the dystrophic symptoms in the mdx mouse.* PLoS One, 2011. **6**(5): p. e19189.
169. Di Certo, M.G., et al., *The artificial gene Jazz, a transcriptional regulator of utrophin, corrects the dystrophic pathology in mdx mice.* Hum Mol Genet, 2010. **19**(5): p. 752-60.
170. Strimpakos, G., et al., *Novel Adeno-Associated Viral Vector Delivering the Utrophin Gene Regulator Jazz Counteracts Dystrophic Pathology in mdx Mice.* J Cell Physiol, 2014.
171. Li, D., et al., *Sarcolemmal nNOS anchoring reveals a qualitative difference between dystrophin and utrophin.* J Cell Sci, 2010. **123**(Pt 12): p. 2008-13.
172. Aartsma-Rus, A., et al., *Theoretic applicability of antisense-mediated exon skipping for Duchenne muscular dystrophy mutations.* Hum Mutat, 2009. **30**(3): p. 293-9.
173. Lu, Q.L., et al., *Systemic delivery of antisense oligoribonucleotide restores dystrophin expression in body-wide skeletal muscles.* Proc Natl Acad Sci U S A, 2005. **102**(1): p. 198-203.
174. Alter, J., et al., *Systemic delivery of morpholino oligonucleotide restores dystrophin expression bodywide and improves dystrophic pathology.* Nat Med, 2006. **12**(2): p. 175-7.
175. Yang, L., et al., *Effective exon skipping and dystrophin restoration by 2'-o-methoxyethyl antisense oligonucleotide in dystrophin-deficient mice.* PLoS One, 2013. **8**(4): p. e61584.
176. Kumar, R., et al., *The first analogues of LNA (locked nucleic acids): phosphorothioate-LNA and 2'-thio-LNA.* Bioorg Med Chem Lett, 1998. **8**(16): p. 2219-22.
177. Aartsma-Rus, A., et al., *Comparative analysis of antisense oligonucleotide analogs for targeted DMD exon 46 skipping in muscle cells.* Gene Ther, 2004. **11**(18): p. 1391-8.
178. Cotten, M., et al., *2'-O-methyl, 2'-O-ethyl oligoribonucleotides and phosphorothioate oligodeoxyribonucleotides as inhibitors of the in vitro U7 snRNP-dependent mRNA processing event.* Nucleic Acids Res, 1991. **19**(10): p. 2629-35.
179. Sazani, P., et al., *Nuclear antisense effects of neutral, anionic and cationic oligonucleotide analogs.* Nucleic Acids Res, 2001. **29**(19): p. 3965-74.
180. Summerton, J., et al., *Morpholino and phosphorothioate antisense oligomers compared in cell-free and in-cell systems.* Antisense Nucleic Acid Drug Dev, 1997. **7**(2): p. 63-70.
181. Amantana, A. and P.L. Iversen, *Pharmacokinetics and biodistribution of phosphorodiamidate morpholino antisense oligomers.* Curr Opin Pharmacol, 2005. **5**(5): p. 550-5.
182. Malerba, A., et al., *Dosing regimen has a significant impact on the efficiency of morpholino oligomer-induced exon skipping in mdx mice.* Hum Gene Ther, 2009. **20**(9): p. 955-65.
183. Malerba, A., et al., *Chronic systemic therapy with low-dose morpholino oligomers ameliorates the pathology and normalizes locomotor behavior in mdx mice.* Mol Ther, 2011. **19**(2): p. 345-54.

184. Vitiello, L., et al., *In vivo delivery of naked antisense oligos in aged mdx mice: analysis of dystrophin restoration in skeletal and cardiac muscle.* Neuromuscul Disord, 2008. **18**(8): p. 597-605.
185. Cartegni, L., S.L. Chew, and A.R. Krainer, *Listening to silence and understanding nonsense: exonic mutations that affect splicing.* Nat Rev Genet, 2002. **3**(4): p. 285-98.
186. Aartsma-Rus, A., et al., *Therapeutic modulation of DMD splicing by blocking exonic splicing enhancer sites with antisense oligonucleotides.* Ann N Y Acad Sci, 2006. **1082**: p. 74-6.
187. Lu, Q.L., et al., *Functional amounts of dystrophin produced by skipping the mutated exon in the mdx dystrophic mouse.* Nat Med, 2003. **9**(8): p. 1009-14.
188. Bremmer-Bout, M., et al., *Targeted exon skipping in transgenic hDMD mice: A model for direct preclinical screening of human-specific antisense oligonucleotides.* Mol Ther, 2004. **10**(2): p. 232-40.
189. Wu, B., et al., *One-year treatment of morpholino antisense oligomer improves skeletal and cardiac muscle functions in dystrophic mdx mice.* Mol Ther, 2011. **19**(3): p. 576-83.
190. Sazani, P., D.L. Weller, and S.B. Shrewsbury, *Safety pharmacology and genotoxicity evaluation of AVI-4658.* Int J Toxicol, 2010. **29**(2): p. 143-56.
191. Sazani, P., et al., *Repeat-dose toxicology evaluation in cynomolgus monkeys of AVI-4658, a phosphorodiamidate morpholino oligomer (PMO) drug for the treatment of duchenne muscular dystrophy.* Int J Toxicol, 2011. **30**(3): p. 313-21.
192. Kinali, M., et al., *Local restoration of dystrophin expression with the morpholino oligomer AVI-4658 in Duchenne muscular dystrophy: a single-blind, placebo-controlled, dose-escalation, proof-of-concept study.* Lancet Neurol, 2009. **8**(10): p. 918-28.
193. Cirak, S., et al., *Exon skipping and dystrophin restoration in patients with Duchenne muscular dystrophy after systemic phosphorodiamidate morpholino oligomer treatment: an open-label, phase 2, dose-escalation study.* Lancet, 2011. **378**(9791): p. 595-605.
194. Mendell, J.R., et al., *Eteplirsen for the treatment of Duchenne muscular dystrophy.* Ann Neurol, 2013. **74**(5): p. 637-47.
195. Flanigan, K.M., et al., *Pharmacokinetics and safety of single doses of drisapersen in non-ambulant subjects with Duchenne muscular dystrophy: results of a double-blind randomized clinical trial.* Neuromuscul Disord, 2014. **24**(1): p. 16-24.
196. Goemans, N.M., et al., *Systemic administration of PRO051 in Duchenne's muscular dystrophy.* N Engl J Med, 2011. **364**(16): p. 1513-22.
197. Malerba, A., L. Boldrin, and G. Dickson, *Long-term systemic administration of unconjugated morpholino oligomers for therapeutic expression of dystrophin by exon skipping in skeletal muscle: implications for cardiac muscle integrity.* Nucleic Acid Ther, 2011. **21**(4): p. 293-8.
198. van Deutekom, J.C., et al., *Local dystrophin restoration with antisense oligonucleotide PRO051.* N Engl J Med, 2007. **357**(26): p. 2677-86.
199. Takeshima, Y., et al., *Intravenous infusion of an antisense oligonucleotide results in exon skipping in muscle dystrophin mRNA of Duchenne muscular dystrophy.* Pediatr Res, 2006. **59**(5): p. 690-4.
200. Derossi, D., et al., *The third helix of the Antennapedia homeodomain translocates through biological membranes.* J Biol Chem, 1994. **269**(14): p. 10444-50.
201. Vives, E., P. Brodin, and B. Lebleu, *A truncated HIV-1 Tat protein basic domain rapidly translocates through the plasma membrane and accumulates in the cell nucleus.* J Biol Chem, 1997. **272**(25): p. 16010-7.

202. Langel, U., et al., *A galanin-mastoparan chimeric peptide activates the Na+,K(+)-ATPase and reverses its inhibition by ouabain.* Regul Pept, 1996. **62**(1): p. 47-52.
203. Amantana, A., et al., *Pharmacokinetics, biodistribution, stability and toxicity of a cell-penetrating peptide-morpholino oligomer conjugate.* Bioconjug Chem, 2007. **18**(4): p. 1325-31.
204. Abes, R., et al., *Delivery of steric block morpholino oligomers by (R-X-R)4 peptides: structure-activity studies.* Nucleic Acids Res, 2008. **36**(20): p. 6343-54.
205. Mitchell, D.J., et al., *Polyarginine enters cells more efficiently than other polycationic homopolymers.* J Pept Res, 2000. **56**(5): p. 318-25.
206. Wu, R.P., et al., *Cell-penetrating peptides as transporters for morpholino oligomers: effects of amino acid composition on intracellular delivery and cytotoxicity.* Nucleic Acids Res, 2007. **35**(15): p. 5182-91.
207. Abes, S., et al., *Vectorization of morpholino oligomers by the (R-Ahx-R)4 peptide allows efficient splicing correction in the absence of endosomolytic agents.* J Control Release, 2006. **116**(3): p. 304-13.
208. Morris, M.C., et al., *A new peptide vector for efficient delivery of oligonucleotides into mammalian cells.* Nucleic Acids Res, 1997. **25**(14): p. 2730-6.
209. Mae, M., et al., *A stearylated CPP for delivery of splice correcting oligonucleotides using a non-covalent co-incubation strategy.* J Control Release, 2009. **134**(3): p. 221-7.
210. Andaloussi, S.E., et al., *Design of a peptide-based vector, PepFect6, for efficient delivery of siRNA in cell culture and systemically in vivo.* Nucleic Acids Res, 2011. **39**(9): p. 3972-87.
211. Ezzat, K., et al., *PepFect 14, a novel cell-penetrating peptide for oligonucleotide delivery in solution and as solid formulation.* Nucleic Acids Res, 2011. **39**(12): p. 5284-98.
212. Yin, H., et al., *Cell-penetrating peptide-conjugated antisense oligonucleotides restore systemic muscle and cardiac dystrophin expression and function.* Hum Mol Genet, 2008. **17**(24): p. 3909-18.
213. Wu, B., et al., *Effective rescue of dystrophin improves cardiac function in dystrophin-deficient mice by a modified morpholino oligomer.* Proc Natl Acad Sci U S A, 2008. **105**(39): p. 14814-9.
214. Jearawiriyapaisarn, N., et al., *Sustained dystrophin expression induced by peptide-conjugated morpholino oligomers in the muscles of mdx mice.* Mol Ther, 2008. **16**(9): p. 1624-9.
215. Moulton, H.M. and J.D. Moulton, *Morpholinos and their peptide conjugates: therapeutic promise and challenge for Duchenne muscular dystrophy.* Biochim Biophys Acta, 2010. **1798**(12): p. 2296-303.
216. Ryser, H.J. and R. Hancock, *Histones and basic polyamino acids stimulate the uptake of albumin by tumor cells in culture.* Science, 1965. **150**(3695): p. 501-3.
217. Youngblood, D.S., et al., *Stability of cell-penetrating peptide-morpholino oligomer conjugates in human serum and in cells.* Bioconjug Chem, 2007. **18**(1): p. 50-60.
218. Moulton, H.M., et al., *Cell-penetrating peptide-morpholino conjugates alter pre-mRNA splicing of DMD (Duchenne muscular dystrophy) and inhibit murine coronavirus replication in vivo.* Biochem Soc Trans, 2007. **35**(Pt 4): p. 826-8.
219. Fletcher, S., et al., *Morpholino oligomer-mediated exon skipping averts the onset of dystrophic pathology in the mdx mouse.* Mol Ther, 2007. **15**(9): p. 1587-92.
220. Goyenvalle, A., et al., *Prevention of Dystrophic Pathology in Severely Affected Dystrophin/Utrophin-deficient Mice by Morpholino-oligomer-mediated Exon-skipping.* Molecular Therapy, 2010. **18**(1): p. 198-205.
221. Deconinck, A.E., et al., *Utrophin-dystrophin-deficient mice as a model for Duchenne muscular dystrophy.* Cell, 1997. **90**(4): p. 717-27.

222. Crisp, A., et al., *Diaphragm rescue alone prevents heart dysfunction in dystrophic mice.* Hum Mol Genet, 2011. **20**(3): p. 413-21.
223. Yin, H., et al., *Functional rescue of dystrophin-deficient mdx mice by a chimeric peptide-PMO.* Mol Ther, 2010. **18**(10): p. 1822-9.
224. Samoylova, T.I. and B.F. Smith, *Elucidation of muscle-binding peptides by phage display screening.* Muscle Nerve, 1999. **22**(4): p. 460-6.
225. Yin, H., et al., *A fusion peptide directs enhanced systemic dystrophin exon skipping and functional restoration in dystrophin-deficient mdx mice.* Hum Mol Genet, 2009. **18**(22): p. 4405-14.
226. Seow, Y., H. Yin, and M.J. Wood, *Identification of a novel muscle targeting peptide in mdx mice.* Peptides, 2010.
227. Perez, F., et al., *Antennapedia homeobox as a signal for the cellular internalization and nuclear addressing of a small exogenous peptide.* J Cell Sci, 1992. **102 (Pt 4)**: p. 717-22.
228. Turner, J.J., et al., *Cell-penetrating peptide conjugates of peptide nucleic acids (PNA) as inhibitors of HIV-1 Tat-dependent trans-activation in cells.* Nucleic Acids Res, 2005. **33**(21): p. 6837-49.
229. Ivanova, G.D., et al., *Improved cell-penetrating peptide-PNA conjugates for splicing redirection in HeLa cells and exon skipping in mdx mouse muscle.* Nucleic Acids Res, 2008. **36**(20): p. 6418-28.
230. Yin, H., et al., *Pip5 transduction peptides direct high efficiency oligonucleotide-mediated dystrophin exon skipping in heart and phenotypic correction in mdx mice.* Mol Ther, 2011. **19**(7): p. 1295-303.
231. Hamer, P.W., et al., *Evans Blue Dye as an in vivo marker of myofibre damage: optimising parameters for detecting initial myofibre membrane permeability.* J Anat, 2002. **200**(Pt 1): p. 69-79.
232. Huang, P., et al., *Impaired respiratory function in mdx and mdx/utrn(+/-) mice.* Muscle Nerve, 2011. **43**(2): p. 263-7.
233. De Troyer, A. and M. Estenne, *Functional anatomy of the respiratory muscles.* Clin Chest Med, 1988. **9**(2): p. 175-93.
234. Ivanova, G.D., et al., *PNA-peptide conjugates as intracellular gene control agents.* Nucleic Acids Symp Ser (Oxf), 2008(52): p. 31-2.
235. Costas, J.M., et al., *Voluntary exercise induces structural remodeling in the hearts of dystrophin-deficient mice.* Muscle Nerve, 2010. **42**(6): p. 881-5.
236. Potter, L.R., et al., *Natriuretic peptides: their structures, receptors, physiologic functions and therapeutic applications.* Handb Exp Pharmacol, 2009(191): p. 341-66.
237. McGrath, M.F., M.L. de Bold, and A.J. de Bold, *The endocrine function of the heart.* Trends Endocrinol Metab, 2005. **16**(10): p. 469-77.
238. Kuroda, J., et al., *NADPH oxidase 4 (Nox4) is a major source of oxidative stress in the failing heart.* Proc Natl Acad Sci U S A, 2010. **107**(35): p. 15565-70.
239. Spurney, C.F., et al., *Dystrophin-deficient cardiomyopathy in mouse: expression of Nox4 and Lox are associated with fibrosis and altered functional parameters in the heart.* Neuromuscul Disord, 2008. **18**(5): p. 371-81.
240. Quinlan, J.G., et al., *Poloxamer 188 failed to prevent exercise-induced membrane breakdown in mdx skeletal muscle fibers.* Neuromuscul Disord, 2006. **16**(12): p. 855-64.
241. Petrof, B.J., et al., *Dystrophin protects the sarcolemma from stresses developed during muscle contraction.* Proc Natl Acad Sci U S A, 1993. **90**(8): p. 3710-4.
242. Loufrani, L., et al., *Flow (shear stress)-induced endothelium-dependent dilation is altered in mice lacking the gene encoding for dystrophin.* Circulation, 2001. **103**(6): p. 864-70.

243. Loufrani, L., B.I. Levy, and D. Henrion, *Defect in microvascular adaptation to chronic changes in blood flow in mice lacking the gene encoding for dystrophin.* Circ Res, 2002. **91**(12): p. 1183-9.
244. Palladino, M., et al., *Angiogenic impairment of the vascular endothelium: a novel mechanism and potential therapeutic target in muscular dystrophy.* Arterioscler Thromb Vasc Biol, 2013. **33**(12): p. 2867-76.
245. Ito, K., et al., *Smooth muscle-specific dystrophin expression improves aberrant vasoregulation in mdx mice.* Hum Mol Genet, 2006. **15**(14): p. 2266-75.
246. Loufrani, L., et al., *Absence of dystrophin in mice reduces NO-dependent vascular function and vascular density: total recovery after a treatment with the aminoglycoside gentamicin.* Arterioscler Thromb Vasc Biol, 2004. **24**(4): p. 671-6.
247. Asai, A., et al., *Primary role of functional ischemia, quantitative evidence for the two-hit mechanism, and phosphodiesterase-5 inhibitor therapy in mouse muscular dystrophy.* PLoS One, 2007. **2**(8): p. e806.
248. Thierry, A.R., et al., *Cellular uptake and intracellular fate of antisense oligonucleotides.* Curr Opin Mol Ther, 2003. **5**(2): p. 133-8.
249. Jearawiriyapaisarn, N., et al., *Long-term improvement in mdx cardiomyopathy after therapy with peptide-conjugated morpholino oligomers.* Cardiovasc Res, 2010. **85**(3): p. 444-53.
250. Sugita, H. and S. Takeda, *Progress in muscular dystrophy research with special emphasis on gene therapy.* Proc Jpn Acad Ser B Phys Biol Sci, 2010. **86**(7): p. 748-56.
251. Gupta, A., et al., *Hydrophobicity drives the cellular uptake of short cationic peptide ligands.* Eur Biophys J, 2011. **40**(6): p. 727-36.
252. Lundin, P., et al., *Distinct uptake routes of cell-penetrating peptide conjugates.* Bioconjug Chem, 2008. **19**(12): p. 2535-42.
253. Lehto, T., et al., *Cellular trafficking determines the exon skipping activity of Pip6a-PMO in mdx skeletal and cardiac muscle cells.* Nucleic Acids Res, 2014. **42**(5): p. 3207-17.
254. Wallace, G.Q. and E.M. McNally, *Mechanisms of muscle degeneration, regeneration, and repair in the muscular dystrophies.* Annu Rev Physiol, 2009. **71**: p. 37-57.
255. Townsend, D., et al., *Emergent dilated cardiomyopathy caused by targeted repair of dystrophic skeletal muscle.* Mol Ther, 2008. **16**(5): p. 832-5.
256. Jansen, M., et al., *Physical training in boys with Duchenne Muscular Dystrophy: the protocol of the No Use is Disuse study.* BMC Pediatr, 2010. **10**: p. 55.
257. Sveen, M.L., et al., *Resistance training in patients with limb-girdle and becker muscular dystrophies.* Muscle Nerve, 2013. **47**(2): p. 163-9.
258. Jansen, M., et al., *Assisted bicycle training delays functional deterioration in boys with Duchenne muscular dystrophy: the randomized controlled trial "no use is disuse".* Neurorehabil Neural Repair, 2013. **27**(9): p. 816-27.
259. Hourde, C., et al., *Voluntary Physical Activity Protects from Susceptibility to Skeletal Muscle Contraction-Induced Injury But Worsens Heart Function in mdx Mice.* Am J Pathol, 2013. **182**(5): p. 1509-18.
260. Zhang, M., et al., *NADPH oxidases in heart failure: poachers or gamekeepers?* Antioxid Redox Signal, 2013. **18**(9): p. 1024-41.
261. Nakamura, A., et al., *Progression of dystrophic features and activation of mitogen-activated protein kinases and calcineurin by physical exercise, in hearts of mdx mice.* FEBS Lett, 2002. **520**(1-3): p. 18-24.
262. Betts, C., et al., *Pip6-PMO, A New Generation of Peptide-oligonucleotide Conjugates With Improved Cardiac Exon Skipping Activity for DMD Treatment.* Mol Ther Nucleic Acids, 2012. **1**: p. e38.

263. Call, J.A., et al., *Endurance capacity in maturing mdx mice is markedly enhanced by combined voluntary wheel running and green tea extract.* J Appl Physiol, 2008. **105**(3): p. 923-32.
264. Buyse, G.M., et al., *Long-term blinded placebo-controlled study of SNT-MC17/idebenone in the dystrophin deficient mdx mouse: cardiac protection and improved exercise performance.* Eur Heart J, 2009. **30**(1): p. 116-24.
265. Jefferies, J.L., et al., *Genetic predictors and remodeling of dilated cardiomyopathy in muscular dystrophy.* Circulation, 2005. **112**(18): p. 2799-804.
266. Sharp, P.S., H. Bye-a-Jee, and D.J. Wells, *Physiological characterization of muscle strength with variable levels of dystrophin restoration in mdx mice following local antisense therapy.* Mol Ther, 2011. **19**(1): p. 165-71.
267. McGeachie, J.K., et al., *Age-related changes in replication of myogenic cells in mdx mice: quantitative autoradiographic studies.* J Neurol Sci, 1993. **119**(2): p. 169-79.
268. Khairallah, M., et al., *Metabolic and signaling alterations in dystrophin-deficient hearts precede overt cardiomyopathy.* J Mol Cell Cardiol, 2007. **43**(2): p. 119-29.
269. Burelle, Y., et al., *Alterations in mitochondrial function as a harbinger of cardiomyopathy: lessons from the dystrophic heart.* J Mol Cell Cardiol, 2010. **48**(2): p. 310-21.
270. Chandrasekharan, K., et al., *A human-specific deletion in mouse Cmah increases disease severity in the mdx model of Duchenne muscular dystrophy.* Sci Transl Med, 2010. **2**(42): p. 42ra54.
271. Smart, N., et al., *Myocardial regeneration: expanding the repertoire of thymosin beta4 in the ischemic heart.* Ann N Y Acad Sci, 2012. **1269**: p. 92-101.
272. Smart, N., K.N. Dube, and P.R. Riley, *Epicardial progenitor cells in cardiac regeneration and neovascularisation.* Vascul Pharmacol, 2013. **58**(3): p. 164-73.